NTNU – Trondheim
Norwegian University of
Science and Technology

Assessment of Low-Frequency Roll Motions on the Semisubmersible Drilling Rig COSL Pioneer

Vibeke Christine Browne

Marine Technology
Submission date: May 2013
Supervisor: Odd Magnus Faltinsen, IMT

Norwegian University of Science and Technology
Department of Marine Technology

Scope of work

Background: The marine personnel on the COSL Pioneer has experienced larger than expected roll motions of the rig. During an investigation of a line failure incident Global Maritime identified roll motions that were magnitudes higher than expected. By examination of the roll motion log one could clearly see that the low frequency motions were the dominant part. The reason for this behaviour is not identified, but some issues with the DP control indicate that the excessive roll motions can be a result of thrust-induced motions.

Task: The student is expected to make a model of the rig and run analyses in time domain in order to reproduce the registered motions during an identified weather situation. All necessary vessel data and a log from MRU and DP system will be made available. The student is free to investigate options that can explain the excessive motions. However, she should also stay in touch with Global Maritime/COSL Drilling Europe as there is planned to be carried out adjustments of the DP settings on the rig. This work can provide useful information.

The thesis should include a discussion of possible reasons for the excessive roll motions and a conclusion with the most probable reason and also possible actions for reducing these motions.

In the thesis the candidate shall present her personal contribution to the resolution of problems within the scope of the thesis work.

Theories and conclusions should be based on mathematical derivations and/or logic reasoning identifying the various steps in the deduction.

The candidate should utilise the existing possibilities for obtaining relevant literature.

The thesis should be organised in a rational manner to give a clear exposition of results, assessments and conclusions. The text should be brief and to the point, with a clear language. Telegraphic language should be avoided.

The thesis shall contain the following elements: A text defining the scope, preface, list of contents, summary, main body of thesis, conclusions with recommendations for further work, list of symbols and acronyms, references and (optional) appendices. All figures, tables and equations shall be numerated.

The original contribution of the candidate and material taken from other sources shall be clearly defined. Work from other sources shall be properly referenced using an acknowledged referencing system.

Supervisor: Prof. Odd M. Faltinsen

Deadline: June 10, 2013

Acknowledgements

This thesis was written in the spring of 2013 and submitted to the Norwegian University of Science and Technology (NTNU) for partial fullfillment of the requirements for the degree of Master of Science in Marine Technology. The main objective of the thesis was to regenerate and study the excessive roll motions registered on the drilling rig COSL Pioneer on January 25th 2012. Three months into the work I was notified that data regarding the dynamic positioning system would not be made available. The scope of the thesis was then shifted to focus more on the theoretical background of the software, programming of dynamic positioning systems and to attempt to generate thruster-induced roll motions in a simulation.

Before starting the work on the thesis I was not familiar with OrcaFlex, had never seen or heard about the programming language Python and had very little knowledge about dynamic positioning systems. A considerable amount of time was therefore spent acquiring this knowledge.

I would like to thank my supervisor Odd M. Faltinsen for his continuous and valuable help and support which provided me with greater insight and understanding of hydrodynamic theory. I am very grateful to Orcina for lending me OrcaFlex and for answering my questions regarding the software quickly with comprehensive and detailed answers. Thanks are directed towards DNV for lending their HydroD software to students at NTNU and for responding to questions regarding the software. I would also like to thank Global Maritime and China Oilfield Services Limited for the opportunity to work with COSL Pioneer and for providing necessary data.

Vibeke Christine Browne

Vibeke Christine Browne
Trondheim, May 29, 2013

Introduction

The first automatic ship steering mechanism for course keeping was developed by Elmer Sperry in the beginning of the 20th century[1]. A large amount of work has been done since then and today's dynamic positioning systems are very advanced. There are many parameters that have to be tuned in order to achieve optimal performance and the tuning of dynamic positioning systems in sea-trials alone may take up to ten days to complete.

The main purpose of a dynamic positioning system is to counteract low-frequency motions in the horizontal plane. Unfortunately, due to the position of the thrusters and the low hydrostatic stiffness of semisubmersibles, they also induce roll and pitch moments. If the forces exerted by the thrusters oscillate with the vessel's roll or pitch resonance frequencies, they may cause large unwanted rotations of the vessel. The natural periods in roll and pitch are usually large for semisubmersibles due to their low water-plane area and low metacentric height. It is suspected that this phenomenon presented itself on the drilling rig COSL Pioneer on January 25th 2012.

The objective of this thesis is to investigate whether the excessive roll motions registered on January 25th 2012 were thruster-induced, but also look for other causes that might have increased the roll motion. Since too little information regarding the dynamic positioning system was available, the work was concentrated on the theoretical background and use of the chosen software as well as the programming of a dynamic positioning system in order to study its effects and try to generate thruster-induced motions.

The potential flow solver Wadam, with the programming interface HydroD, was chosen for the frequency-domain analysis of the bare hull. The output from Wadam was imported to the time-domain analysis program OrcaFlex together with information about the environment and mooring system. The dynamic positioning system was represented by forces and moments calculated in a separately written Python-script using a PID Controller.

Background theory and earlier work regarding thruster-induced roll motion is discussed in Chapter 1. Chapter 2 treats the work performed in Wadam and its theoretical background. The modelling of COSL Pioneer in OrcaFlex and how OrcaFlex performs time-domain simulations can be found in Chapter 3. Computational difficulties that were encountered during the work and sensitivity studies are described in Chapter 4. Chapter 5 presents the set-up for different time-domain simulations. Results from the frequency-domain and time-domain analyses may be found in Chapter 6 and Chapter 7, respectively. Discussion of the results, conclusions and suggestions for further work are presented in Chapter 8.

Summary

Excessive roll motions were registered on the drilling rig COSL Pioneer on January 25th 2012. Calculations performed by Global Maritime showed less roll motions than registered, but were consistent with the other five degrees of freedom. It was suspected that the excessive motions could have been induced by the low-frequency forces from the thrusters. The main objective of this thesis was to regenerate and identify the cause of these excessive roll motions.

A frequency-domain analysis of the bare hull was performed in HydroD, with the potential flow solver Wadam. A panel model and structural data for the frequency-domain analysis were provided by Global Maritime. The hydrodynamic data from Wadam was exported to OrcaFlex, the program used for the time-domain analysis. The rig and its anchor lines were modelled in OrcaFlex while the drilling riser was omitted from the analysis due to its small influence on the motions of the rig. The forces from the thrusters were calculated in a separate program written in the programming language Python. A very simple dynamic positioning system was applied since only scarce information about the thrusters and the dynamic positioning system was made available.

The thruster forces calculated in the Python-program were implemented in OrcaFlex as two forces and a moment acting in the earth-fixed horizontal plane. The thruster forces were calculated using an algorithm for a Proportional Integral Derivative controller, also known as a PID controller. A PID controller has three controller gain coefficients that were estimated on the basis of a uncoupled and linear simplification of the real system. Simulations were also run for the same PID controller with gains that were 50% higher and 50% lower than the original estimate. A simulation without any inclusion of thruster forces was run and used as reference.

No thruster-induced motions were registered in the time-domain simulations with PID controllers. The transverse thruster force was therefore replaced with a harmonic force with a period in roll equal to that of the simulation with the PID controller and in a direction that was initially in phase with the roll motion. However, the harmonic thruster load increased the roll motions, but they were still significantly smaller than on January 25th 2012.

A real dynamic positioning system calculates the thruster forces on the basis of the low-frequent horizontal motions of the vessel. This was initially attempted, but then abandoned as the second-order Butterworth filter that OrcaFlex applies in order to filter low-frequency from wave-frequency motions introduced a phase lag. The phase lag was of approximately 25°and the caused the amplitudes of the motion to diverge.

The standard deviations for surge, sway, heave, roll and pitch from all the simulations in OrcaFlex were compared to the standard deviations of the registered motions between 18:00 and 18:55 on January 25th 2012. The registered motions had standard deviations that were approximately twice as large in roll and had half the values in heave. The standard deviations in surge, sway and yaw were of the same magnitude in the time-domain simulations and on January 25th 2012.

The deviations between the registered motions and the simulations are assumed to be predominantly due to the simplifications regarding the thrusters. The most significant simplifications were the forces' point of application, direction and that the wave frequency motion was included in the calculation of the forces.

Sammendrag

Rullebevegelser som var større enn forventet ble registrert på boreriggen COSL Pioneer 25. januar 2012. Beregninger foretatt av Global Maritime viste lavere rullebevegelser enn de som ble registrert, men var i overensstemmelse med bevegelsene i de andre frihetsgradene. Det var antatt at de store rullebevegelsene kan ha blitt forårsaket av lavfrekvente krefter fra thrusterne. Hovedformålet med denne masteroppgaven var å regenerere de registererte rullebevegelsene og identifisere årsaken til at rullebevegelsene var større enn forventet.

En analyse i frekvensdomenet ble utført ved å modellere skroget til COSL Pioneer i HydroD og løst ved hjelp av potensialteori i programmet Wadam. En panelmodell og strukturelle data ble fremskaffet av Global Maritime. Hydrodynamiske data for skroget ble deretter eksportert til OrcaFlex, programmet som ble brukt til tids-domene analyser. Riggen med ankerlinene ble modellert i OrcaFlex, mens borestrengen ble utelatt fra beregningene ettersom den ikke ville hatt noen betydelig effekt på riggens bevegelser. Kreftene fra thrusterne ble beregnet i et separat program og ble skrevet i programmeringsspråket Python. Et veldig forenklet dynamisk posisjoneringssystem ble brukt ettersom kun svært begrenset informasjon om det faktiske dynamiske posisjoneringssystemet var tilgjengelig.

Kreftene fra thrusterne som ble beregnet i Python-programmet ble implementert i OrcaFlex som to krefter og et moment som ble påsatt i det globale horisontale planet. Kreftene fra thrusterne ble beregnet med en algoritme for en Proportional Integral Derivative kontroller, ofte kalt en PID kontroller. En PID kontroller har tre parametere som ble estimert på bakgrunn av en ukoblet, lineær forenkling av det virkelige systemet. Simuleringer ble også kjørt med kontroller parametere som var 50% høyere og 50% lavere enn det originale estimatet. En simulering som ble kjørt uten noen thrusterkrefter ble brukt som referanse.

Ingen thruster-induserte rullebevegelser ble registrert i tidsdomene-simuleringene med PID kontrollere. De tverrgående kreftene fra thrusterne ble derfor byttet ut med en harmonisk kraft som hadde en periode lik den gjennomsnittelige perioden i rull som ble registrert under simuleringen med den originale PID kontrolleren og hadde en retning slik at den var i fase med rullebevegelsen i begynnelsen av simuleringen. Dette økte rullebevegelsene, men rullebevegelsene var fortsatt mye mindre enn det som ble registrert på COSL Pioneer den 25. januar 2012.

Et ekte dynamisk posisjonerings system beregner kreftene fra thrusterne på bakgrunn av de lavfrekvente horisontale bevegelsene til fartøyet. Dette ble forsøkt, men forkastet ettersom det andre-ordens Butterworth filteret som OrcaFlex bruker for å skille ut lavfrekvente bevegelser også introduserte en faseforskjell. Denne faseforskjellen var på rundt 25° og fikk amplituden til bevegelsene til å divergere.

Standardavviket til bevegelsene i jag, svai, hiv, rull og stamp for alle simuleringene i OrcaFlex ble sammenlignet med standardavviket for de bevegelsene som ble registrert mellom 18:00 og 18:55 25. januar 2012. De faktiske bevegelsene hadde et standardavvik som var cirka dobbelt så stort i rull og halvparten så stort i hiv. Standardavvikene i jag, svai og stamp var av samme størrelsesorden for simuleringene i OrcaFlex og som for de registrerte bevegelsene fra januar 2012.

Avviket mellom de registrerte bevegelsene er antatt å være hovedsaklig grunnet foren-

klingene som ble gjort under modelleringene av kreftene fra thrusterne. Spesielt gjelder dette punktet kreftene ble påført, retningen til kreftene og at alle komponentene av alle de horisontal bevegelsene til riggen ble inkludert i beregningen av disse kreftene istedenfor kun de lavfrekvente bevegelsene.

Nomenclature

α	Parameter in the Jonswap Spectrum
α	Ratio of group velocity and phase velocity used for calculation of wave-drift damping
β	Direction of incoming wave
β_e	Encounter heading
$\boldsymbol{\alpha}$	First-order rotation vector
$\boldsymbol{\xi}$	Location of source in computation of velocity potential
$\boldsymbol{\xi}$	Translational displacement vector in the calculation of the second-order pressure
δ	Phase angle
δ_d	Phase lag of wave drift QTF
ϵ	Offset from set-point
Γ	Gamma function
γ	Parameter in the Jonswap Spectrum
$\Im$[x]	Imaginary part of the complex number x
λ	Expansion factor
ν	Poisson ratio
ω	Frequency of oscillation
ω_0	Arbitrary frequency of oscillation used in Newman's approximation method
ω_e	Encounter frequency of oscillation
Φ	Total velocity potential
ϕ	Velocity potential
ϕ_0	Velocity potential of the incoming wave
ϕ_1	First-order velocity potential
ϕ_2	Second-order velocity potential
ϕ_D	Diffraction velocity potential
ϕ_R	Radiation velocity potential
ϕ_{exc}	Excitation velocity potential
ψ	Heading of vessel
$\Re$[x]	Real part of the complex number x
ρ	Water density
σ	Standard deviation
σ_A	Parameter in the Jonswap Spectrum

σ_B Parameter in the Jonswap Spectrum

τ Period of oscillation

τ_e Encounter period

θ Wave direction variable

θ_P Principal wave direction

ε Mean axial strain

φ Component of radiation velocity potential for degree of freedom j

ξ Complex amplitude of rigid body motion in discretization of radiation potential

ζ Wave amplitude

ζ_{max} Maximum wave elevation

Q_{diag} Diagonal QTF value

2q Spreading exponent

n Normal vector

r Vector of point on body

x Position vector

A Cross sectional stress area

a Acceleration

a_d Amplitude of wave drift QTF

A_e Aranha scaling factor

A_{DOF} Vessel projected are above or beneath the waterline in surge where DOF = surge, sway or yaw

A_{kj} Added mass coefficient

B Damping coefficient matrix

B_{kj} Damping coefficient

B10 Buoy with buoyancy of 100 MN

B5 Buoy with buoyancy of 50 MN

C Effective curvature in the calculation of the moment of the line segments

C Restoring coefficient matrix

C_d Drag coefficient

C_g Wave group velocity

C_p Wave phase velocity

C_{DOF} Vessel wind or current coefficient where DOF = surge, sway or yaw

C_{kj} Restoring coefficient

C76 Chain with bar diameter of 76 mm

C84	Chain with bar diameter of 84 mm
D	Diameter of line segment
DOF	Degree of freedom
DP	Dynamic positioning
E	Modulus of elasticity
F	Force matrix
f	Frequency variable
f_i	Random frequency used in the calculation of the Impulse Response Function
f_m	Parameter in the Jonswap Spectrum, frequency of maximum spectral value
G	Green's function
g	Constant of gravity
GM_T	Transverse metacentric height
H	Rotation matrix
H_S	Significant waveheight
i	Variable denoting number of frequency wave component in an irregular sea, unless specified otherwise
IRF	Impulse Response Function
j	Degree of freedom for rigid body motion, unless specified otherwise
k	Degree of freedom for force or moment, unless specified otherwise
k_0	Wave number
K_d	Controller gain for derivative controller
K_i	Controller gain for integrative controller
K_n	Seabed normal stiffness
K_p	Controller gain for proportional controller
L	Length of line segment
l	Variable denoting number of directional wave component in an irregular sea, unless specified otherwise
LF	Low frequency oscillations
M	Inertial coefficient matrix
m	Variable denoting number of a wave component in an irregular sea, unless specified otherwise
N	Number of wave components in a given sea state
n	Variable denoting number of a wave component in an irregular sea, unless specified otherwise
n_k	Unit vector normal to body

N_t Number of current time step in OrcaFlex

OCIMF Oil Companies International Marine Forum

p Hydrodynamic pressure

p Position

PID Proportional Integral Derivative (controller)

Q_d Quadratic Transfer Function for the difference-frequency load for a pair of wave components

Q_{de} Value of Quadratic Transfer Function modified for encounter effects

QTF Quadratic transfer function

RAO Response Amplitude Operator or transfer function

s Sign of $Q_{diag}(\beta, \tau)$)

s Time-lag variable used in the calculation of the Impulse Response Function

S_b Wet surface of body

$S_d(\theta)$ Directional spectrum

$S_f(f)$ Frequency wave spectrum

S_{WL} Water line area

S(f,θ) Wave spectrum

t Time variable

T_c Mean crest period between local maxima

T_e Effective linear axial stiffness

T_w Wall tension

T_z Zero-crossing period

u Velocity

U_L Vessel low-frequency velocity in the wave direction

v Velocity

v_c Current velocity

VIV Vortex Induced Vibrations

W Wire

WDL Wave Drift Load

WF Wave frequency oscillations

X_k Exciting force or moment

Contents

List of Figures

List of Tables

1 | Thruster induced roll motion

As the weather conditions on earth become more extreme the drilling process becomes more dependent on stationkeeping. Wind, waves and current induce motions which can be counteracted by mooring, dynamic positioning systems or both. Wave-frequency motions cannot be counteracted by thrusters since they do not react fast enough and because such use would cause to much wear and tear of the thrusters. The thrusters are therefore only used to counteract low-frequency forces. Due to the position of the thrusters and the relatively low hydrostatic stiffness of semisubmersibles, the thruster forces cause roll and pitch moments while counteracting the horizontal, low-frequency wave-drift forces. This is illustrated in Figure 1.1.

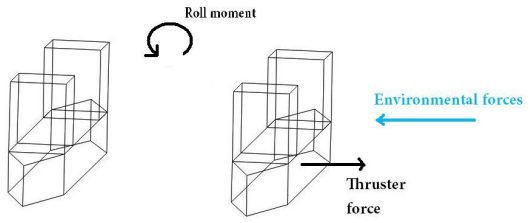

Figure 1.1: Illustration of roll moment caused by thruster forces

Semisubmersibles usually have large natural periods in roll and pitch due to the low waterplane area and may therefore oscillate with frequencies close to those of the forces and motions in the horizontal plane. The thrusters may induce large resonance motions in roll or pitch if the period of oscillation of the thrusters and the natural periods in roll or pitch coincide and have the same phase. According to Sørensen and Strand[2], the thrusters may amplify the pitch and roll motions of a semisubmersible with up to two degrees in the resonance frequency range[2]. Huse and Børresen[3] state that the thrusters may induce damping of the same order of magnitude as the viscous damping in heave, pitch and roll.

The thrusters do not necessarily increase the roll and pitch motions, provided that the phase of the thruster forces is controlled, they may even reduce them. Sørensen and Strand[2] proposed a multi-variable control law accounting for both vertical and horizontal plane motions. Their controller provided a thruster force given by

$$F_{\text{thruster}} = -\mathbf{K}_p\mathbf{e} - \mathbf{K}_d\dot{\mathbf{e}} + \mathbf{A}_{wi}\mathbf{F}_i + \mathbf{K}_i\mathbf{z} - \mathbf{K}_w\hat{\mathbf{F}}_{wind} - \mathbf{K}_{rpd}\mathbf{e}_{rot} \tag{1.1}$$

where the first, second and fourth term are the proportional, derivative and integrative terms of a horizontal PID controller, which will be described in more detail in Chapter 3.6.2. The third term is an anti-wind up term which counteracts wind-up of the integrative term and the fifth term is a wind feed forward control law counteracting the wind forces. The sixth and final term is the roll-pitch-damping term which may be written as

$$\begin{bmatrix} F_x \\ F_y \\ F_\psi \end{bmatrix} = \begin{bmatrix} 0 & g_{xq} \\ g_{yp} & 0 \\ g_{\psi p} & 0 \end{bmatrix} \cdot \begin{bmatrix} \hat{p} \\ \hat{q} \end{bmatrix} \tag{1.2}$$

where $\hat{p}$ and $\hat{q}$ are the estimated roll and pitch rates and g_{xq}, g_{yp} and $g_{\psi p}$ are their respective controller gains. For further details of Equation 1.1, the reader is referred to the paper by Sørensen and Strand[2]. Their study showed that the pitch and roll

motions could be significantly reduced by the multi-variable controller without any large increase in thruster force compared to a horizontal controller. This can be seen from the time-domain simulation with the horizontal and multi-variable controllers applied to the semisubmersible West Future, found in Figure 1.2 and Figure 1.3. The applied draught and displacement of West Future are 24 meters and 45 000 ton compared to 15.75 meters and 34 330 ton for COSL Pioneer.

A pitch-damping controller similar to that of Sørensen and Strand was applied and studied by Jenssen[4]. The pitch rate was multiplied by a controller gain, as in the second row of Equation 1.2. Jenssen discovered that a too high gain would influence the surge motion negatively and thereby increase the pitch motion. This is one example of why it is important to select the gain coefficients carefully. Jenssen[4] estimated that for a well tuned pitch controller the improvement could be as much as ten times in relative damping without any significant additional thrust.

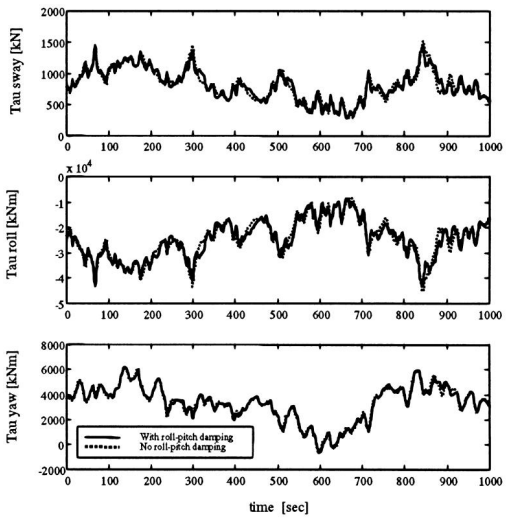

Figure 1.2: Time history of thrust components in sway, roll and yaw. Analysis and figure by Sørensen and Strand[2].

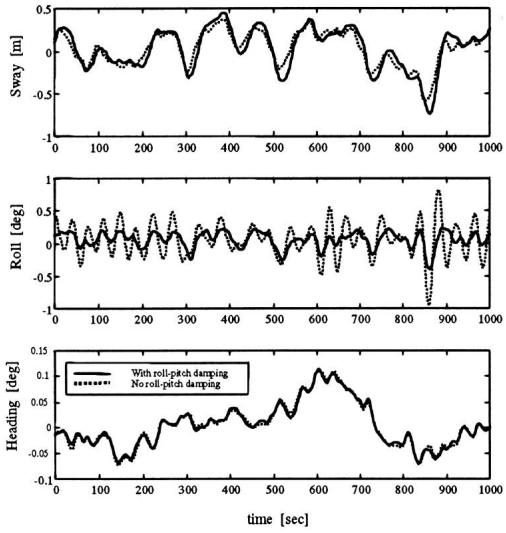

Figure 1.3: Time history of sway position, roll and yaw angles. Analysis and figure by Sørensen and Strand[2].

2 Wadam - Frequency domain analysis of hull

The potential solver Wadam was chosen to calculate the hydrostatic and hydrodynamic properties of the bare hull of COSL Pioneer. It is run by the hydrodynamic design tool and integrated program package HydroD[5]. Wadam uses first- and second-order three-dimensional potential theory to calculate the different load components acting on the body[5]. This chapter describes the input to Wadam and explains the computational choices. The complete input can be found in Appendix E.

2.1 Input of physical conditions in Wadam

The properties of the hull of COSL Pioneer were represented by a panel model and a mass model. The panel model was used to calculate hydrodynamic loads according to potential theory and the mass model was used to calculate inertia forces.

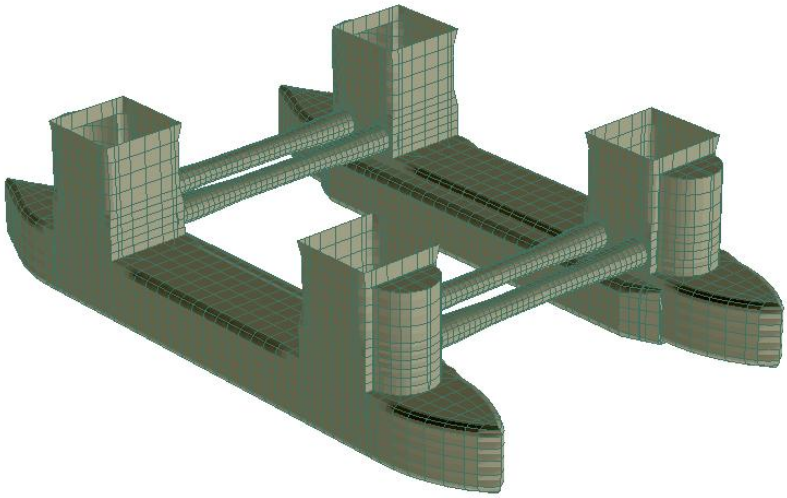

Figure 2.1: Panel Model for use in frequency-domain analysis.

Global Maritime provided the panel model and structural data such as the weight, radii of gyration and transverse metacentric height of COSL Pioneer. The panel model can be seen in Figure 2.1 and consists of 6628 panels.

Graphs of the motion transfer functions for COSL Pioneer were provided by Global Maritime and used as reference for the results from Wadam. Several analyses were performed in Wadam in order to find an estimate for the viscous damping. An additional damping in heave of five percent of the critical damping ensured that the peak value was equal to the reference peak value.

The structural data found in Table 2.1 was used as input for the mass model. The center of gravity was found by iterating until the transverse metacentric height in an even keel condition had the correct value.

Added mass and damping coefficients as well as transfer functions were computed for periods of oscillation for the incoming waves between 2.5 and 30 seconds with intervals

Mass	34 330 ton
Transverse metacentric height	2.7 m
Longitudinal center of gravity	-0.0454 m
Transverse center of gravity	0 m
Vertical center of gravity	4.87 m
Radius of gyration, roll	39.5 m
Radius of gyration, pitch	38.9 m
Radius of gyration, yaw	44.6 m

Table 2.1: Key properties of COSL Pioneer for survival condition

of 0.25-1 seconds. The exact intervals can be found in Table E.1. As the vessel is symmetric about the longitudinal axis, the transfer functions were only computed for incoming wave directions between 0-180°, with an interval of 15°. The transfer functions are presented in Chapter 6.

2.2 Computational choices in Wadam

The computational choices were based on two main aspects; accuracy of the results and running time. As the author had very little experience with the software, the following choices were made on the basis of recommendations in the Wadam User Manual [5].

To limit running time, a direct LU factorisation method was chosen for the solution of the potential theory integral equations (given in Appendix A.2.5) and the mass matrices were calculated in HydroD.

Mean-drift forces were computed by pressure integration in six degrees of freedom. Control volume calculations were also available, but disregarded since they only provide results for surge, sway and yaw. The mean-drift force coefficients would later be used by OrcaFlex in order to calculate second-order wave loads on the vessel using Newman's approximation. See Chapter 2.3.3 and Chapter 3.3- *Wave Drift Loads*, for further details on the calculations.

An analytical integration of the logarithmic singularities of the Green's functions was chosen on the background of recommendations in the Wadam User Manual[5]. Analytical integration was recommended for panel models that contain panels with large width-to-length ratio, which can be seen in the columns of the panel model in Figure 2.1. One node Gauss numerical integration was chosen for the Green's functions and its derivatives. Four node Gauss integration would yield more accurate results, but would also have significantly increased the running time of the computation.

The distance between the panel centroids are compared to a panel dimension of the user's choice. The panel dimension can either be the square of the area of the panel or the maximum diagonal, the latter being the default option which was chosen for this analysis.

2.3 Output from Wadam

The desired output from Wadam consisted of the stiffness matrix, the damping matrices, the added mass matrices, the linear load transfer function and the quadratic load transfer function. All but the restoring matrix are frequency dependent and were calculated for all prescribed frequencies of oscillation. The desired output was stored in a Wamit-formatted output file and directly imported to OrcaFlex.

This chapter summarizes how Wadam obtained the desired output for OrcaFlex as described in the Wadam User Manual[5], the Wamit User Manual[6] and Marine Hydrodynamics by Newman[7]. If the reader is not familiar with classical potential wave theory, he or she is referred to Fluid Mechanics by Frank M. White[8].

2.3.1 Restoring matrix

As the panel model only consisted of a floating hull without risers or anchor lines, the only contribution to the stiffness matrix was the hydrodynamic stiffness of the hull. The hydrostatic coefficients calculated by Wadam were calculated with the formulas given in the Wamit User Manual[6][9] which are given below.

$$C_{33} = \rho g \iint_{S_{WL}} n_3 dS \tag{2.1a}$$

$$C_{34} = \rho g \iint_{S_{WL}} y n_3 dS \tag{2.1b}$$

$$C_{35} = -\rho g \iint_{S_{WL}} x n_3 dS \tag{2.1c}$$

$$C_{44} = \rho g \iint_{S_{WL}} y^2 n_3 dS + \rho g \nabla z_b - m g z_g \tag{2.1d}$$

$$C_{45} = -\rho g \iint_{S_{WL}} x y n_3 dS \tag{2.1e}$$

$$C_{46} = -\rho g \nabla x_b + m g x_g \tag{2.1f}$$

$$C_{55} = \rho g \iint_{S_{WL}} y^2 n_3 dS + \rho g \nabla z_b - m g z_g \tag{2.1g}$$

$$C_{56} = -\rho g \nabla y_b + m g y_g \tag{2.1h}$$

ρ is the water density, g is the constant of gravity, S_{WL} is the water line area, n_3 is the normal vector in the z-direction, ∇ is the volume displacement and m is the mass of the body. Subscripts b and g denotes the center of buoyancy and the center of gravity, respectively. C_{jk} is the coefficient for the force or moment in the j'th degree of freedom due to a motion in the k'th degree of freedom.

Equation 2.2 is valid for the remaining combinations of i,j = 3..6. The restoring coefficients of the horizontal plane i,j=1,2,6 are zero.

$$C_{kj} = C_{jk} \qquad \text{except for (ij) = (46) or (56)} \tag{2.2}$$

2.3.2 Damping, added mass and linear load transfer functions

Potential theory contributions

Wadam applies first-order potential theory to calculate the potential, excitation and radiation forces and moments. The vessel is represented by a three-dimensional panel model where each panel is represented by a source with constant strength. The flow is assumed to be ideal and the velocity potential of the fluid domain thereby satisfies the Laplace equation, given below in Equation 2.3. The assumption of harmonic oscillations allows for the simplification given in Equation 2.4.

$$\nabla\Phi = 0 \tag{2.3}$$

$$\Phi = \Re(\phi e^{i\omega t}) \tag{2.4}$$

The combined free-surface condition enforces that a fluid particle on the free surface always stays on the free surface and that the pressure on the free surface is equal to the atmospheric pressure [10]. The combined free-surface condition has to be satisfied on the free surface and is given by the following equation.

$$g\frac{\partial\phi}{\partial z} - \omega^2\phi = 0 \qquad \text{on z} = 0 \tag{2.5}$$

Since the problem at hand is linear the velocity potential, ϕ, can be divided as

$$\phi = \phi_{exc} + \phi_R = \phi_0 + \phi_D + \phi_R \tag{2.6}$$

ϕ_0 is the velocity potential of the incoming wave. ϕ_D is the diffraction velocity potential due to the presence of the vessel and the reflection of the incoming waves. ϕ_{exc} is the sum of the velocity potential of the incoming wave and the diffraction velocity potential. ϕ_R is the radiation velocity potential due to the motion of the vessel and is given by Equation 2.7.

$$\phi_R = i\omega\sum_{j=1}^{6}\xi_j\varphi_j \tag{2.7}$$

In Equation 2.7, ξ is the complex amplitude of rigid body motion and j denotes the degree of freedom. Equations 2.8a and b have to be satisfied on the body in order to ensure no fluid flow through the body.

$$\frac{\partial\varphi_j}{\partial n} = n_j \tag{2.8a}$$

$$\phi_{exc} = 0 \tag{2.8b}$$

where

$$\begin{aligned}\mathbf{r} &= (x, y, z) = \text{point on the body}\\ \mathbf{n} &= (n_1, n_2, n_3) = \text{unit vector pointing normally outwards from the body}\\ \mathbf{r}\times\mathbf{n} &= (n_4, n_5, n_6)\end{aligned}$$

The global excitation and radiation velocity potentials are determined by solving the integral equations (Equation 2.9 and Equation 2.10) which are obtained by using Green's theorem with the free-surface potentials as the Green's functions. The velocity potentials are assumed to be constant over each of the panels and the given integral equations

are discretizised by the panels in the panel model in order to find the velocity potentials in the fluid domain. The integral equation for the radiation potentials is given by

$$2\pi\varphi_j(\mathbf{x}) + \iint_{S_b} \left[\varphi_j(\boldsymbol{\xi})\frac{\partial G(\boldsymbol{\xi},\mathbf{x})}{\partial n_\xi}d\boldsymbol{\xi} - n_j G(\boldsymbol{\xi},\mathbf{x})\right]d\boldsymbol{\xi} = 0 \tag{2.9}$$

The integral equation for the excitation potential is given by

$$2\pi\phi_{exc}(\mathbf{x}) + \iint_{S_b} \phi_{exc}(\boldsymbol{\xi})\frac{\partial G(\boldsymbol{\xi},\mathbf{x})}{\partial n_\xi}d\boldsymbol{\xi} = 4\pi\phi_0(\mathbf{x}) \tag{2.10}$$

A derivation of the integral equations, explanations of their components as well as how they are discretizised can be found in Appendix A. When the radiation velocity potential is found, Equation 2.11 and Equation 2.12 are used to calculate the coefficients of the frequency-dependent damping and added mass matrices.

$$B_{kj}(\omega) = -\omega\,\Im\left[\rho\iint_{S_b} n_k\varphi_j dS\right] \tag{2.11}$$

$$A_{kj}(\omega) = \Re\left[\rho\iint_{S_b} n_k\varphi_j dS\right] \tag{2.12}$$

In Equation 2.11 and Equation 2.12, S_b is the wetted surface of the body, φ_j is the radiation velocity potential components given by Equation 2.7 and n_k is the component of the normal vector pointing out of the body in the direction of the force. The exciting forces and moments are calculated by integrating the dynamic pressure of the excitation velocity potential over the wet surface of the body, as given by Equation 2.13. These forces and moments are then divided by the wave amplitude in order to find the linear load transfer function.

$$X_k = -i\omega\rho\iint_{S_b} n_k\phi_{exc}dS \tag{2.13}$$

2.3.3 Quadratic load transfer functions - mean drift forces

The second order mean-drift forces and moments are calculated by pressure integration for all six degrees of freedom. The second order hydrodynamic loads acting on the hull are calculated by integrating the Bernoulli pressure over the wetted area of the body to second order accuracy. The second order Bernoulli pressure can be written as

$$p_{\text{2nd order}} = -\rho g z - \rho\frac{\partial\phi_1}{\partial t} - \rho\cancelto{\text{zero mean contribution}}{\frac{\partial\phi_2}{\partial t}} - \frac{1}{2}\rho\nabla\phi_1\nabla\phi_1 \tag{2.14}$$

The time-average of the contribution from the second-order potential is zero and can therefore be omitted from the calculation of the mean-drift forces[11].

If $\mathbf{n} = (n_1, n_2, n_3)$ are the components of a unit vector pointing out of the body in the body fixed coordinates $\mathbf{x}$ = (x,y,z) and (n_4, n_5, n_6) are given by $\mathbf{x}\times\mathbf{n}$, then the forces and moments acting on the hull can be given by

$$\mathbf{F} = \iint_{S_b} \mathbf{n}p dS \tag{2.15}$$

where S_b is the instantaneous wetted surface of the body. In a space fixed coordinate system, the unit vector $\mathbf{N}$ is given as

$$\mathbf{N} = \mathbf{n} + \boldsymbol{\alpha} \times \mathbf{n} + \mathrm{H}\mathbf{n} \tag{2.16}$$

where $\boldsymbol{\alpha}$ is the first-order rotation vector and H is quadratic in the first-order motions. The definition of H can be found in the paper by Ogilvie [12]. The pressure on the instantaneous position on the body as stated by Lee *et. al*[11] is then given by

$$\begin{aligned} p_{\text{2nd order}} = &- \rho g(z + \xi_3 + \alpha_1 y - \alpha_2 x) - \rho\frac{\partial \phi_1}{\partial t} - \cancel{\rho\frac{\partial \phi_2}{\partial t}} \quad \text{zero mean contribution} \\ &- \frac{1}{2}\rho \boldsymbol{\nabla}\phi_1 \cdot \boldsymbol{\nabla}\phi_1 - \rho(\boldsymbol{\xi} + \boldsymbol{\alpha} \times \mathbf{x}) \cdot \boldsymbol{\nabla}\frac{\partial \phi_1}{\partial t} - \rho g H \mathbf{x} \cdot \nabla \mathbf{z} \end{aligned} \tag{2.17}$$

where $\boldsymbol{\xi}$ is the translational displacement vector. Inserting 2.16 and 2.17 into Equation 2.15 and adjusting S_b to correct for first order change in wave run up yields the representation of the forces and moments up to second order[11]. These forces and moments are divided by the square of the wave amplitude to obtain the Newman quadratic transfer function.

3 | OrcaFlex - Time-domain analysis

Time-domain analyses were performed in the program OrcaFlex, which is developed by Orcina. Hydrodynamic data for the rig was imported from Wadam, while anchor lines were modelled directly in OrcaFlex and thruster forces were calculated in a separate Python program. The riser was omitted from the analysis due to its complexity and small effect on the roll motion.

The next sections will describe the input to OrcaFlex, explain the choices made for the analysis and outline the calculation methods of OrcaFlex. A complete set of the input to OrcaFlex can be found in Appendix F.

3.1 General data

3.1.1 Coordinate systems

The coordinate systems in OrcaFlex are illustrated in Figure 3.1. The z-axes of the global and the vessel coordinate systems are directed upwards. The z-axis of the lines are directed from End A to End B, End A is fixed at the seabed and End B is connected to the Vessel.

Rotations are defined as positive when the rotation is clockwise looking in the positive direction of the axis of rotation. As an example, positive rotation around the Z-axis(Rotation 3) is rotation from the positive X-axis towards the positive Y-axis. When rotations of the vessel is performed during time-domain analyses, rotations of the Vessel is performed in the following order:

Rotation around the z-axis → Rotation around the y-axis → Rotation around the x-axis

3.1.2 Statics

The static analysis calculates the equilibrium position of the system, which is used as a starting point for the dynamic analysis[13]. The calculation of the static equilibrium position of the vessel includes hydrostatic and inertial loads of the vessel, connection loads from the mooring system, mean wave-drift loads and the constant part of wind and current loads.

OrcaFlex provides two different methods for calculation of the static equilibrium; 'Whole System Statics' and 'Separate Buoy and Line Statics'. The former calculates the equilibrium position of all the components of the model in a single iterative process. The latter applies an inner and an outer loop. The inner loop computes the static equilibrium position of the lines in the model whereas the outer computes the position of the buoys and vessels. Whole system statics was chosen because it is generally both faster and more robust[13].

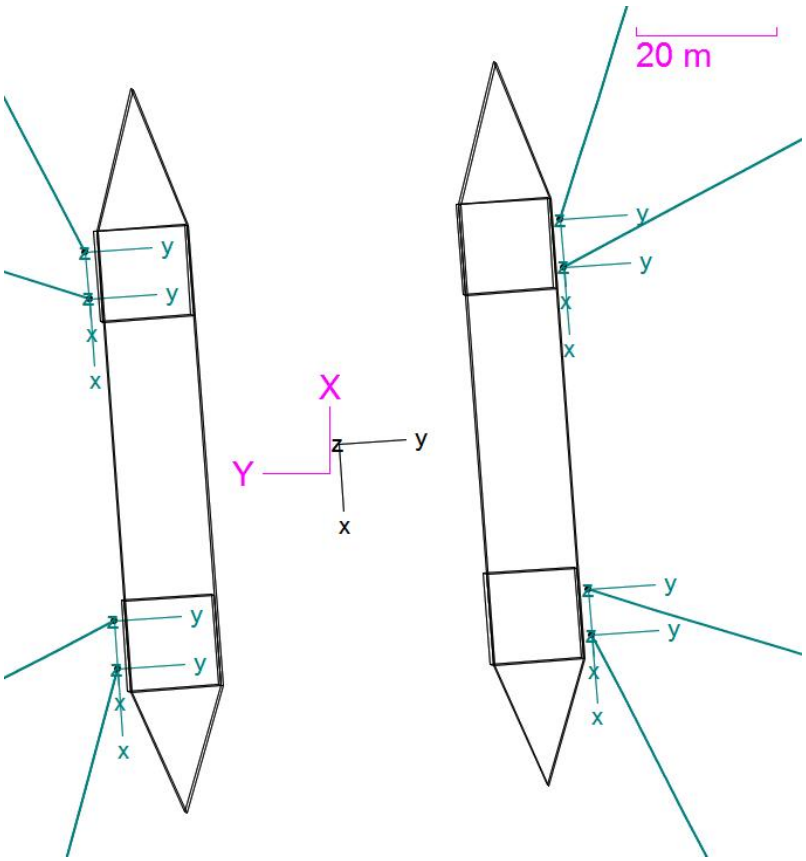

Figure 3.1: Overview of coordinate systems in OrcaFlex. The vessel is in it's equilibrium position and seen from above.

The static equilibrium is obtained by calculating the out-of-balance forces of the initial positions of the objects in the model and using the out-of-balance forces to estimate the next possible equilibrium position. This is repeated until a satisfactory accuracy, which is defined by the user, is obtained.

The statics convergence parameters, such as the maximum number of iterations and the tolerance of error, were set to default as this is normally satisfactory according to the OrcaFlex User Manual[13].

3.1.3 Dynamics

The dynamic simulation was divided into two parts; a period for build-up and a period for the simulation. The wave and system dynamics are slowly built up from zero to full level during the build-up period. The objective of the build-up is to avoid sudden transients when the simulation is started[13].

The results were saved at an interval of 0.1 second and saved with single precision, which gives about seven significant figures[13].

3.1.4 Integration and time steps

The two available integration methods in OrcaFlex are explicit Euler integration and implicit integration using the Generalised-α scheme. Both methods use the static equi-

librium position as the initial position for all objects in the model. For each time step forces and moments are calculated for all lines and bodies. The equation of motion is set up for all lines and bodies as given in Equation 3.1.

$$M(p) \cdot a = F(p, v) - B(p, V) - C(p) \tag{3.1}$$

All terms in Equation 3.1 are vectors. *M(p)·a* are the mass inertial forces and moments, *F(p,v)* are the external forces, *B(p,v)* are the damping contributions and *C(p)* are the stiffness contributions. p are the positions, v are the velocities and a are the accelerations. The equation of motion is solved at the beginning of the time step if the explicit integration scheme is used and at the end of the time step if the implicit integration scheme is used.

When implicit integration is applied, iterations have to be performed for each time-step as the position, velocity and acceleration are unknown at the end of a the time step [13]. The consequence of this is that the implicit integration is significantly more time-consuming than the explicit integration for one time-step. However, the implicit integration is typically more stable for longer time steps and is therefore often the faster choice[13]. The implicit method was chosen because it was recommended by Orcina User Support[14] on the grounds that it generally runs more efficiently.

The Generalised-α method is described in Appendix B and may be considered as a synthesis of the HHT-α and the WBZ-α methods. It is unconditionally stable and accurate to the second order[15]. High-frequency dissipation is used to damp high-frequency response while simultaneously minimizing undesired low-frequency dissipation[15]. The numerical details can be found in Appendix B.

The simulation was performed with a time-step of 0.1 second, limited to 100 iterations per time-step and equilibrium positions were measured against the default tolerance of $25{\cdot}10^{-6}$.

3.2 Environment

Weather data was provided by Global Maritime for the day and night of January 25th 2012. The data collected between 18:00 and 18:55 was chosen for the computational analysis described in this chapter.

3.2.1 Water and seabed properties

The average temperature during the chosen period was four degrees Celsius, which was used to determine the kinematic viscosity by the 1978 ITTC Performance Prediction Method [16] for sea water. The water density was assumed to be constant and as no description of the seabed was provided, the seabed was constructed as a flat surface at the given depth of 109 meters.

3.2.2 Waves

The wave elevation was generated by using an energy density spectrum to create a set of random wave components. The phases assigned to each linear wave component

are pseudo-random. A random set of phases are generated and then saved such that the same wave train can be simulated repeatedly. The energy spectrum is given by a frequency spectrum multiplied by a directional spreading spectrum as given below.

$$S(f,\theta) = S_f(f) \cdot S_d(\theta) \tag{3.2}$$

The Jonswap spectrum was the chosen frequency spectrum and is given, as by Isherwood[17], in Equation 3.3. The significant wave height, H_S, the zero crossing period, T_z and the incoming wave direction, θ_p were extracted from weather data for January 25th 2012. The parameters γ, α, σ and T_p or f_m were calculated by OrcaFlex with Equations 3.4a-f because accurate values for these parameters were not available.

$$S_f(f) = \frac{\alpha g^2}{16\pi^4} f^{-5} e^{-\frac{5}{4}(\frac{f_m}{f})^4} \gamma^b \tag{3.3}$$

The parameters in the Jonswap spectrum are given by

$$b = e^{-\frac{1}{2}\sigma^{-2}(\frac{f}{f_m}-1)^2} \tag{3.4a}$$

$$s = \frac{2\pi H_s}{g T_z^2} \tag{3.4b}$$

$$\gamma = \begin{cases} 10.54 - 1.34 s^{-1/2} - e^{-19+3.775 s^{-1/2}} & \text{for s}\geq 0.037 \\ 0.9 + e^{18.86-3.67 s^{-1/2}} & \text{for s} < 0.037 \end{cases} \tag{3.4c}$$

$$\alpha = s^2(2.964 + 0.4788\gamma^{1/2} - 0.3430\gamma + 0.04225\gamma^3/2) \tag{3.4d}$$

$$f_m = \frac{1}{T_z}(0.6063 + 0.1164\gamma^{1/2} - 0.01224\gamma) \tag{3.4e}$$

$$\sigma = \begin{cases} \sigma_A = 0.07 & \text{for } f \leq f_m \\ \sigma_B = 0.09 & \text{for } f < f_m \end{cases} \tag{3.4f}$$

Equations 3.4 d and e are only valid for $0.6 < \gamma < 8.0$ and the given σ.

The directional spectrum is given by

$$S_d(\theta) = K(q)\cos^{2q}(\theta - \theta_p) \qquad \text{for} -\pi/2 \leq \theta - \theta_p \leq \pi/2 \tag{3.5}$$

where $K(q)$ is given by

$$K(q) = \pi^{-1/2}\frac{\Gamma(q+1)}{\Gamma(q+1/2)} \tag{3.6}$$

2q is the spreading exponent, θ is the wave direction, θ_p is the principal wave direction and Γ is the Gamma function. The spreading exponent was chosen to be equal to that of another analysis in the same weather conditions performed by Global Maritime.

The minimum and maximum relative frequencies were set to their default values of 0.5 and 10 as the OrcaFlex User Manual[5] indicates that these usually provide a good representation of the continuous spectrum. This means that the integration of the spectrum will start at a frequency of $0.5 \cdot f_m$ and stop at $10 \cdot f_m$, where f_m is the frequency of the peak of the spectrum given by Equation 3.4. The wave amplitude of a wave component with a given frequency and direction is given by

$$\zeta_{il} = \sqrt{2S(\omega_i, \beta_l)\Delta\omega\Delta\beta} \tag{3.7}$$

Significant wave height, H_s	8.8 m
Zero-crossing period, T_z	9.2 s
Principal wave direction, θ_P	152°
Spreading exponent, 2q	10
Number of wave directions	9
Number of wave components per direction	100

Table 3.1: Wave data for 25.01.12 19:00-19:10

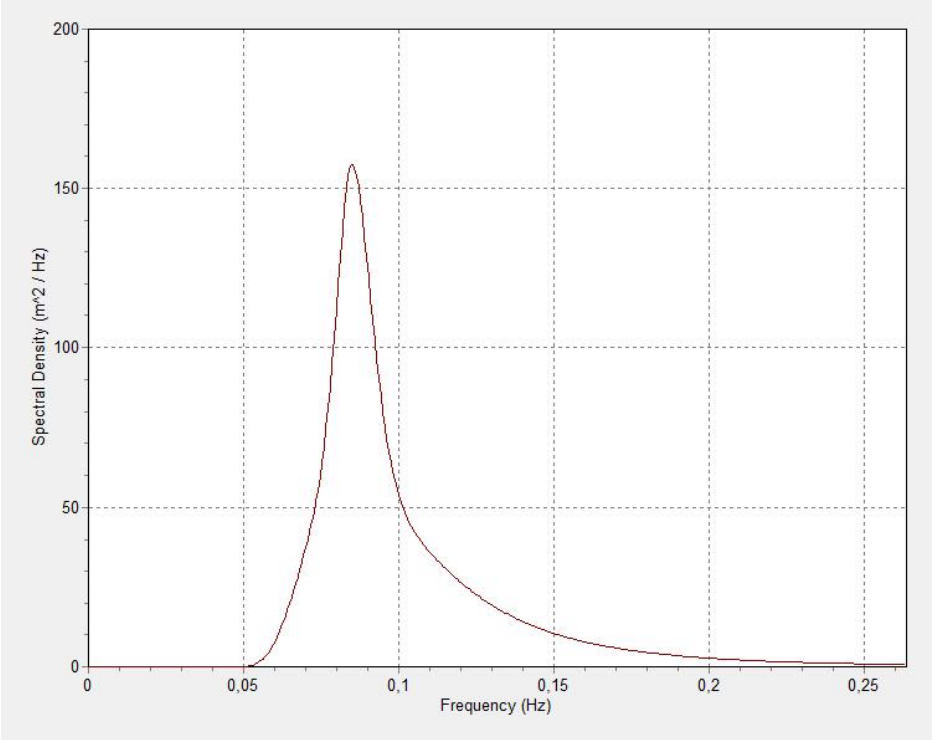

Figure 3.2: JONSWAP frequency spectrum

A summary of the wave input data can be found in Table 3.1, the frequency spectrum in Figure 3.2 and the directional spectrum in Figure 3.3.

Linear wave theory is not applicable for the calculation of the kinematics of the waves above the mean water level because it only defines the wave kinematics up to the mean free surface. OrcaFlex offers three different kinds of stretching of the wave kinematics above the mean free-surface, they are listed below and illustrated in Figure 3.4.

- **Vertical stretching:** Replaces the values for z>0 with the values at the mean water level (z=0).
- **Wheeler stretching:** Linearly stretches (wave crest) or compresses (wave trough) the values along the z-axis.
- **Extrapolation stretching:** Linearly extrapolates the tangent at the mean water level.

Several studies comparing these methods have been performed in order to determine which is the superior to the others, but the results have been inconsistent[18]. The Wheeler method seems to be working well, but may underpredict the velocities in the region around z=0 for large and steep waves[19]. Stansberg *et. al* [20] estimated that

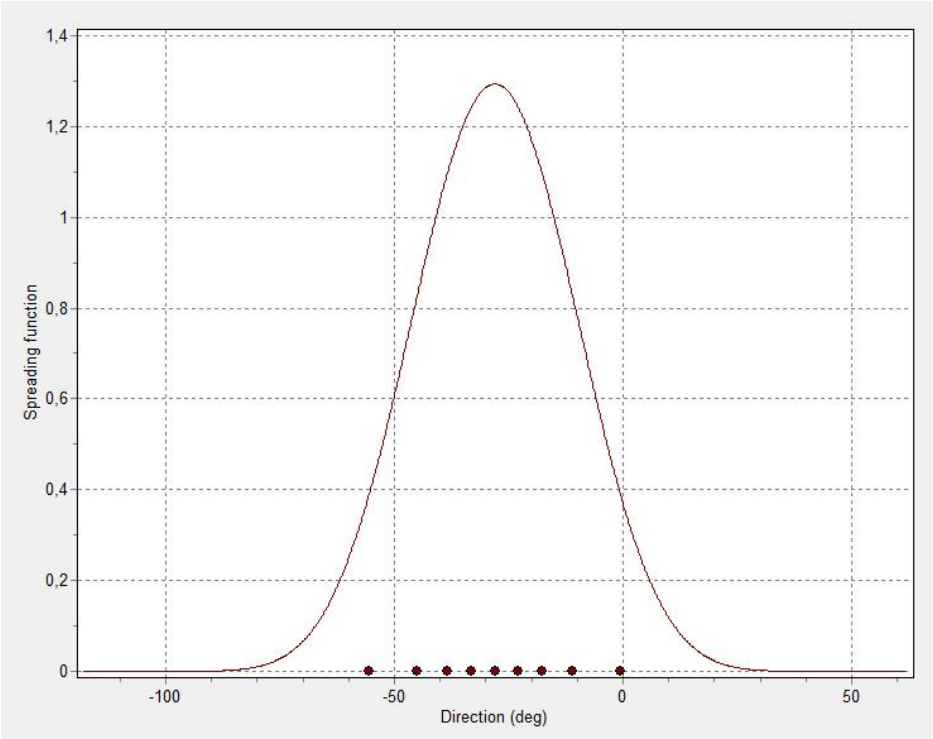

Figure 3.3: Directional spectrum. The dots represent the discretisation of the spectrum.

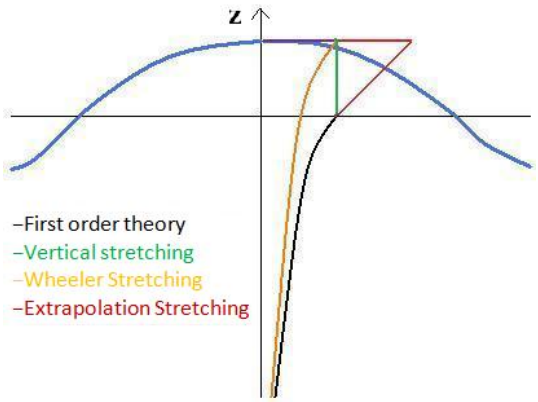

Figure 3.4: Methods for stretching of wave kinematics above the mean free-surface.

the order of magnitude of this reduction is given as

$$\frac{\Delta u}{u_0} \approx k_0 \zeta_{max} \tag{3.8}$$

where u is the horizontal velocity, k_0 is the wave number and ζ_{max} is the maximum wave elevation. According to the results of Longridge *et. al*[21], Wheeler stretching provide more accurate results than linear extrapolation.

Zhang *et. al*[18] presented a study on the three stretching methods with the objective of studying the influence of wave field characteristics. Both experimental and numerical results were used for comparison with the theoretical approximations. A regular wave was used to conceptually represent a narrow-banded spectrum and a wave train with two regular wave components was used to conceptually represent a broad-banded spectrum. Their results indicated that the Wheeler method is a better approximation for broad-banded spectra and that the linear extrapolation stretching is superior for

narrow-banded spectra[18]. As illustrated by Figure 3.2, the frequency spectrum is fairly narrow-banded, which means that according to Zhang *et. al*[18], the extrapolation stretching should be chosen.

The extrapolation stretching was chosen on the grounds of the aforementioned studies and because it is the most conservative option.

3.2.3 Current and wind

As detailed specifications were not provided, the current was defined as a constant flow with a velocity of 0.5 m/s propagating in northern direction. A power law distribution, given by Equation 3.9, was applied in order to satisfy the boundary condition of zero velocity at the seabed.

$$v_c(z) = v_{c,seabed} + (v_{c,surface} - v_{c,seabed}) \cdot \left(\frac{z - z_{seabed}}{z_{surface} - z_{seabed}} \right)^{\frac{1}{\text{exponent}}} \tag{3.9}$$

In Equation 3.9, v_c is the current velocity and 'exponent' determines the degree of the decay. The value of the exponent was not known and was determined such that it increased to 0.5 m/s rather quickly. The exponent was set to 30 and the current profile can be seen in Figure 3.5.

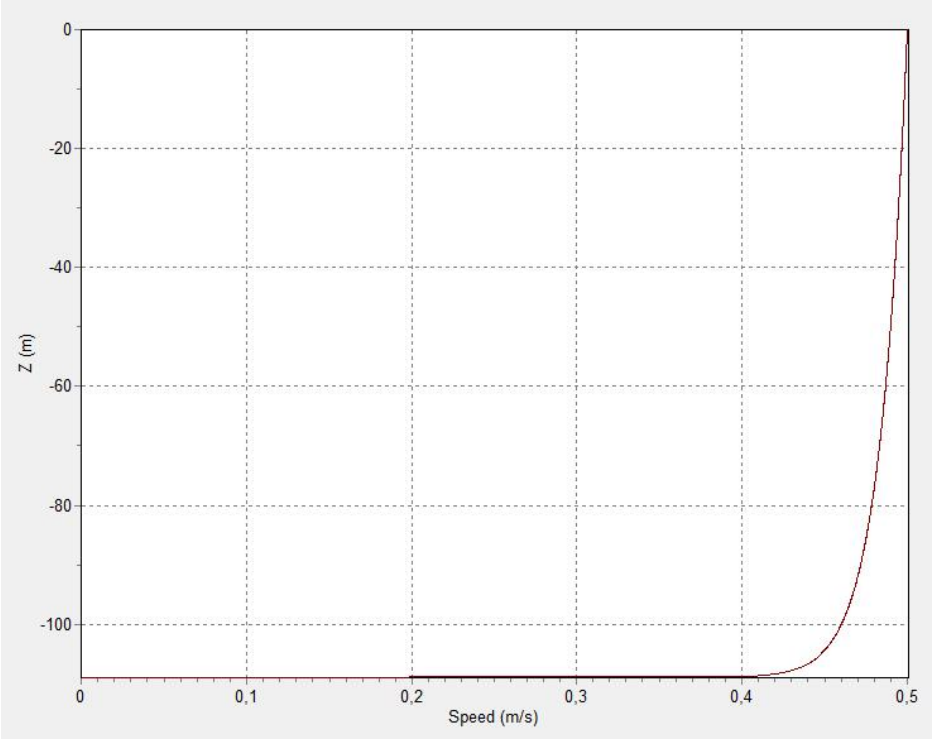

Figure 3.5: Vertical current profile

The wind velocity was determined from weather data provided by Global Maritime for the location of COSL Pioneer on January 25th 2012. The wind was modelled as constant with a velocity of 25.8 m/s with a direction of 154 degrees.

3.3 Vessel

The static equilibrium for all six degrees of freedom of the vessel was computed in an iterative process in connection with the rest of the model and was set to be the starting position for the dynamic analysis.

There are various alternatives for the calculation of the motions of the vessel. OrcaFlex provides the opportunity to superimpose two main vessel motions; Primary Motion and Superimposed Motion. As there was no reason to separate the contributions to the motion of COSLPioneer, the Superimposed Motion was set to None and the Primary Motion of the rig was calculated in six degrees of freedom.

OrcaFlex separates low-frequency motion from wave-frequency motion when computing the different loads acting on the vessel. The low- and high-frequency motions are separated by a period of oscillation given by the user, the Dividing Period. The Dividing Period should ideally be set such that all significant low-frequency contributions oscillate with periods sufficiently longer than the Dividing Period. Similarly, all significant wave-frequency contributions should oscillate with periods well below the Dividing period. As recommended by OrcaFlex User Support[14], the Dividing Period was calculated with the formula below.

$$\text{Dividing Period} = \frac{1}{{}^1\!/_2(\text{Wave Frequency} + \text{Low Frequency})} \tag{3.10}$$

The Wave Frequency was set to the frequency of the peak of the spectrum, f_m, given by Equation 3.4e and the Low Frequency was set by using the highest natural period from the decay test in OrcaFlex (anchor lines included). This method gave a Dividing Period of 25 seconds.

The included environmental forces acting on the vessel are listed below, many of which depend on the motion of the vessel. The parentheses indicate whether the forces are dependent on the low-frequency Primary Motion (LF), the wave-frequency Primary Motion (WF) or both.

- First order wave loads (LF)
- Wave drift loads (LF)
- Wave drift damping (LF)
- Added mass and damping (WF+LF)
- Current loads (LF)
- Wind loads (LF)

The loads do not necessarily depend on the primary motion directly. They may for example only be affected by the primary motion change of heading and the consequent change of incoming direction of the waves[14]. The following sections contain a description of how OrcaFlex calculate the load components listed above.

3.3.1 First order wave loads

The first order wave loads are defined by the linear load transfer functions, or Response Amplitude Operators(RAOs). The Load RAOs define the exciting force (or moment)

induced by regular waves as a function of wave amplitude, wave period of oscillation and the incoming direction of the wave. For a given sea state and a given degree of freedom, the first order wave load is given as

$$\text{First order wave load} = \sum_{i=1}^{N}\sum_{l=1}^{N} RAO_{load}(\omega_i, \beta_l)\zeta_{il}\cos(\omega_i t - \delta_i) \tag{3.11}$$

where i and l denotes the wave frequency and directional components, ζ_{il} is given by Equation 3.7 and it's spectrum, S, is given by equations number 3.2-3.5.

The Load RAOs for COSL Pioneer were calculated in Wadam and imported to OrcaFlex via Wamit output files. They may be found in Figure 6.3 and Figure 6.4.

OrcaFlex performs linear interpolation for wave frequencies and directions that do not have available RAOs. Periods shorter than the shortest period given will be found by taking the RAO to be zero at a period of zero and then performing linear interpolation between zero and the shortest period. For periods higher than the highest frequency given, the RAO is given the value equal of the RAO of the highest frequency available[13]. The OrcaFlex User Manual[13] recommends to use steps of 30° or less and steps of 15° were applied for this analysis.

3.3.2 Wave-drift loads

Wave-drift loads are second-order, difference-frequency loads calculated using Quadratic Transfer Functions (QTFs). The QTFs define the force (or moment) induced by the interaction of two regular waves with certain amplitudes, periods of oscillation and incoming directions. The force (or moment) on the vessel induced by the two wave components oscillate with the difference in frequency of oscillation between the two wave components. A wave component's interaction with itself induce a mean-drift load that is included in both the static and dynamic calculations[13].

When a Full QTF calculation is used to calculate the Wave Drift Load (WDL) in a given degree of freedom, the load is given as the sum of the contributions from the interaction of every wave component in the sea state with all the others, as given below.

$$\text{WDL} = \sum_{m=1}^{N}\sum_{n=1}^{N} \Re[Q_d(\tau_m, \tau_n, \beta_m, \beta_n)]\zeta_m\zeta_n e^{i((\omega_m-\omega_n)t-(\delta_m-\delta_n))} \tag{3.12}$$

m and n denotes the numbers of two wave components and N is the total number of wave components. The value of the QTF for a given degree of freedom and a given wave pair (components m and n) is given by

$$Q_d(\beta_m, \beta_n, \tau_m, \tau_n) = a_d(\beta_m, \beta_n, \tau_m, \tau_n)e^{-i\delta_d(\beta_m,\beta_n,\tau_m,\tau_n)} \tag{3.13}$$

where $a_d(\beta_m, \beta_n, \tau_m, \tau_n)$ is the wave drift response amplitude divided by the product of the wave amplitudes for the two wave components and $\delta_d(\beta_m, \beta_n, \tau_m, \tau_n)$ is the corresponding phase lag. The calculation of Equation 3.12 requires a double summation over all the wave components. The running time is proportional to N^2 which causes the calculations are to be very computationally expensive[13].

OrcaFlex provides the option of applying Newman's approximation method. The Newman approximation only use the diagonal of the QTF-matrices and approximate the

off-diagonal terms by averaging the diagonal terms. Newman used the arithmetic mean of the diagonal terms, whereas OrcaFlex use the geometric mean as later developed by Standing *et. al*[22]. The QTF component for a given wave pair in OrcaFlex is given by

$$Q_d(\beta_m, \beta_n, \tau_m, \tau_n) = \begin{cases} s_m \sqrt{|Q_{diag}(\beta_m, \tau_m) \cdot Q_{diag}(\beta_n, \tau_n)|} & \text{if } s_m = s_n \\ 0 & \text{if } s_m \neq s_n \end{cases} \tag{3.14}$$

where s gives the sign of $Q_{diag}(\beta, \tau))$. s has the value $+1$ if Q_{diag} is positive and -1 if it is negative. Equations 3.12 and 3.14 give the following expression for the Wave Drift Load.

$$\text{WDL} = \sum_{m=1}^{N} \sum_{n=1}^{N} \Re \left[\frac{s_m + s_n}{2} \sqrt{|Q_{diag}(\beta_m, \tau_m) \cdot Q_{diag}(\beta_n, \tau_n)|} \right] \zeta_m \zeta_n e^{i((\omega_m - \omega_n)t - (\delta_m - \delta_n))} \tag{3.15}$$

As described by Standing *et. al* [22], the wave drift load can be written as

$$\begin{aligned} \text{WDL} = \Re \Bigg[\Bigg(\sum_{m=1}^{N} \frac{s_m + s_n}{2} \sqrt{|Q_{diag}(\beta_m, \omega_m)|} \zeta_m e^{i((\omega_m - \omega_0)t - \delta_m)} \Bigg) \\ \cdot \Bigg(\sum_{n=1}^{N} \sqrt{|Q_{diag}(\beta_n, \omega_n)|} \zeta_n e^{i((\omega_n - \omega_0)t - \delta_n)} \Bigg) \Bigg] \end{aligned} \tag{3.16}$$

where m and n denotes the number of the wave components, N is the total number of wave components and ω_0 is an arbitrary frequency. The Newman approximation reduces the double summation to single summations[10]. Newman's approximation gives satisfactory results when the components of the QTFs do not have large variations with frequency and the main contribution comes from components with similar frequency[10]. Unless there is a large spread in the wave directions, the components that are far away from the diagonal (which oscillates with a larger frequency) are usually not as significant[13].

The QTFs are imported to OrcaFlex in the same way as the Load RAOs. The method using Newman's approximation was chosen because the interval of interest is oscillations with small frequencies, i.e. the components close to the diagonal, and because this reduces the running time significantly.

When Newman's approximation is applied and the diagonal value of the QTFs are used, the interpolation is performed separately for the direction and the period of oscillation. The default value is zero for infinite period and is linearly extrapolated on frequency towards zero for zero frequency (infinite period). The value for the shortest specified period is used for all shorter periods.

3.3.3 Wave-drift damping

Wave drift-damping is caused by the rapid oscillation of the waves interacting with the slow-drift motion of the vessel[23]. This type of damping can be observed by comparing free-decay tests in still water to free-decay tests in regular waves[10].

The wave-drift damping in OrcaFlex is calculated using the encounter effects approach of Molin, from Aranha's original deep water analysis with shallow water extensions, according to the results of Malenica *et al.*[24][13]. The method is outlined below and

can be found in the OrcaFlex User Manual[13]. The method uses modified QTF values that allow for encounter effects and are given by

$$Q_{de}(\beta, \beta, \tau, \tau) = A_e Q_d(\beta_e, \beta_e, \tau_e \tau_e) \tag{3.17}$$

where

$$A_e = 1 + \big(\omega \frac{\partial \alpha}{\partial \omega} - 2\big) \frac{U_L}{C_g} = \text{Aranha scaling factor} \tag{3.18a}$$

$$\alpha = \frac{C_g}{C_p} \tag{3.18b}$$

$$\beta_e = \beta + \frac{U_T}{C_g} = \text{encounter heading} \tag{3.18c}$$

$$\tau_e = \frac{2\pi}{\omega_e} = \text{encounter period} \tag{3.18d}$$

$$\omega_e = \omega\big(1 - \frac{U_L}{C_p}\big) = \text{encounter frequency} \tag{3.18e}$$

$$C_g = \frac{\partial \omega}{\partial k_0} = \text{wave group velocity} \tag{3.18f}$$

$$C_p = \frac{\omega}{k_0} = \text{wave phase velocity} \tag{3.18g}$$

k_0 is the wave number, U is the vessel low-frequency velocity at the wave drift QTF origin and L and T denote components in the longitudinal wave direction and the transverse of the wave direction, respectively.

By altering the diagonal QTF values before applying Newman's approximation method, OrcaFlex can include the effect of the time-varying wave-drift damping[13]. Both the current's effect on the wave drift load and the damping effect on the vessel's low-frequent motion are included since the velocity applied is the low-frequent velocity relative to the current. OrcaFlex only applies wave-drift damping in surge and sway[13].

3.3.4 Stiffness, added mass and damping

The restoring loads as well as the components of added mass and damping loads that are not frequency dependent are calculated as given below.

$$\mathbf{F} = -\mathbf{K}\mathbf{x} \tag{3.19}$$

$\mathbf{F}$ is an array containing the loads on the vessel in six degrees of freedom, $\mathbf{K}$ is the stiffness, damping or added-mass coefficient matrix and $\mathbf{x}$ is an array containing the offset, velocity or acceleration, respectively.

The frequency-dependent added-mass and damping forces are included by use of the method proposed by Cummins and implemented by Wicker[13]. The Impulse Response Function, IRF, is calculated and applied by the use of a convolution integral at each time-step. The convolution integral takes the previous vessel motion into account. The frequency-dependent added-mass and damping forces exerted on the vessel is given by Equation 3.20[13]. The infinite-frequency added-mass matrix is calculated and included

in the inertial matrix of the vessel. The following equations (3.20, 3.21 and 3.22) are given in the OrcaFlex User Manual[13].

$$\mathrm{F}(t) = -\mathrm{A}(\infty)a(t) + \int_0^{T_c} \mathrm{IRF}(s)v(t-s)ds \tag{3.20}$$

$\mathrm{A}(\infty)$ is the added mass for infinite-frequency approximated by Equation 3.21, a is the acceleration, T_c is the Cutoff Time (discussed at the end of the section), IRF is the Impulse Response Function given by Equation 3.22, v is the velocity, t is the current time and s is a time-lag integration variable. The IRF is assumed to be zero for time lags larger than the Cutoff Time[13]. The infinite-frequency added mass is given by

$$\mathrm{A}(\infty) = A(f_i) + \frac{1}{2\pi f_i}\int_0^{T_c} IRF(s)\sin(2\pi f_i \cdot s)ds \tag{3.21}$$

where f_i is a random frequency for which the added-mass and damping coefficients are known and the rest of the terms are the same as for Equation 3.20. The Impulse Response Function is given by

$$\mathrm{IRF}(t) = 4\int_0^{\infty} B(f)\cos(2\pi f \cdot t)df \tag{3.22}$$

The IRF matrix is calculated from the user-specified, frequency-dependent damping matrices. The damping coefficients are assumed to vary linearly between the given frequencies, go to zero at zero frequency and decay proportionally with f^{-3} for frequencies higher than the highest given frequency.

Equation 3.20 and Equation 3.21 should ideally be integrated from time zero up to infinity. However, the IRFs decay and approach zero with increasing time lag, as seen in Figure 3.6 for the roll-roll component. The IRFs for the other combinations of degrees of freedom have similar qualities. The user has to set the Cutoff Time such that all significant contributions are included. After a study of all the IRFs, the Cutoff Time was set to 100 seconds. A sensitivity analysis was performed in order to evaluate the Cutoff Time and these results are given in Chapter 4.3.4.

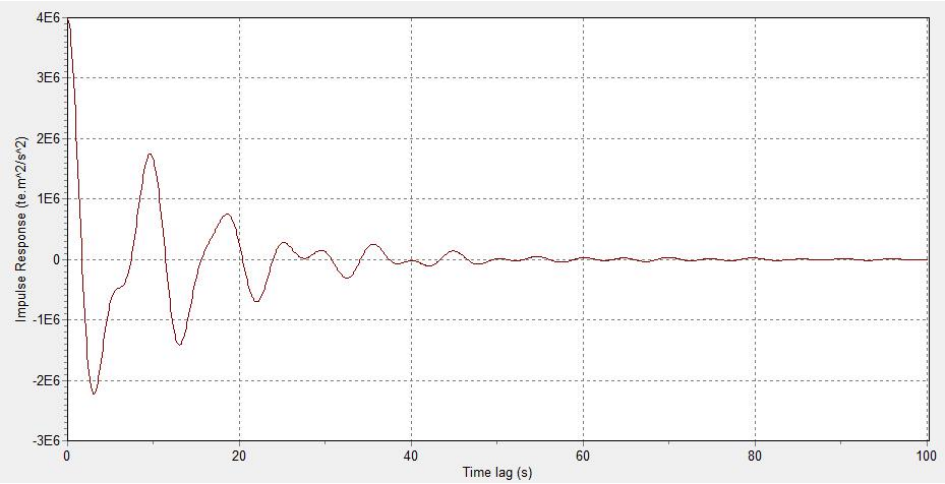

Figure 3.6: Impulse Response Function, roll-roll component.

3.3.5 Manoeuvring loads

Manoeuvring loads arise from rigid body motions in inviscid fluid and depend on the low-frequency added mass as well as the translational and rotational velocities of the vessel[13]. The manoeuvring loads are given by

$$F_1 = \sum_{j=1}^{6}[A_{2j}u_6u_j - A_{3j}u_5u_j] \tag{3.23a}$$

$$F_2 = \sum_{j=1}^{6}[A_{3j}u_4u_j - A_{1j}u_6u_j] \tag{3.23b}$$

$$F_3 = \sum_{j=1}^{6}[A_{1j}u_5u_j - A_{2j}u_4u_j] \tag{3.23c}$$

$$F_4 = \sum_{j=1}^{6}[A_{2j}u_3u_j - A_{3j}u_2u_j + A_{5j}u_6u_j - A_{6j}u_5u_j] \tag{3.23d}$$

$$F_5 = \sum_{j=1}^{6}[A_{3j}u_1u_j - A_{1j}u_3u_j + A_{6j}u_4u_j - A_{4j}u_6u_j] \tag{3.23e}$$

$$F_6 = \sum_{j=1}^{6}[A_{1j}u_2u_j - A_{2j}u_1u_j + A_{4j}u_5u_j - A_{5j}u_4u_j] \tag{3.23f}$$

where A_{ij} is the added mass coefficient and u_j is the low-frequency velocity. These manoeuvring loads are calculated with the added mass matrix for the lowest given frequency and for velocities relative to the current. OrcaFlex omits the components of the Munk moment (given in Equation 3.24) from Equation 3.23f because the current loads are explicitly calculated and are therefore already included when the current loads are calculated with the OCIMF method.

$$\text{Munk moment} = A_{11}u_2u_1 - A_{12}u_2u_2 + A_{21}u_1u_1 - A_{22}u_1u_2 \tag{3.24}$$

3.3.6 Current and wind loads

OrcaFlex uses the Oil Companies International Marine Forum (OCIMF) method for current and wind loads on a stationary vessel. This is extended in OrcaFlex by altering the current and wind velocities to account for the low-frequency primary velocity of the vessel itself and apply the relative velocity past the vessel[13]. The wind and current loads are calculated by the OCIMF formulae found in Equations 3.25 a, b and c.

$$F_{surge} = {}^1\!/_2 C_{surge}\rho v^2 A_{surge} \tag{3.25a}$$

$$F_{sway} = {}^1\!/_2 C_{sway}\rho v^2 A_{sway} \tag{3.25b}$$

$$M_{yaw} = {}^1\!/_2 C_{yaw}\rho v^2 A_{yaw} \tag{3.25c}$$

A wind-tunnel test was performed by FORCE Technology for COSL Pioneer. The current and wind load coefficients and corresponding areas were collected from these results. The load coefficients can be found in Figure 3.7 and Figure 3.8.

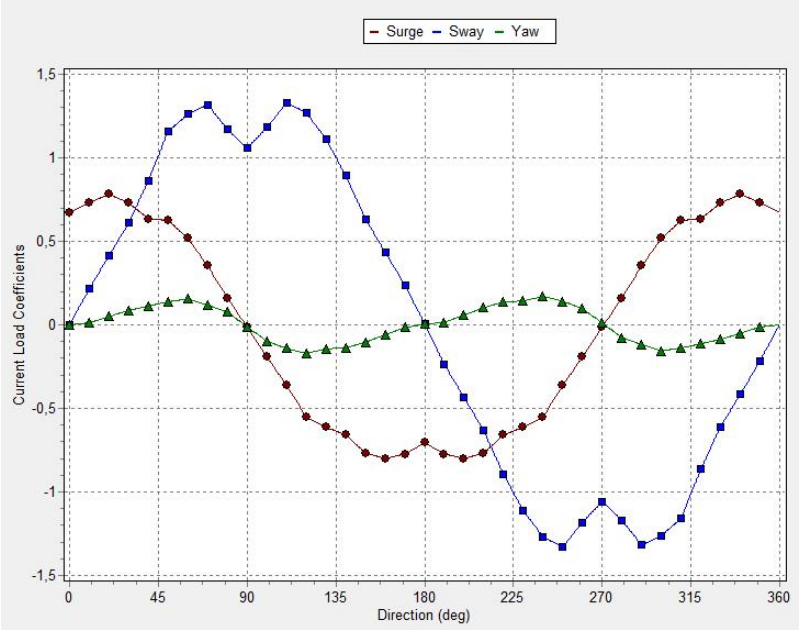

Figure 3.7: Current load coefficients from wind-tunnel test performed by FORCE Technology.

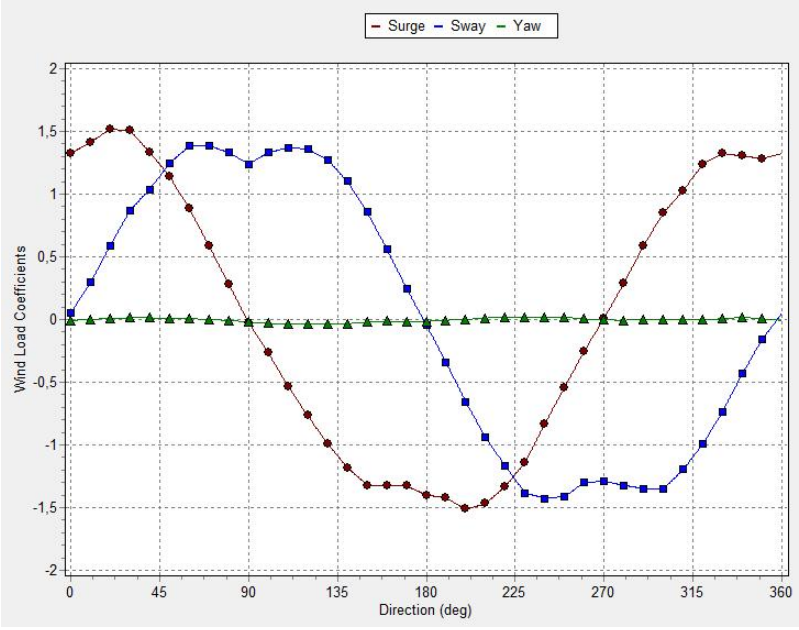

Figure 3.8: Wind load coefficients from wind-tunnel test performed by FORCE Technology.

3.4 Anchor Line System

COSL Pioneer has eight anchors and anchor lines. Eight subsurface buoys are attached to lines number 6 and 7 (see Figure 3.9) in order to provide clearance to pipelines on the sea bed.

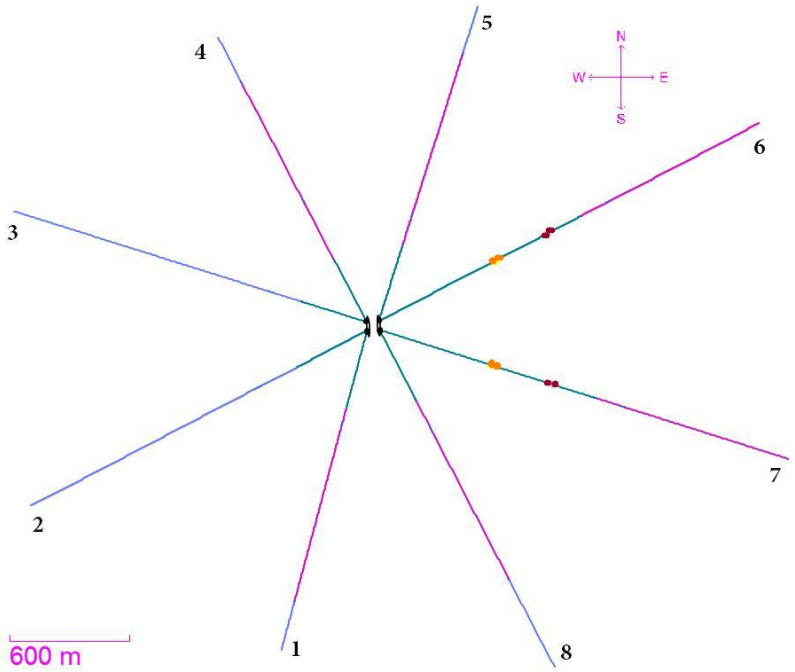

Figure 3.9: Overview of the mooring system of COSL Pioneer.

The forces on COSL Pioneer from its anchor lines were modelled using Lines in OrcaFlex. The anchor lines of COSL Pioneer are made up of two different types of chain and subsurface buoys as well as wires. The subsurface buoys are represented by OrcaFlex Attachments connected to the lines. The chain and wire properties are described in Chapter 3.4.2 whereas the buoys are described in Chapter 3.4.3. Table 3.2 describes the composition of all the lines. The complete input to OrcaFlex may be found in Appendix F.

Line 1	C84 (250 m), C76 (1013 m), W (398 m)
Line 2	C84 (500 m), C84 (1013 m), W (398 m)
Line 3	C84 (250 m), C84 (1013 m), W (350 m)
Line 4	C84 (250 m), C76 (1013 m), W (350 m)
Line 5	C84 (250 m), C76 (1013 m), W (398 m)
Line 6	C76 (1013 m), W (167 m), B10, W (20 m), B10, W (280 m), B5, W (20 m), B5, W (313 m), W (341 m)
Line 7	C76 (1013 m), W (227 m), B10, W (20 m), B10, W (280 m), B5, W (20 m), B5, W (253 m), W (341 m)
Line 8	C84 (250 m), C76 (1013 m), W (398 m)

Table 3.2: Anchor line components. The components are listed from anchor to vessel. Lengths of Line Sections are given in the parentheses. Abbreviations are explained in Table 3.3 and Table 3.4.

3.4.1 General Line properties and boundary conditions

Each line in OrcaFlex is constructed from one or several sections with a specific Line Type and attachments which are connected to specific nodes in the lines. As torsion and bending of the anchor chains and wires do not have any significant effect on the vessel motions, torsion of the lines were omitted and the end connections of the lines were set to be free to rotate. Calculation of wake effects requires significant computation[13] and were assumed to have a small influence on the results. These effects were thus disregarded. The frequencies of oscillation of Vortex Induced Vibrations (VIV) are significantly larger than the area of interest for this case and VIV were therefore ignored.

Each of the Line Sections were discretizised in to a number of segments (see description of segments in Chapter 3.4.4). The number of segments were defined by Target Segment Length. Larger variations call for a better degree of accuracy, therefore two meter target segment length was applied in the vicinity of change of line type and at seabed touchdown where the curvature of the lines are larger. Ten meter target segment length was applied for the other parts of the lines. The complete input regarding target segment lengths can be found in Table F.10 and Table F.11.

Calculation parameters regarding convergence were kept at their default values, except for Line 5 which presented convergence issues. The number of iterations was increased from default at 400 to 2000 iterations for Line 5. The default convergence parameters can be found in Table F.8.

3.4.2 Line types

Each line in the OrcaFlex model consists of one or several different Line Types. The main properties of the line types used for the anchor lines can be found in Table 3.3.

	ChainNVR4-76	**ChainNVR4-86**	**Wire(6x49WS+IWRC)**
Abbreviation	C76	C86	W
Diameter	0.076 m	0.086 m	0.090 m
Mass	0.1127 ton/m	0.1340 ton/m	0.0320 ton/m
Break load	6 003 kN	7 210 kN	7 250 kN
Axial stiffness	508 158 kN	620 973 kN	667 983 kN

Table 3.3: Anchor line types

As mentioned, the chains and the wire were assumed to have zero torsional stiffness and as the lines did not have any significant compressibility the bulk modulus was set to infinity as suggested in the OrcaFlex User Manual[13]. Some convergence problems were encountered due to slack in the lines and the bending stiffness was set to 0.1 kNm^2 as suggested by OrcaFlex User Support, this is discussed in more detail in Chapter 4.1. Structural damping of the lines was assumed to be insignificant for the vessel motions.

Drag and lift coefficients and corresponding diameters were provided by Global Maritime for the chains. The OrcaFlex Line Type Wizard was applied to obtain the drag and lift parameters for the wire as well as added mass, inertia and seabed friction coefficients for all three line types.

Line clashing was assumed not to occur and was therefore not calculated. This was beneficial since line clashing calculations significantly increase the running time for the simulation.

3.4.3 Subsurface buoys

The subsurface buoys connected to lines number 6 and 7 were modelled as Clumps in OrcaFlex. Clumps are defined by mass, volume, height, added mass and drag areas and coefficients. Accurate description of the buoys connected to COSL Pioneer were not available. The net buoyancy was given and the remaining parameters were determined by estimates. The buoys were assumed to be rectangles of quadratic cross section that had heights twice the width. The drag coefficient of the buoys was estimated to be 1.5 and the added mass coefficient to be 1. The volume was found by estimating the mass of the buoy and correcting the volume to give the right buoyancy. The main properties of the buoys can be found in Table 3.4.

	Buoy5	**Buoy10**
Abbreviation	B5	B10
Mass	0.1 ton	0.2 ton
Volume	4.97 m^3	9.94 m^3
Height	2.71 m	3.41 m

Table 3.4: Subsurface buoys

3.4.4 Theoretical background for the calculations of the line loads

Line model

The lines consist of nodes connected by segments, as can be seen in Figure 3.10. The different properties of the lines are divided between the segments and the nodes, the segments handle the axial and torsional properties while the nodes hold the other properties such as mass, weight, buoyancy and drag. The bending properties are modelled as rotational springs and dampers between the segments and the nodes as seen in Figure 3.11.

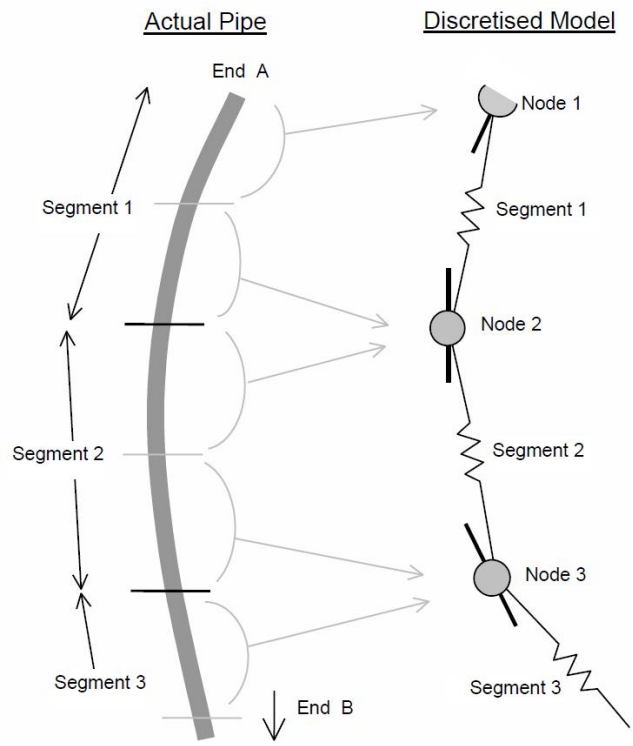

Figure 3.10: Segmentation of OrcaFlex Line. Figure by Orcina[13]

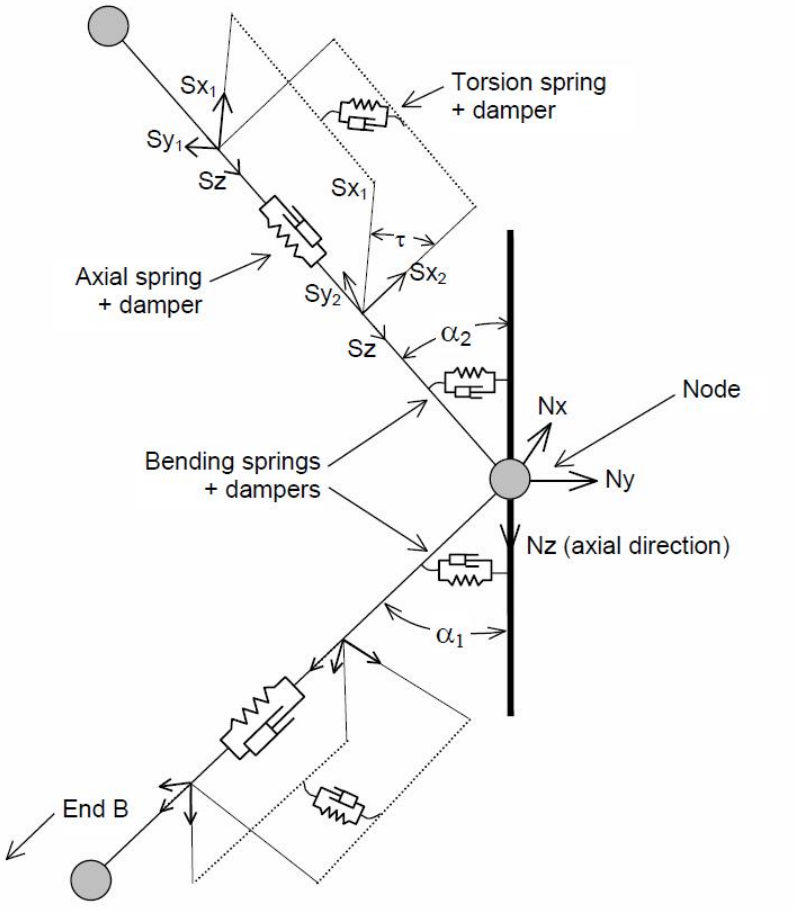

Figure 3.11: Mathematical model of a Line in OrcaFlex. Figure by Orcina[13]

Calculations

The forces and moments acting on the lines in OrcaFlex are assembled at the nodes, each node assimilates the forces from half of the segments on either side. The forces and moments on a mid-node are calculated in the following order:

Tension Forces → Bend Moments → Shear Forces → Torsion Moments → Total Load

The effective linear axial tension is given by

$$T_e = T_w + (p_o A_o - p_i A_i) \tag{3.26}$$

where p_o and p_i is the outer and inner pressure and A_o and A_i is the outer and inner cross sectional stress area. The pressure effects are small as neither the wire nor the chains have any contents (i.e. A_i=0). When implicit integration is applied, the wall tension, T_w, is given by

$$T_w = EA\varepsilon - 2\nu(p_0 A_0 - p_i A_i) \tag{3.27}$$

where E is the modulus of elasticity and ε is the mean axial strain given as

$$\varepsilon = \frac{L - \lambda L_0}{\lambda L_0} \tag{3.28}$$

where λ is the time-varying expansion factor of the segment, due to for example thermal expansion. The bending moment for linear isotropic bending stiffness is

$$M = EI|C| \tag{3.29}$$

where EI is the bending stiffness and C is the effective curvature which is given by

$$C = \frac{\alpha}{{}^1\!/_2 L_0} \tag{3.30}$$

where α is the angle between the segment axial axis and the axial direction of the line (see Figure 3.11). The shear force is given by

$$\text{Shear Force} = z \times \frac{M_2 - M_1}{L} \tag{3.31}$$

where z is the segment axial direction and M_1 and M_2 are the bending moments on either side of the segment. Drag forces acting on the lines are given by Equations 3.32a-c, which are valid for both wind and current loads.

$$F_x = P \cdot {}^1\!/_2 \rho A_x C_{d_x} V_n |V_n| \tag{3.32a}$$
$$F_y = P \cdot {}^1\!/_2 \rho A_y C_{d_y} V_n |V_n| \tag{3.32b}$$
$$F_z = P \cdot {}^1\!/_2 \rho A_z C_{d_z} V_z |V_z| \tag{3.32c}$$

where

$$A_x = D_n L$$
$$A_y = D_n L$$
$$A_z = \pi D_a L$$

P is the proportion of the line that is wet or dry, for current and wind loads, respectively. C_d is the drag coefficient, A is the projected area and V is the fluid velocity relative to the line in the normal or axial direction. The hydrodynamic lift force is given by

$$\mathbf{F}_{\text{lift}} = P \cdot |\mathbf{n}_n \times \mathbf{n}_z| \cdot 1/2 \rho D_n l C_l |V_t|^2 \mathbf{n}_l \tag{3.34}$$

where $\mathbf{n}_n$ is a unit vector in the seabed outward normal direction, $\mathbf{n}_z$ is a unit vector in the node z-direction, D_n is the normal lift diameter, C_l is the lift coefficient, V_t is the component of the relative velocity in the transverse direction $\mathbf{n}_t$ and $\mathbf{n}_l$ is a unit vector in the lift force direction given by

$$\mathbf{n}_l = \mathbf{n}_z \times \mathbf{n}_t = \mathbf{n}_z \times \left(\frac{\mathbf{n}_n \times \mathbf{n}_z}{|\mathbf{n}_n \times \mathbf{n}_z|} \right) \tag{3.35}$$

where $\mathbf{n}_t$ is the flow direction for lift purposes (normal to the line axis and in the seabed plane). The added mass of the line in a given direction is given as

$$F_{\text{added mass}} = -C_a m_{\text{fluid}} a_{\text{line}} + C_m m_{\text{fluid}} a_{\text{fluid}} \tag{3.36}$$

where C_a is the added mass coefficient for the given direction, C_m is the inertia coefficient for the given direction, m_{fluid} is the mass of the fluid displaced by the line, a_{line} is the acceleration of the line in the given direction and a_{fluid} is the acceleration of the fluid in the given direction. The first term is due to the extra inertial force due to added mass and acceleration of the line relative to the earth. The second term is caused by the accelerating fluid exerting forces on the line.

Restoring loads due to interaction with the seabed are calculated with the following formula.

$$F_{\text{reaction}} = K_n A d \tag{3.37}$$

K_n is the seabed normal stiffness, A is the area of contact and d is the depth of the penetration into the seabed. There are no seabed damping forces acting on the lines when implicit integration is applied.

Torsion forces and moments may be calculated, but these calculations are not described here as they are excluded from the analysis in this thesis. The total force and moment acting on a mid-node is finally given as the sum of the recently mentioned effects, connection loads and non-structural loads such as weight and buoyancy. The final forces and moments are used to calculate resulting translational and rotational acceleration of the node which is integrated to find the position and velocity at the next time step.

Compression

Wires and chains can support very little compression and the compression of these line types was therefore set to 'Limited' in OrcaFlex. This means that OrcaFlex issues a warning if the compression of the line exceeds the Euler load. The Euler load is given by

$$F_{\text{Euler}} = \frac{\pi^2 EI}{L_0^2} \tag{3.38}$$

EI is the bending stiffness and L_0 is the unstretched length of the element. The chains can in reality not support any compression at all and the bending stiffness is in reality zero. However, when the bending stiffness of the wires were set to zero, the analyses became unstable when the lines became slack. The bending stiffness of the chains was therefore given a small value, 0.1 kNm^2, in order to circumvent this instability issue. This is discussed further in Chapter 4.1.

3.5 Drilling riser

The drilling riser was disconnected at the Lower Marine Riser Package (LMRP) at the time of interest. The riser was connected to the rig by a flex-joint which would not transfer any significant moment to the rig. After a discussion with employees at Global Maritime it was decided to omit the riser from the time-domain analysis.

3.6 Thrusters

The thruster forces were computed in a separate program and included in the OrcaFlex time-domain analysis as Applied Loads acting on the Vessel. Only a very simple dynamic positioning (DP) system was implemented in the time-domain analysis as the information regarding the thrusters and the DP system was very limited.

3.6.1 Complete DP systems and simplifications

Dynamic positioning systems are made with many variations but they are often based on the same principles, as presented in Figure 3.12[25]. Sensors on-board the vessel use different methods to measure the position of the vessel. *Signal processing* is the reception, analysis and check of signals from the sensors. Filtering of the signals removes noise caused by the sensors and separates low-frequency and wave-frequency components[1]. Only the low-frequency motions and velocities should be counteracted by the thrusters. State estimation and wave filtering is performed by the *vessel observer*. In the case of a lost signal the vessel observer have to make predictions for the necessary signals, this situation is called dead reckoning[1]. The *controller* uses the filtered signals to calculate the necessary forces in surge, sway and the necessary yaw moment from the thrusters. This information is sent to the *thruster allocator* which uses an optimalization technique to calculate the most efficient way to distribute the forces of the thrusters[25].

Because the DP system of this thesis did not collect signals from sensors in the real world, but could obtain them directly from the time-domain simulation, signal processing and a vessel observer were not necessary. OrcaFlex could have provided the separate program with the current position in all degrees of freedom and separated between low- and high-frequency motions, which meant that filtering was not necessary either. This possibility was not used for reasons explained in Chapter 4.2.

Thruster allocation is a complex optimalization process that requires information regarding the power management system as well as detailed information about the functionality of the thrusters. The allocation algorithm should be optimised with respect to maintenance issues, fuel consumption, available power in addition to the necessary thrust[1]. This task was omitted since the necessary data was not available. The dynamic positioning system was simplified such that the required forces were calculated from the vessel's position only. The reason why the wave-frequency part of the motion was also included in the analyses is explained in Chapter 4.2. The calculated forces in the global x- and y- direction and the required moment around the global z-axis were applied at the correct draught at the center of the rig.

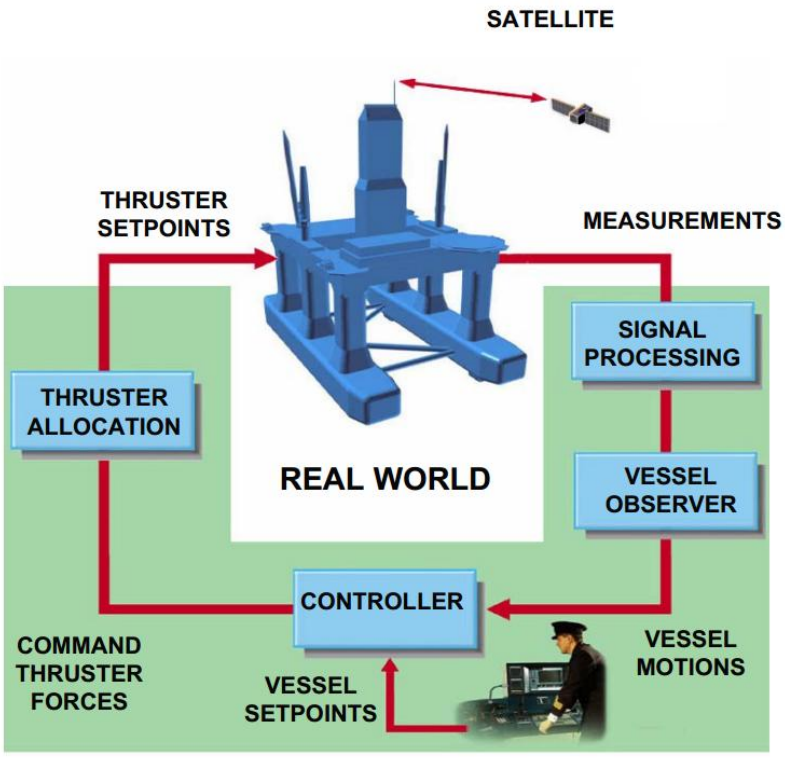

Figure 3.12: Overview dynamic positioning system. Figure by Sørensen [26]

3.6.2 PID Controller

The method which was implemented in order to calculate the necessary forces and moment was a Proportional Integral Derivative controller, commonly known as a PID controller. The PID controller was presented by Nicholas Minorsky in 1922 and was motivated by a study of how a helmsman steered a ship[1]. The offset from the desired position, the integration of the previous offset and the derivative of the offset are used as input to calculate the required corrections. A linear horizontal-plane positioning feedback controller of the PID type is given as

$$\mathbf{F_{T,k}} = -\mathbf{R_e^T K_p e} - \mathbf{K_d \tilde{v}} - \mathbf{R^T K_i z} \tag{3.39}$$

where

$$\begin{aligned}
\mathbf{x} &= [x, y, \psi]^T \\
\mathbf{z} &= \mathbf{x} - \mathbf{x}_d \\
\mathbf{v} &= \dot{\mathbf{x}} \\
\tilde{\mathbf{v}} &= \mathbf{v} - \mathbf{R}^T(\psi_d)\mathbf{x}_d \\
\mathbf{R}(\psi) &= \begin{bmatrix} \cos(\psi) & -\sin(\psi) & 0 \\ \sin(\psi) & \cos(\psi) & 0 \\ 0 & 0 & 1 \end{bmatrix} \\
\mathbf{e} &= \mathbf{R}^T(\psi_d)(\mathbf{x} - \mathbf{x}_d) \\
\mathbf{R}_e &= \mathbf{R}^T(\psi_d)R(\psi)
\end{aligned}$$

$\mathbf{x}$ is current horisontal position and heading in the global (earth-fixed) coordinate system. $\mathbf{z}$ is the integrator states and $\mathbf{x}_d$ is the desired position. $\mathbf{v}$ is the velocity and $\tilde{\mathbf{v}}$ is the velocity deviation vector, which in the current problem is equal to the velocity as

the desired velocity is zero. $\mathbf{R}(\psi)$ is the rotation matrix and $\mathbf{e}$ is the three dimensional deviation vector. $\mathbf{K}_p$, $\mathbf{K}_d$ and $\mathbf{K}_i$ are the three-dimensional non-negative controller gain matrices that need to be determined.

As a further simplification, the three degrees of freedom were considered to be uncoupled and the only forces and moments to be determined were the forces in the global x- and y- direction and the moment around the global z-axis. The force calculated by the simplified PID controller for a given degree of freedom could then be expressed as

$$F(t) = -K_p\epsilon(t) - K_i \int_0^t \epsilon(t')dt' - K_d\frac{d\epsilon(t)}{dt} \tag{3.40}$$

where *F(t)* is the control signal or the required force or moment, $\epsilon(t)$ is the difference between the current value and the set-point. K_p is the gain for the proportional controller, K_i is the gain for the integral controller and K_d is the gain for the derivative controller.

3.6.3 Implementation in OrcaFlex

The thruster forces were included in OrcaFlex as 'Applied Loads'; forces in the global x- and y-direction and a moment around the global z-axis. The Applied Loads were applied at origo in the horizontal plane at the draught of the thrusters, given in global coordinates: (0m,0m, -16.1m). These forces and moment were calculated in a separate program and incorporated in the OrcaFlex simulation via an 'External Function'.

An External Function communicates with an external program and OrcaFlex via the programming interface OrcFxAPI[27]. The External Function is defined by the name of the program, what programming language it is written in and which version of the programming language that is used as well as which functions in that program it should run. The program was the script 'PIDthruster.py', which can be found in Appendix C and was written using the programming language Python[28].

At the beginning of the simulation, OrcaFlex creates one instance of the External Function per data item that uses it. Three instances are created in this model; one for the force in the global x-direction, one for the force in the global y-direction and one for the moment around the global z-axis. The External function then collects parameters given in the External Function data form in the OrcaFlex model that will be used for the entire simulation. For each iteration of each time-step the External Function collects necessary data from the simulation, such as current low-frequency position and heading, and returns the required values, thruster forces and moments.

Mathematical discretization

The equation implemented in the python script is a discretisation of Equation 3.40, given by Equation 3.41.

$$F(n_t) = -K_p\epsilon(n_t) - K_i \sum_{n_t=0}^{N_t} \epsilon(n_t')\Delta t' - K_d\frac{\Delta\epsilon(n_t)}{\Delta t} \tag{3.41}$$

where

$$\begin{aligned}
\epsilon(n_t) &= (\text{Current Position} - \text{Desired Position}) \\
\Delta\epsilon(n_t) &= (\text{Current Error} - \text{Last Error}) \\
\Delta t' &= \Delta t = \text{Time Step} \\
n_t &= \text{Time Step number variable} \\
N_t &= \text{Current Time Step} \\
K_p &= \text{Proportional gain} \\
K_i &= \text{Integrative gain} \\
K_d &= \text{Derivative gain}
\end{aligned}$$

The three gain coefficients, K_p, K_i and K_d were initially unknown and needed to be determined for surge, sway and yaw.

Tuning of the PID controller

The proportional and derivative gains were determined by using a simplified method by Faltinsen[10] and slightly altering the method to include stiffness from the mooring system. A single degree of freedom slow-drift motion is given by

$$(M + A)\ddot{\eta} + (B + B^{DP})\dot{\eta} + (C + C^{DP}) = F^{SW} + F^{W} + F^{C} \tag{3.43}$$

where M is the mass, A is the added mass, B is the hydrodynamic damping, B^{DP} is the damping from the DP system, C is restoring force from the anchor lines, C^{DP} is the restoring force from the DP system, F^{SW} is the force from the slow-drift wave excitation force, F^{W} is the slowly-varying wind force and F^{C} is the slowly-varying current force.

For this PID controller, the set-point is constant and equal to the equilibrium position of COSL Pioneer without any environmental loads. By comparing Equation 3.40 and Equation 3.43 one can see that the proportional term of Equation 3.40 is equivalent to the restoring term, C^{DP}, of Equation 3.43 and the derivative term of Equation 3.40 is equivalent to the damping term, B^{DP}, of Equation 3.43. It is assumed that the forces on the right hand side of the equation have a zero mean. Equation 3.43 can then provide an estimate for the proportional controller by assuming harmonic motions and using the equation for the undamped natural period as shown below.

$$K_p = C^{DP} = \left(\frac{2\pi}{T_n}\right)^2 (M + A) - C \tag{3.44}$$

T_n is the natural period of the system for the given degree of freedom. As recommended by Faltinsen[10], the damping coefficient of the DP system was set to 60% of critical damping to provide an estimate for the derivative controller.

$$K_d = B^{DP} = 1.2\sqrt{(M + A)(C + C^{DP})} \tag{3.45}$$

The method by Faltinsen does not provide an equivalent for the integral gain. However, the same method for the restoring and damping forces of the PID controller is also presented by Fossen[29]. Fossen gives an estimate for the integral gain as

$$K_i = \frac{1}{T_n} K_p \tag{3.46}$$

The stiffness from the anchor lines were found by manually changing the offset in OrcaFlex and using the following equation to calculate the stiffness.

$$C = \frac{F - F_{\text{equilibrium}}}{\text{offset}} \tag{3.47}$$

This was done for several offsets in all three degrees of freedom, ranging from 1-20 meters in surge and sway and 1-20° in yaw. The final stiffness was chosen by studying the registered motions of COSL Pioneer January 25th 2012 and choosing the stiffness corresponding to the offsets of the largest registered motions. The added-mass coefficient was taken as the one for the longest period given, 30 s, and the natural periods applied were determined by decay tests in OrcaFlex(mooring system included). The results of the aforementioned work and study can be found in Table 3.5.

	Surge	**Sway**	**Yaw**
Stiffness mooring system, C	460 $^{\text{kN}}/_{\text{m}}$	520 $^{\text{kN}}/_{\text{m}}$	10 500 $^{\text{kNm}}/_{^\circ}$
Natural period, T_n	42.3 s	66.7 s	88.0 s
Proportional gain, K_p	500 $^{\text{kN}}/_{\text{m}}$	105 $^{\text{kN}}/_{\text{m}}$	488 895 $^{\text{kNm}}/_{^\circ}$
Integrative gain, K_i	12 $^{\text{kN}}/_{\text{ms}}$	1.6 $^{\text{kN}}/_{\text{ms}}$	5 556 $^{\text{kNm}}/_{\text{s}^\circ}$
Derivative gain, K_d	7 744 $^{\text{kNs}}/_{\text{m}}$	7 935 $^{\text{kNs}}/_{\text{m}}$	8 392 479 $^{\text{kNms}}/_{\text{deg}^\circ}$

Table 3.5: Results from tuning of PID controller.

Equation 3.41 and the gain coefficients found in Table 3.5 are the basis for the thruster forces that were applied via the Applied Loads setting in OrcaFlex. However, several simulations were run with and without forces from the thrusters, with different gain coefficients and one simulation was run with a harmonic load instead of the load calculated by the PID controller. The set-up for these simulations can be found in Chapter 5 and the results in Chapter 7.

4 | Computational difficulties and sensitivity studies

4.1 Convergence issues

The first simulations proved to be dynamically unstable due to slack in the downstream lines. The slack occurred because most of the environmental loads acted in the same direction; north. OrcaFlex uses the out-of-balance force in order to find the static or dynamic equilibrium for the nodes of the lines. This means that when a line goes slack, the tension goes to zero and OrcaFlex will encounter difficulties when trying to find the equilibrium position.

The instability was helped by assigning a small bending stiffness of 0.1 kNm^2 to the lines in order to avoid slack and reducing the number of segments in the lines. Line number 5 (see Figure 3.9) presented more difficulties than the other lines and the maximum number of iterations was increased for this line only.

4.2 Filtering and instability issues

Originally, the program PIDThruster used the low-frequency position of the vessel to calculate the thruster forces. The motion of the vessel was filtered by OrcaFlex into low-frequency and high-frequency motion using a second-order Butterworth filter.

The Butterworth filters are low-pass filters which are optimized in order to make the passband as flat as possible[30], see Figure 4.1 for illustration. A phase lag is introduced when the Butterworth filter is applied and its magnitude depends on the Dividing Period and the order of the filter, as seen in Figure 4.2.

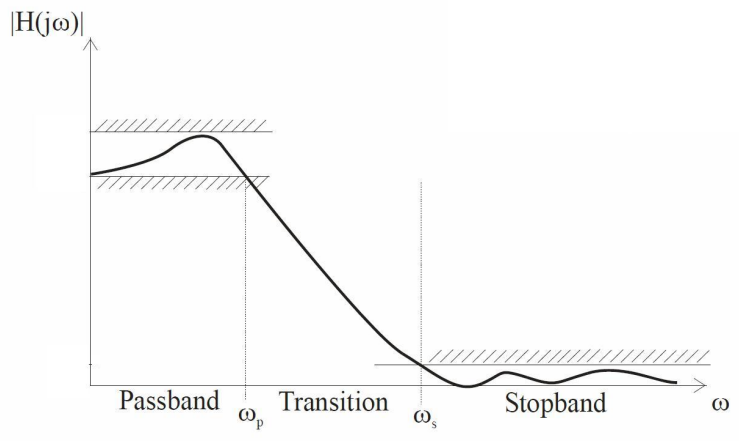

Figure 4.1: Definition of the passband of a filter. Figure from Sørensen[30]

The Dividing Period of 25 seconds (oscillation frequency equal to 0.25 rad/sec) and a second-order Butterworth filter gave a phase lag of approximately 25 degrees. The first simulations gave rise to unanticipated divergence of the motion amplitudes. This was assumed to be a result of the phase lag introduced by the filter causing the forces and

moments to be applied at the wrong time and thereby causing negative damping of the system. When the filtration of the motion that was used as input to the PID controller was removed, the increasing amplitude of the motions disappeared.

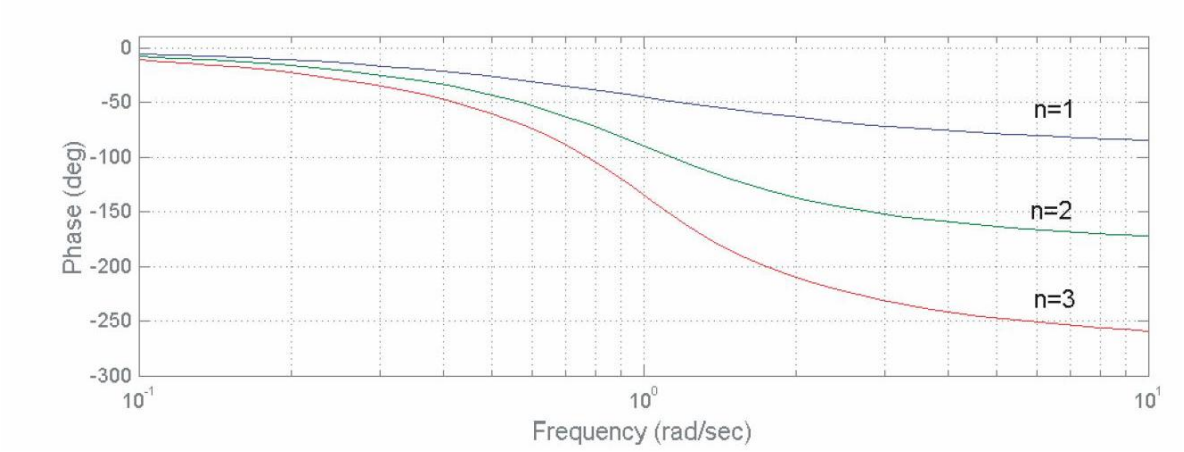

Figure 4.2: Phase lag as a function of frequency of oscillation for Butterworth filter of order n. Figure by Sørensen[30]

4.3 Sensitivity Studies

Some of the parameters set in the time-domain simulations were based on the estimate of the author and were tested to see if the estimated values could significantly influence the results of interest. The parameters tested were changed in the direction of what was assumed to yield a less stable analysis and then compared to the original simulation. A simulation with the standard settings given in Appendix F was used as reference and will henceforth be referred to as the Normal Simulation. No thruster forces were applied for the simulations in the sensitivity study.

The statistical parameters used for the sensitivity study are listed below and were compared for the motion, position and acceleration in all six degrees of freedom. These parameters will from here on be referred to as the Test Parameters.

- Mean up-crossing period, T_z, estimated as the average time between successive up-crossings of the mean value
- Mean crest period, T_c, estimated as the average time between successive local maxima
- Standard deviation, σ, given by equation 4.1
- Mean value
- Maximum value
- Minimum value

The standard deviation is given by

$$\sigma = \sqrt{\int_0^\infty S_{\text{value}}(f)df} \tag{4.1}$$

where S_{value} is the spectrum for the value of interest. In order to obtain a basis for the statistical Test Parameters, the simulations had a duration of 20 minutes. The difference between the Normal Simulation and the test simulations for the Test Parameters was studied with an accuracy of one percent.

4.3.1 Bending stiffness of the lines

A sensitivity test was performed for the bending stiffness of the lines because, as mentioned in Chapter 3.4.1 and Chapter 4.1, the lines were given a non-physical bending stiffness. The test simulation applied a bending stiffness of 0.02 kNm^2, which was twice the value of the bending stiffness for the Normal Simulation.

The change of bending stiffness did not result in any difference of the Test Parameters with the given degree of accuracy and was therefore assumed not to affect the results.

4.3.2 Length of segments in the anchor lines

The second test simulation was performed with altered target segment lengths for all the anchor lines (see Chapter 3.4.1 for explanation of target segment length). The target segments lengths were increased from ten to twelve meters or from two to three meters. Sections and segment lengths are described in Chapter 3.4.1 and the complete set-up for the Normal Simulation is found in Table F.10 and Table F.11.

The alteration of the of the target segment lengths did not cause any variation of the Test Parameters for motions and velocities and only small variations of 1-2% were registered for the accelerations. On the basis of these results, the target segment lengths were assumed not to have any significant effect on the motions, velocities and accelerations of the Vessel for this analysis.

4.3.3 Time Step

In order to test the sensitivity of the time step in the simulation, it was increased from 0.1 s to 0.15 s. This change presented no variation of the Test Parameters for the motions and only small variations of 1-2% was observed for heave and pitch velocities. There was differences of up to 21% for the accelerations, but when accelerations of less than 0.1 m/s^2 and 0.1 deg/s^2 were omitted, the results did not show any significant percentual change. The time step of 0.1 second was assumed to give a sufficient degree of accuracy for the analysis.

4.3.4 Cutoff Time

The use of the Cutoff Time is described at the end of Chapter 3.3.4. It was set to 100 seconds in the Normal Simulation and reduced to 80 seconds for the sensitivity study. This rather large change in Cutoff Time did not present any variation in the Test Parameters for the motions. A 5% difference in the mean vertical velocity was registered, but this was assumed to be insignificant since the absolute value was less than 0.1 m/s. Only small variations of 1-2% were observed for the accelerations with absolute values larger than 0.1 m/s^2 and 0.1 deg/s^2.

On the basis of the study of the Impulse Response Functions(see Chapter 3.3.4) and this sensitivity analysis, the Cutoff Time of 100 seconds was deemed to be sufficiently high.

4.3.5 Dividing Period

As described in Chapter 3.3 and Chapter 4.2, the Dividing Period separates the low- and high- frequency responses. The Dividing Period was set to 25 seconds in the Normal Simulation and was tested by changing it to 18 and 35 seconds.

Change of Dividing Period yielded larger differences in the Test Parameters than for the other tests. Test Parameters of absolute value of less than 0.1 (s, m, deg, m/s, deg/sec, m/s^2 or deg/sec^2) are not included in the discussion below.

For the Dividing Period of 18 seconds, the roll and pitch motions showed the largest deviations with approximately 10% in the standard deviation, 10-15% in the up-crossing period and 4-42% difference for the maximum and minimum values measured. The differences for the Dividing Period of 35 seconds were smaller, but still of significance. The maximum and minimum values in roll and pitch showed differences of 2-25%, but all of the other parameters varied with 5% or less.

These results show that the Dividing Period may have a significant impact on the results and especially the most important parameter for this thesis; the roll motion.

A period of 18 seconds corresponds to a frequency of 0.056 Hz, a period of 35 seconds corresponds to a frequency of 0.029 Hz and a period of 25 seconds corresponds to a frequency of 0.04 Hz. The energy of the spectrum located at these frequency ranges can be evaluated by considering the wave spectrum in Figure 3.2.

As mentioned at the end of Chapter 3.2.2, the integration of the spectrum of COSL Pioneer starts at a frequency of 0.042 Hz (see Chapter 3.2.2). This implies that responses oscillating with frequencies less than this will be excluded. In other words, a frequency of 35 seconds define all responses as wave frequency responses. When all motion is regarded as wave-frequency motion, the loads listed below will not be dependent on the motion of the vessel (as described in Chapter 3.3) but only on the environmental loads.

- First order wave loads
- Wave drift loads
- Wave drift damping
- Current loads
- Wind loads

The sensitivity test did not clarify whether the Dividing Period is accurate nor whether it is too small or too large. The original value of 25 seconds was applied for the analyses, but the effect of the Dividing Period should be taken into consideration when the results are evaluated.

5 | Set-up of simulations in OrcaFlex

5.1 Static analysis

The calculation method for the static analysis is described in Chapter 3.1.2 and the input to the OrcaFlex model is found in Appendix F. The starting point for the static analysis was at the origin with zero heel and trim at a heading of -175 degrees.

5.2 Decay test

In order to find the natural periods of COSL Pioneer while including all the effects such as hydrodynamic damping and stiffness from the anchor lines, a decay test was performed in OrcaFlex. The dynamic simulation was started with the Vessel in non-equilibrium position in all degrees of freedom and the time-domain simulation was run without any waves, wind or current present. The natural periods were taken as the mean up-crossing periods for the motions of the simulation.

5.3 Set-up of time-domain simulations

As mentioned, the time-domain simulations are based on the input described in appendix F. The programs that were used to calculate the thruster forces, *PIDthruster.py* and *harmonicThruster.py*, can be found in Appendix C and Appendix D and a description of their implementation in OrcaFlex is given in Chapter 3.6.3. All simulations had a duration of 20 minutes and had the same settings with regard to the environment, mooring system and inertial and hydrodynamic properties of the hull.

The only input that was varied for the simulations was the Applied Loads (the thruster forces). All the simulations are briefly listed below and the complete input to the External Function can be found in Table 5.1. The name of the simulations are listed in bold text and are followed by a description of the thruster forces that were included as Applied Loads. The programs and parameters used in the calculation of the thruster forces can be found in Table 5.1.

- **noThruster:** No forces from thrusters were included.
- **normalThruster:** Loads from the thrusters were calculated with the program PIDthruster. The controller gains are given in Table 3.5 and the set-points in the global x- and y- directions and rotation about the global z-axis may be found in the 'Still Water' column in Table 7.1.
- **lowGainsThruster:** Loads from the thrusters were calculated as for normalThruster, but with 50% lower controller gains.
- **highGainsThruster:** Loads from the thrusters were calculated as for normalThruster, but with 50% higher controller gains.

- **statNormalThruster:** Loads from the thrusters were calculated as for normalThruster with the inclusion of static loads that counteracted the mean-drift forces, constant current forces and constant wind forces.
- **harmonicThruster:** Loads from the thrusters applied in the global x-direction and moment around the global z-axis were calculated as for normalThruster. The load applied in the global y-direction was a harmonic load of amplitude 3000 kN oscillating with a period equal to the mean up-crossing period for the roll motion from the simulation normalThruster.

Simulation	**Global X-force**	**Global Y-force**	**Global Z-moment**
noThruster	None	None	None
normalThruster	PIDtruster: target1 = 0.153 m kp1 = 500 $^{kN}/_{m}$ ki1 = 12 $^{kN}/_{ms}$ kd1 = 7744 $^{kNs}/_{m}$ stat1 = 0 kN	PIDtruster: target2 = -2.2473 m kp2 = 105 $^{kN}/_{m}$ ki2 = 1.6 $^{kN}/_{ms}$ kd2 = 7935 $^{kNs}/_{m}$ stat2 = 0 kN	PIDtruster: target6 = -174.7363 ° kp6 = 488895 $^{kNm}/_{°}$ ki6 = 5556 $^{kNm}/_{°s}$ kd6 = 8392479 $^{kNms}/_{°}$ stat6 = 0 kNm
statNormalThruster	PIDtruster: target1 = 0.153 m kp1 = 500 $^{kN}/_{m}$ ki1 = 12 $^{kN}/_{ms}$ kd1 = 7744 $^{kNs}/_{m}$ stat1 = 1875 kN	PIDtruster: target2 = -2.2473 m kp2 = 105 $^{kN}/_{m}$ ki2 = 1.6 $^{kN}/_{ms}$ kd2 = 7935 $^{kNs}/_{m}$ stat2 = 535 kN	PIDtruster: target6 = -174.7363 ° kp6 = 488895 $^{kNm}/_{°}$ ki6 = 5556 $^{kNm}/_{°s}$ kd6 = 8392479 $^{kNms}/_{°}$ stat6 = -12820 kNm
lowGainsThruster	PIDtruster: target1 = 0.153 m kp1 = 250 $^{kN}/_{m}$ ki1 = 6 $^{kN}/_{ms}$ kd1 = 3872 $^{kNs}/_{m}$ stat1 = 0 kN	PIDtruster: target2 = -2.2473 m kp2 = 53 $^{kN}/_{m}$ ki2 = 0.8 $^{kN}/_{ms}$ kd2 = 3968 $^{kNs}/_{m}$ stat2 = 0 kN	PIDtruster: target6 = -174.7363 ° kp6 = 244298 $^{kNm}/_{°}$ ki6 = 2778 $^{kNm}/_{°s}$ kd6 = 4196240 $^{kNms}/_{°}$ stat6 = 0 kNm
highGainsThruster	PIDtruster: target1 = 0.153 m kp1 = 750 $^{kN}/_{m}$ ki1 = 18 $^{kN}/_{ms}$ kd1 = 11616 $^{kNs}/_{m}$ stat1 = 0 kN	PIDtruster: target2 = -2.2473 m kp2 = 157.5 $^{kN}/_{m}$ ki2 = 2.4 $^{kN}/_{ms}$ kd2 = 11903 $^{kNs}/_{m}$ stat2 = 0 kN	PIDtruster: target6 = -174.7363 ° kp6 = 733343 $^{kNm}/_{°}$ ki6 = 8334 $^{kNm}/_{°s}$ kd6 = 12588719 $^{kNms}/_{°}$ stat6 = 0 kNm
harmonicThruster	PIDtruster: target1 = 0.153 m kp1 = 500 $^{kN}/_{m}$ ki1 = 12 $^{kN}/_{ms}$ kd1 = 7744 $^{kNs}/_{m}$ stat1 = 0 kN	harmonicTruster: amp = 3000 kN	PIDtruster: target6 = -174.7363 ° kp6 = 488895 $^{kNm}/_{°}$ ki6 = 5556 $^{kNm}/_{°s}$ kd6 = 8392479 $^{kNms}/_{°}$ stat6 = 0 kNm

Table 5.1: Input to Applied Loads (External Function) which calculates the thruster forces in the OrcaFlex time-domain simulations. The input consist of the name of external function and the parameters defined on the External Function data form.

6 | Results from frequency-domain analysis in Wadam

The hydrodynamic stiffness calculated in Wadam can be found in Table 6.1. The damping and added mass matrices are not presented in this chapter because they contain a large amount of data, but they can be found in the OrcaFlex-file in the electronic attachment.

	Heave	Roll	Pitch
Heave	8319.37 kN/m	-0.01878 kNm/m	-0.8063 kNm/m
Roll	-0.01878 kN/°	908.374E3 kNm/°	0.920185 kNm/°
Pitch	-0.8063 kN/°	0.920185 kNm/°	1.94314E6 kNm/°

Table 6.1: Hydrostatic stiffness calculated in Wadam.

The principal incoming direction of the waves in the vessel local coordinate system is 33°. The transfer functions were not calculated for all degrees, but OrcaFlex interpolated to obtain the missing components. The transfer functions are shown for an incoming direction of 30°, which was the closest of the incoming directions for which the transfer functions were calculated in Wadam.

6.1 Motion transfer functions

The motion transfer functions were calculated in Wadam and provide the motion response of COSL Pioneer as if it were freely floating without any loads from thrusters or anchor lines. The linear motion transfer functions are included here as a reference to the reader in order to provide an understanding of the motion characteristics of COSL Pioneer.

As can be seen by the Figure 6.1, there are two cancellations for the heave RAO, the first is caused by phase difference between the pontoons and the second is caused by a cancellation period.

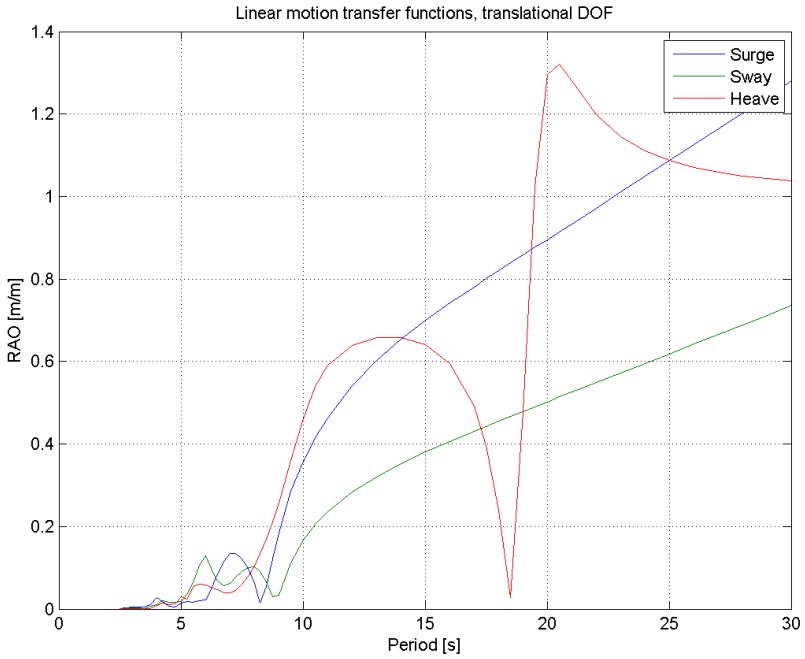

Figure 6.1: Motion transfer functions, translational DOF.

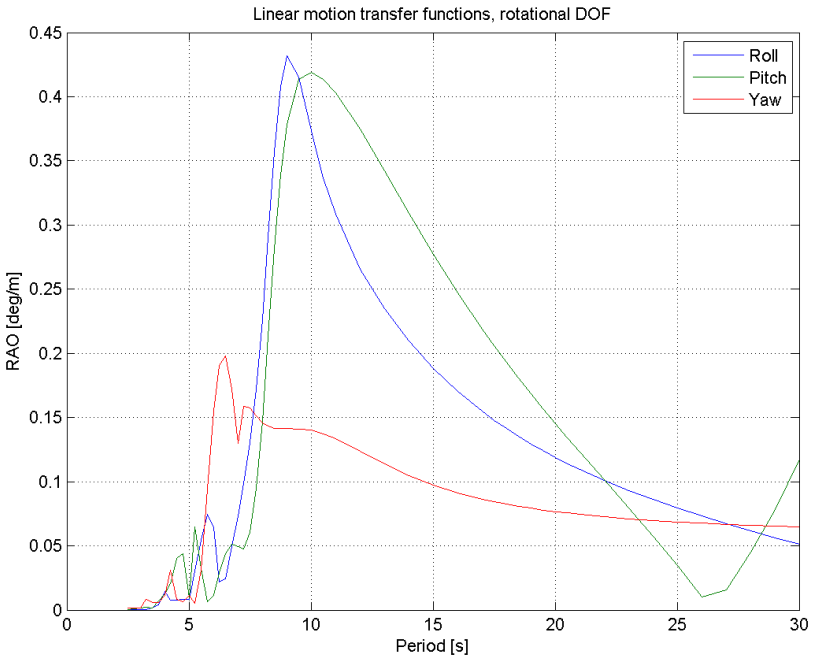

Figure 6.2: Motion transfer functions, rotational DOF.

6.2 Linear load transfer function

The load transfer functions calculated in Wadam were imported to OrcaFlex and are shown in Figure 6.3 and Figure 6.4. All degrees of freedom have their peaks in an area of the Jonswap spectrum with significant energy, see Figure 3.2.

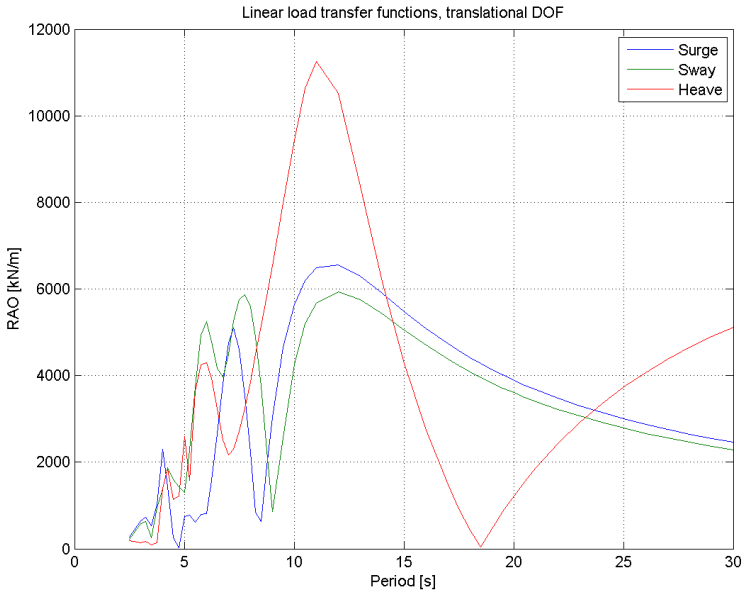

Figure 6.3: Load transfer functions, translational DOF.

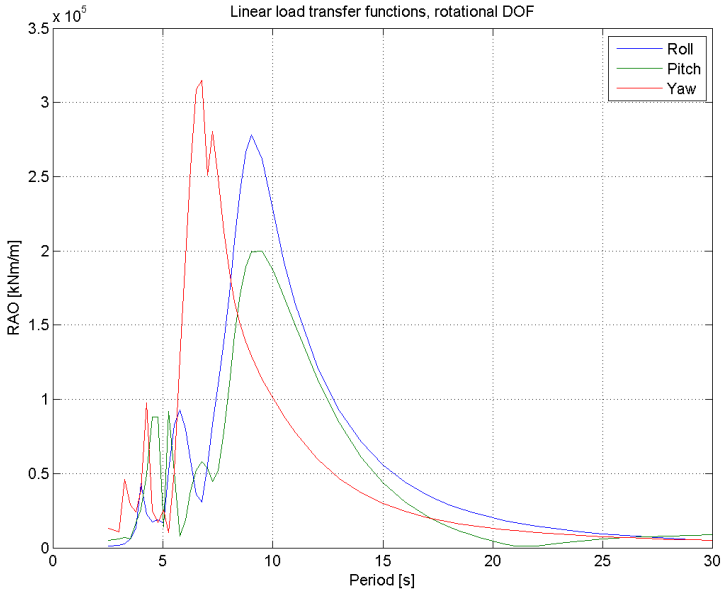

Figure 6.4: Load transfer functions, rotational DOF.

6.3 Quadratic load transfer functions

As can be seen by Figure 6.5, Figure 6.7 and Figure 6.8, there are larger variations for the second-order quadratic load transfer functions than for the linear motion and load transfer functions. As the author did not have any experience with quadratic load transfer functions, they were compared to other studies of wave drift forces on semisubmersibles to see if they were reasonable. The accuracy of the quadratic load transfer functions could be of large significance if second-order wave loads are the reason for the excessive slowly-varying roll motions. The quadratic load transfer functions were compared to the work by Hong *et. al*[31], Hermans[32] and Schellin and Kirsch[33].

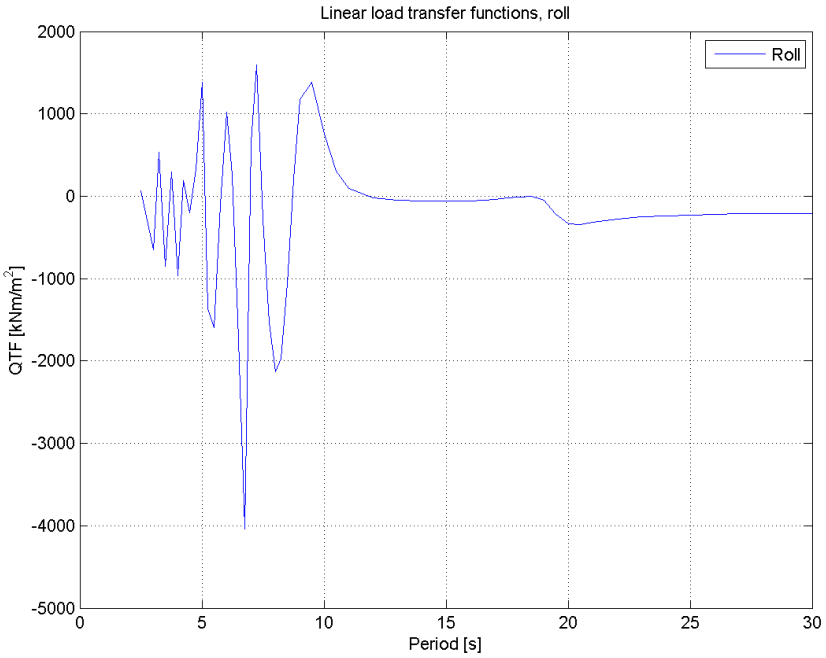

Figure 6.5: Wave drift transfer functions, roll.

The roll quadratic transfer function (QTF) found in Figure 6.5 was compared to the work of Hong *et. al*[31]. Note that the graphs by Hong are plotted against frequency and not period. The roll QTF calculated in Wadam is more jagged than the QTF calculated by Hong *et. al*, found in Figure 6.6, and the absolute value of the peak for a period of seven seconds is 73% smaller. It is not the same semisubmersible, but the difference in displacement is only 10% and the difference in draught only 9%.

The surge and sway QTFs found in Figure 6.7 are similar to the ones calculated by Schellin and Kirsch[33] and Hermans[32], but like the roll QTF they are more jagged.

The work by Hong *et. al*[31] and Voogt and Soles[34] show that the roll wave drift forces are strongly dependent on the heel angle of the semisubmersible. This effect is not included in the current analysis as the wave drift forces are calulated in an even keel condition, but should be taken into consideration if the Vessel should experience a mean heel angle.

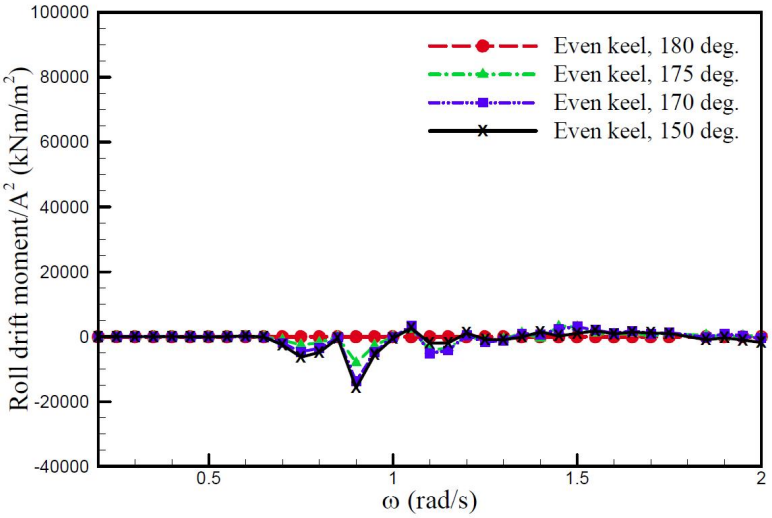

Figure 6.6: Wave drift transfer functions in roll for comparison. Figure by Hong *et. al.*

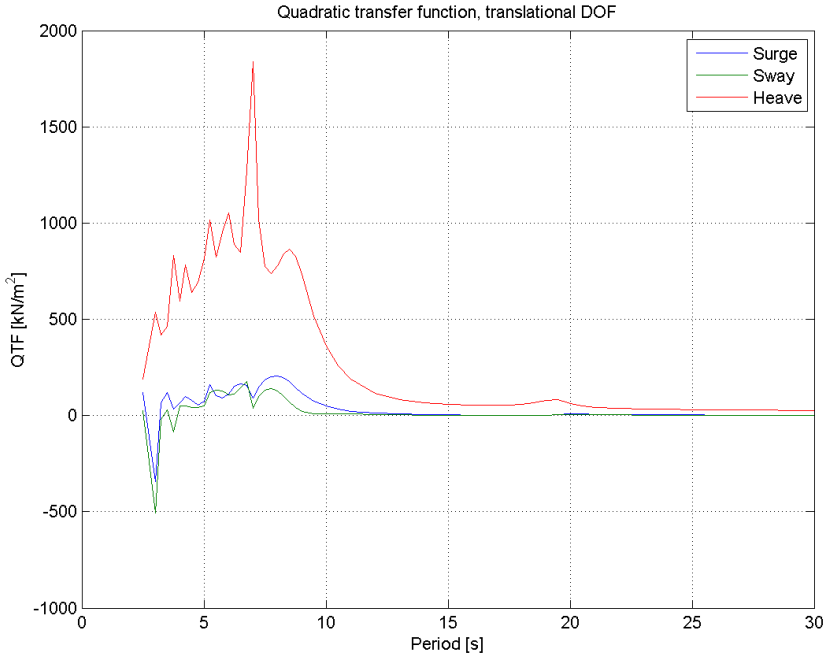

Figure 6.7: Wave drift transfer functions, translational DOF.

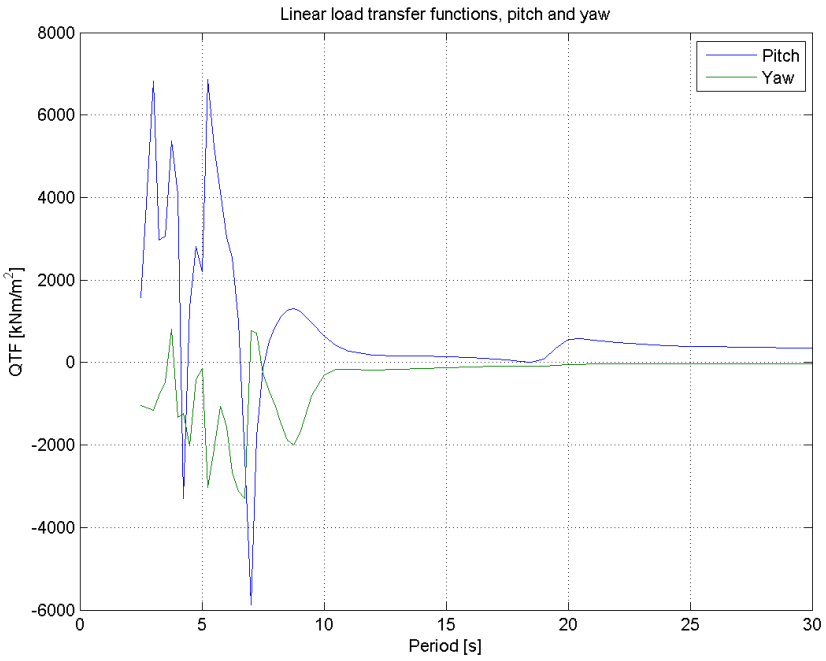

Figure 6.8: Wave drift transfer functions, pitch and yaw.

7 | Results from analyses in OrcaFlex

7.1 Static analysis

The set-up for the static analysis is described in Chapter 5.1. The final equilibrium position in still water can be found in the left column of Table 7.1 and was used as the set-point for the thrusters.

The static equilibrium was also calculated with the inclusion of mean-drift forces, constant current loads and constant wind loads and is given in right column in Table 7.1. This equilibrium position was used as the starting point for the dynamic analysis.

	Still water equilibrium	**Included constant wave, wind and current forces**
X - position	0.25 m	4.13 m
Y - position	-2.26 m	-1.35 m
Z - position	-0.20 m	0.19 m
X - rotation	0.63°	1.33°
Y - rotation	-0.02°	-0.57°
Z - rotation	-174.6°	-175.6°

Table 7.1: Static equilibrium position for COSL Pioneer, calculated both in still water and with the inclusion of mean-drift forces and constant wind- and current forces.

7.2 Decay test

A description of the decay test can be found in Chapter 5.2. The objective of the decay test was to find the natural periods of COSL Pioneer with the effects of anchor lines included. The results were used to determine the Dividing Period and the gain coefficients of the PID controller, as described in Chapter 3.3 and Chapter 3.6.3. The mean up-crossing period from the 20 minute simulation can be found in Table 7.2.

	Mean up-crossing period
Surge	46.2 s
Sway	68.4 s
Heave	19.4 s
Roll	52.6 s
Pitch	37.1 s
Yaw	88.1 s

Table 7.2: Results from decay test in OrcaFlex

7.3 Comparison of time-domain simulations in OrcaFlex

The time-domain results are computed with the input found in appendix F unless specified otherwise. The set-up for the different time-domain simulations can be found in Chapter 5.3. Sources of error will be discussed in Chapter 8.1.

It should be noted that the mean, maximum and minimum values discussed in this chapter are not the absolute mean values relative to the global origin, but mean values given relative to the set-point for the thrusters in the global coordinate system. The set-point for the thrusters is given in the 'Still Water' column in Table 7.1. The thruster forces (Applied Loads) are given in the local coordinate system of the vessel which is rotated approximately -175°about the global z- axis, as can be seen in Figure 3.1. The rotations around the global x-,y- and z-axes will be referred to as Rotation 1, Rotation 2 and Rotation 3, respectively.

All of the Test Parameters studied during the sensitivity studies are listed in Chapter 4.3 and were also used for the evaluation of the time-domain simulations. The Test Parameters were evaluated for all degrees of freedom for the motions of the rig and for the forces from the thrusters, but only a limited selection will be presented and discussed. The focus in the description of the results will be on the the mean values and the standard deviation as they give a measure of the efficiency of the thrusters and the degree of motion of the rig. The roll motion and applied load in the y- direction will be more thoroughly evaluated than the other motions and forces. The statistical properties were calculated in OrcaFlex and post-processed in Microsoft Excel.

7.3.1 Comparison of simulations with and without thruster forces

Statistical properties for the the simulations noThruster and normalThruster, described in Chapter 5.3, can be found in tables number 7.3, 7.4 and 7.5. The equation used to calculate the percentual differences in Table 7.5 is given below.

$$\text{Difference} = \frac{\text{Value(normalThruster)} - \text{Value(noThruster)}}{\text{Value(noThruster)}} \tag{7.1}$$

The thruster loads were programmed to counteract the motions in the horizontal plane but could also, as discussed in Chapter 1, induce roll and pitch motions. Whether or not roll and pitch motions were increased by the thrusters was dependent on the phase of the thruster forces and the phase of the roll and pitch motions. The program written to calculate the thruster forces did not include any settings to account for these phases or the frequency of oscillation of the forces. The rate of occurrence of roll- and pitch-induced motions could therefore not be anticipated, nor was it possible to foresee whether the thrusters would have a positive or negative effect on the roll and pitch motions.

As can be seen in Table 7.5, Figure 7.1 and Figure 7.2, the thrusters generally reduced the motions but increased the value of the mean heel and trim angles. The mean up-crossing and crest periods were also reduced, except for the mean crest period in roll. Reduced motions and periods of oscillations indicate that the thrusters were generally diminishing the motions of the rig.

	X (m)	Y (m)	Z (m)	Rot 1 (°)	Rot 2 (°)	Rot 3 (°)
Mean	4.27	0.76	0.41	0.60	-0.58	-1.04
Standard Deviation	1.51	0.83	2.67	0.88	1.30	0.97
Mean up-crossing period, Tz (s)	18.34	15.37	18.82	12.89	22.42	41.12
Mean crest period, Tc (s)	11.64	11.89	16.04	10.33	11.52	9.56
Maximum value	11.22	4.760	7.09	3.415	2.66	1.364
Minimum value	0.03	-2.02	-7.4314	3.13	-4.83	-3.31

Table 7.3: Statistical properties for motions in the simulation noThruster. The input for noThruster is described in Appendix F and Table 5.1

	X (m)	Y (m)	Z (m)	Rot 1 (°)	Rot 2 (°)	Rot 3 (°)
Mean	0.003	0.17	0.42	0.71	-1.74	-0.14
Standard Deviation	1.07	0.66	2.57	0.84	1.22	0.06
Mean up-crossing period (s)	13.21	13.56	18.57	12.24	15.46	9.62
Mean crest period (s)	11.42	11.77	16.03	10.60	11.18	7.90
Maximum value	4.16	3.14	7.20	3.28	2.75	0.01
Minimum value	-3.43	-1.49	-7.25	-2.73	-6.85	-0.725

Table 7.4: Statistical properties for motions in the simulation normalThruster. The input for normalThruster is described in Appendix F and Table 5.1

	X	Y	Z	Rot 1	Rot 2	Rot 3
Mean	-99.9%	-77%	2%	19%	202%	-87%
Standard Deviation	-29%	-20%	-4%	-4%	-6%	-94%
Mean up-crossing period	-28%	-12%	-1%	-5%	-31%	-77%
Mean crest period	-2%	-1%	0%	3%	-3%	-17%
Difference between max and min	-32%	-32%	-0.5%	-8%	28%	-84%

Table 7.5: Percentual difference between statistical properties of the motions in the simulations noThruster and normalThruster.

Stationkeeping efficiency of the thrusters

As can be seen from Table 7.5 and Figure 7.1, the thruster forces significantly reduce the mean offset for all horizontal motions. Figure 7.2 shows that the standard deviation was slightly reduced for all degrees of freedom except for yaw, for which the standard deviation was reduced to almost zero.

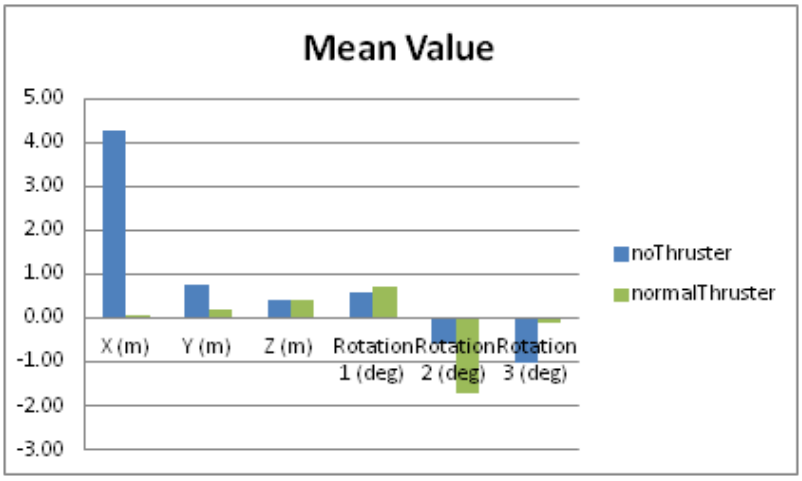

Figure 7.1: Mean value for motions in noThruster and normalThruster.

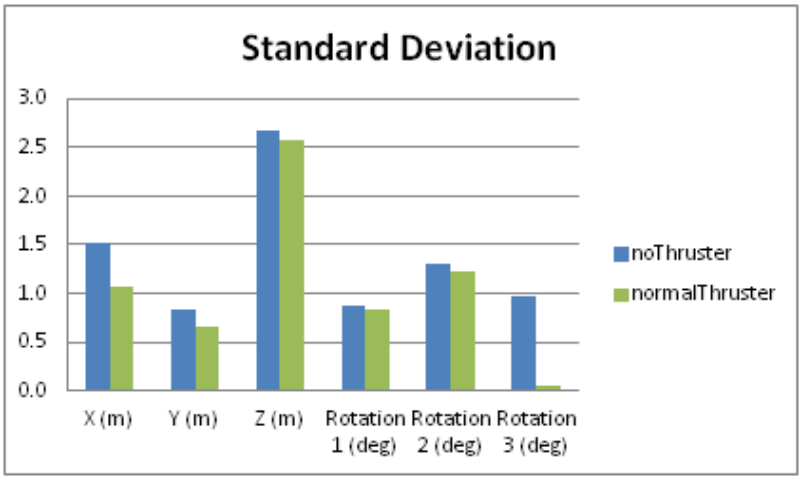

Figure 7.2: Standard deviations for motions in noThruster and normalThruster.

As can be seen in Figure 7.3, the Applied Loads accounted for almost half of the total loads acting in the local y-direction and the mean load has the opposite sign of the other forces, as it should.

The thrusters' influence on the roll motion

The time-domain roll motion in the simulations noThruster and normalThruster can be found in Figure 7.4 and Figure 7.5 and the applied load in the local y-direction can be found in figure 7.6. The standard deviation of the applied load in the vessel local y- direction is about half of the total force in that direction, as seen in Figure 7.3. Figure 7.4 and Figure 7.5 show that there is only a small difference between these two simulations with regard to the roll-motion. As seen in Table 7.5, the mean deviation

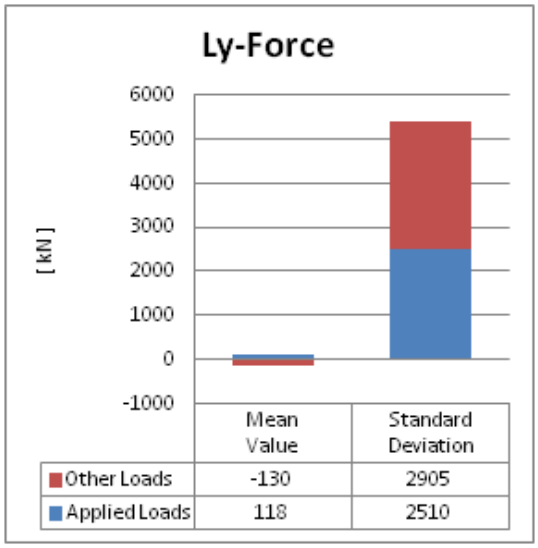

Figure 7.3: Mean and standard deviation for different components of the total load in the local y-direction for normalThruster.

from the desired roll angle increased with 19% and the standard deviation actually decreased with 4%.

The up-crossing period of the low-frequency roll motion from the simulation normalThruster was 33.7 seconds, which is not close to the natural period in roll found from the decay test, which was 52.6 seconds. The period of oscillation of the slowly-varying roll motion from the registered motions from January 25th 2012 was in the order of magnitude of one minute. This indicates that there are dominant low-frequency forces that were not properly modelled.

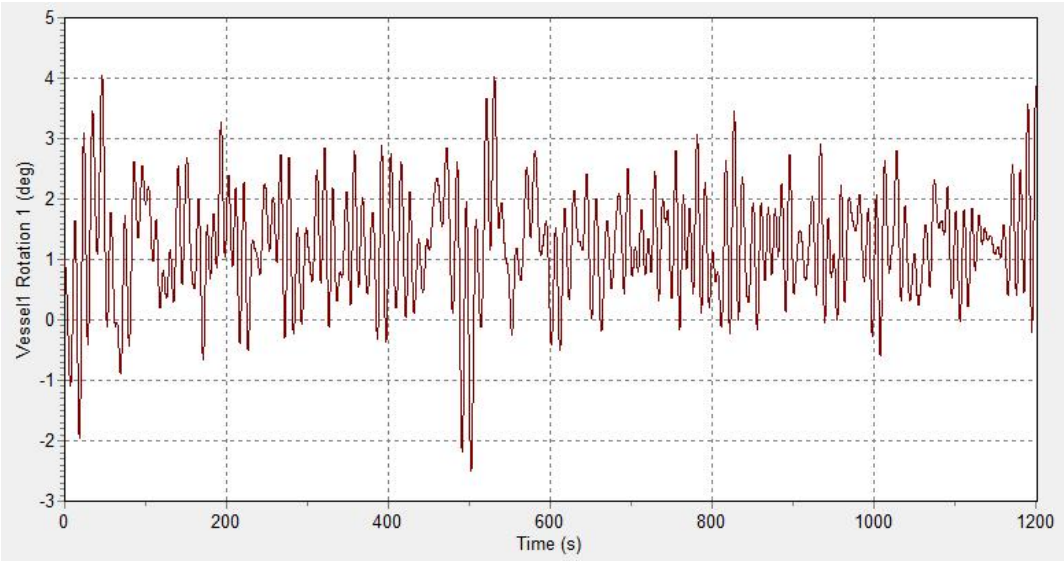

Figure 7.4: Time-domain roll motion for noThruster

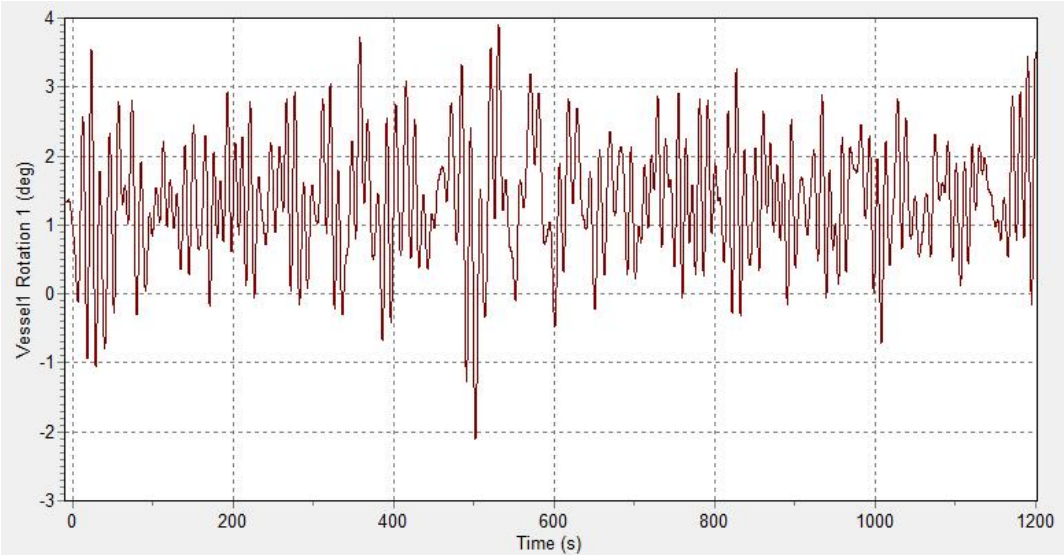

Figure 7.5: Time-domain roll motion for normalThruster

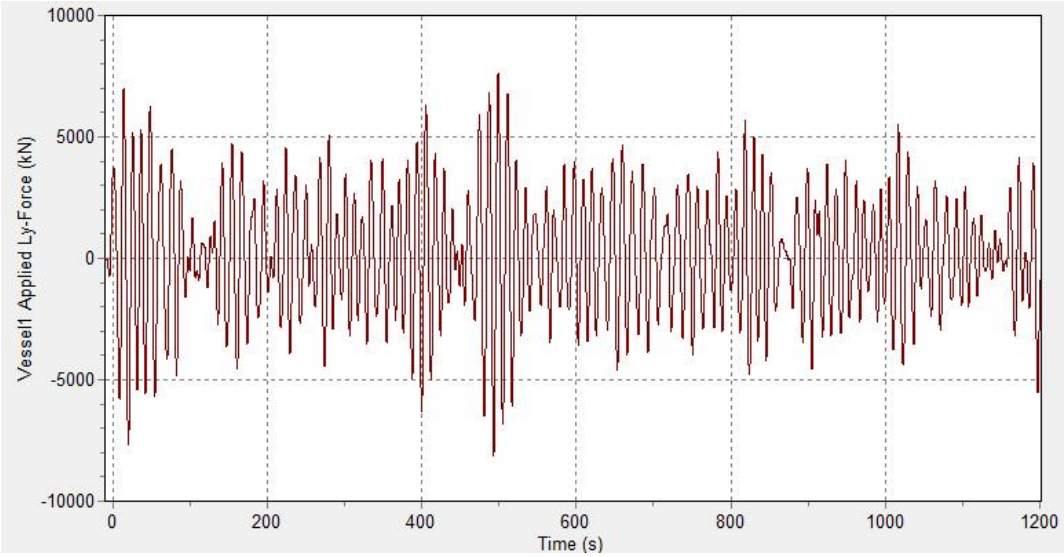

Figure 7.6: Time-domain thruster force in the vessel local y-direction for normalThruster

7.3.2 Effect of different gain coefficients

This chapter will discuss the effect of different gain coefficients. As described in Chapter 5.3, simulations were performed for controller gains that were 50% higher and 50% lower than the controller gains used in the simulation normalThruster. The controller gains used in the simulation normalThruster can be found in Table 3.5 and all the controller gains can be found in Table 5.1. The equation for the PID controller is given by equation 3.40 and given below for reference.

$$F(t) = -K_p\epsilon(t) - K_i\int_0^t \epsilon(t')dt' - K_d\frac{d\epsilon(t)}{dt}$$

Stationkeeping efficiency of the thrusters

The results show that increasing controller gains lead to smaller mean offset for all horizontal motions and smaller standard deviation for the motion in all degrees of freedom.

The global y-position (relative to the set-point) and the applied load in the vessel local y-direction were used to demonstrate the stationkeeping efficiency of the thrusters. The mean value and standard deviation for the three sets of gain coefficients for the global y-position and the applied load in the vessel local y-direction can be found in Figure 7.7 and Figure 7.8. These figures show that increased gain coefficients lead to larger thruster forces in the opposite direction of the offset which leads to smaller mean offset and smaller standard deviation of the motion. The global y-position and rotation around the global z-axis show the same tendencies. It can from this be concluded that the thruster forces are acting as desired in the horizontal plane.

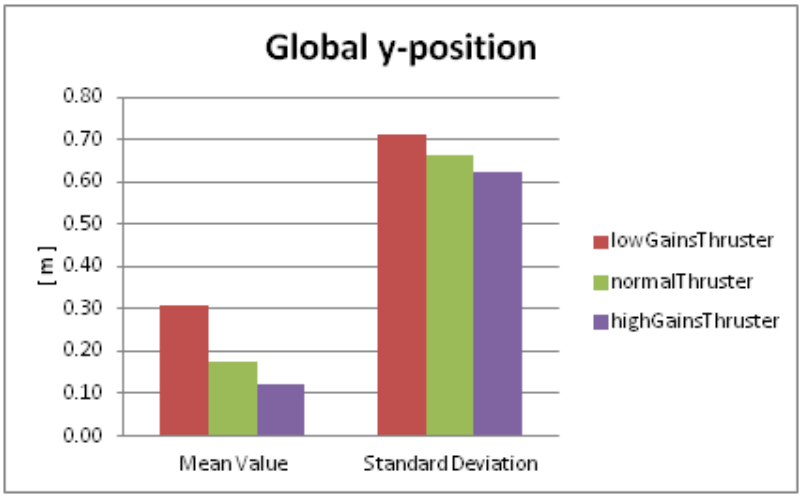

Figure 7.7: Mean value and standard deviation for the y- position for different controller gains.

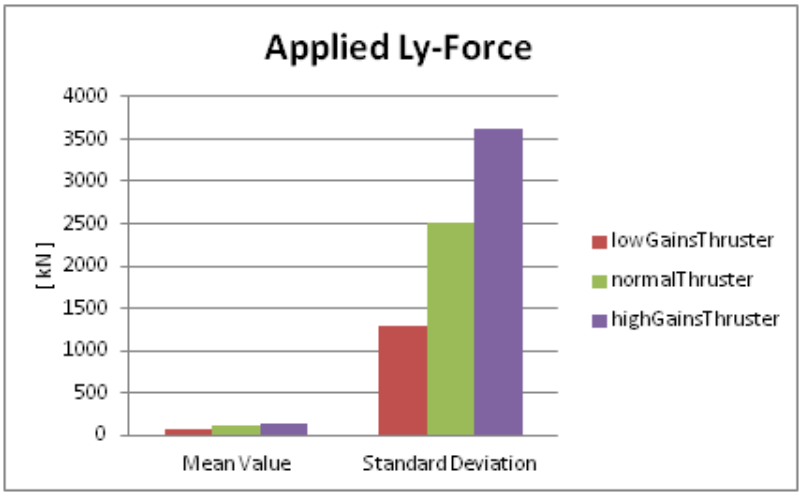

Figure 7.8: Mean value and standard deviation for the Applied Ly-force for different controller gains.

The thrusters' influence on the roll motion

The mean value and standard deviation of the rotation around the global x-axis and the applied moment around the local x-axis were used to illustrate the effect of the thrusters on the roll motion. The applied moment around the local x-axis is mainly a result of the applied load in the global y-direction and the rotation around the global x-axis has approximately the same value and opposite sign as the rotation around the local x-axis of the vessel. The rotation around the global x-axis can be found in Figure 7.9 and the applied moment around the local x-axis of the vessel can be found in Figure 7.10.

It can be seen from Figure 7.8, Figure 7.9 and Figure 7.10 that increased gain coefficients lead to larger forces in the local y-direction and thereby induce a moment around the local x-axis and cause a larger mean roll angle. However, there does not seem to be a clear connection between the standard deviation of applied moment around the local x-axis and the standard deviation of the resulting roll motion. This may be connected to the phase of the applied load and the roll motion. There does seem to be a connection for the pitch motion, which can be seen in Figure 7.11 and 7.12. The pitch motion show the same qualities regarding the mean value as the roll motion.

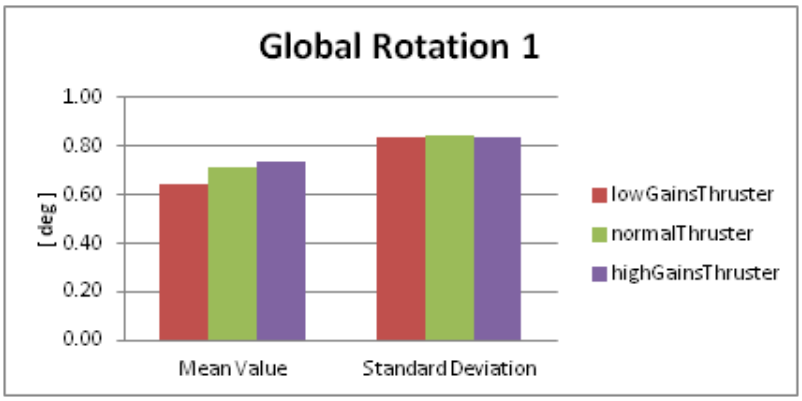

Figure 7.9: Mean value and standard deviation for Rotation 1 for different controller gains.

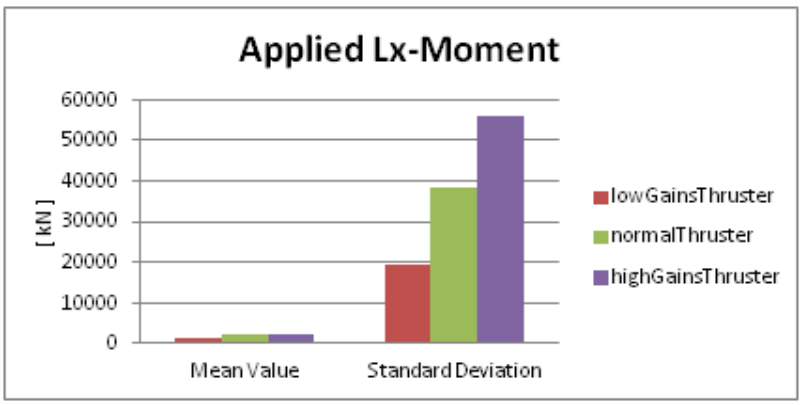

Figure 7.10: Mean value and standard deviation for the Applied X-moment for different controller gains.

Compared to normalThruster, lowGainsThruster decrease the mean up-crossing period in roll by 1% and highGainsThruster increase it with 5%. However, both lowGain-

sThruster and highGainsThruster increase the mean up-crossing period in pitch with 3%, so there does not seem to be a definite connection.

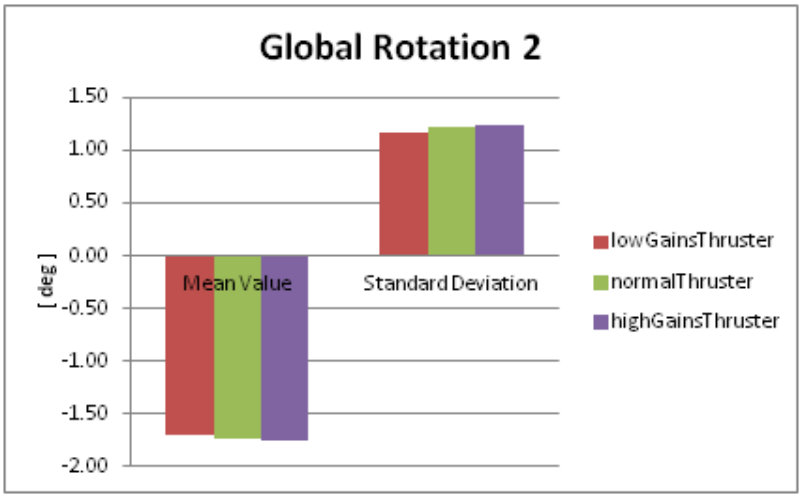

Figure 7.11: Mean value and standard deviation for Rotation 2 for different controller gains.

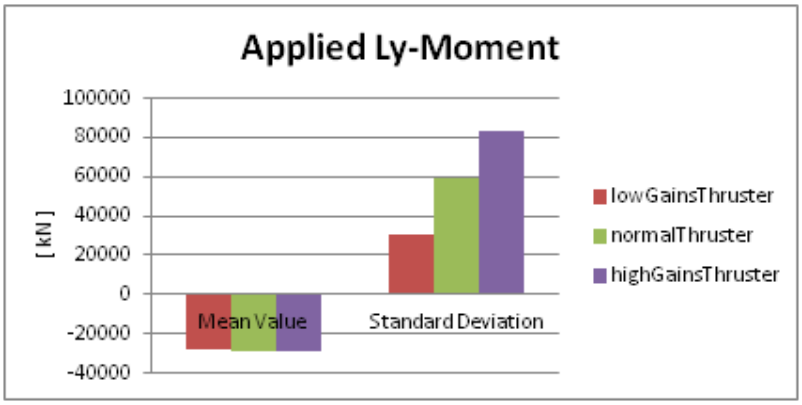

Figure 7.12: Mean value and standard deviation for the Applied Y-moment for different controller gains.

7.3.3 Effect of constant thruster force to counteract mean environmental loads

In an attempt to reduce the standard deviation of the motion caused by the thrusters, constant thruster forces were added in order to counteract the mean-drift forces, the constant current load and the constant wind load. The simulation statThruster is equal to normalThruster except for an additional, constant load in the global x- and y- directions and a constant moment around the global z-axis which were of equal magnitude and opposite direction of the forces mentioned above. These forces were calculated at the same time as the static equilibrium position when the mean-drift loads and constant wind- and current-loads were included.

The extra constant thruster forces increased the mean offset in the global x- and y-directions, but had no significant value on the rotation around the global z-axis. The

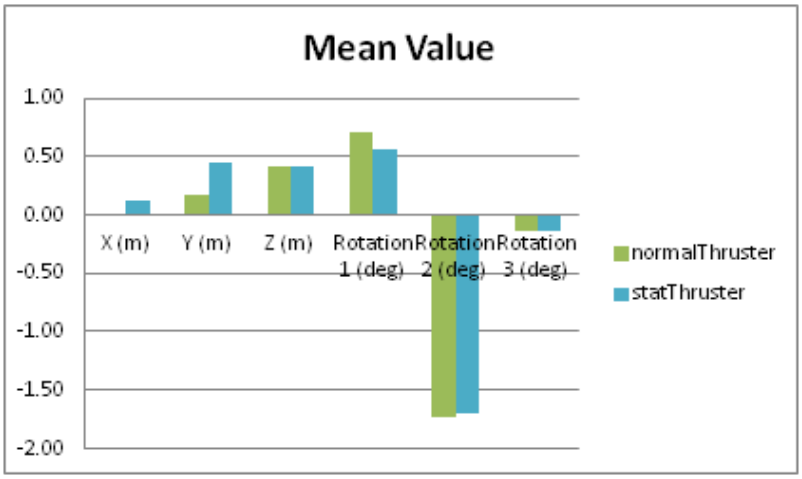

Figure 7.13: Mean value of motions for normalThruster and statThruster

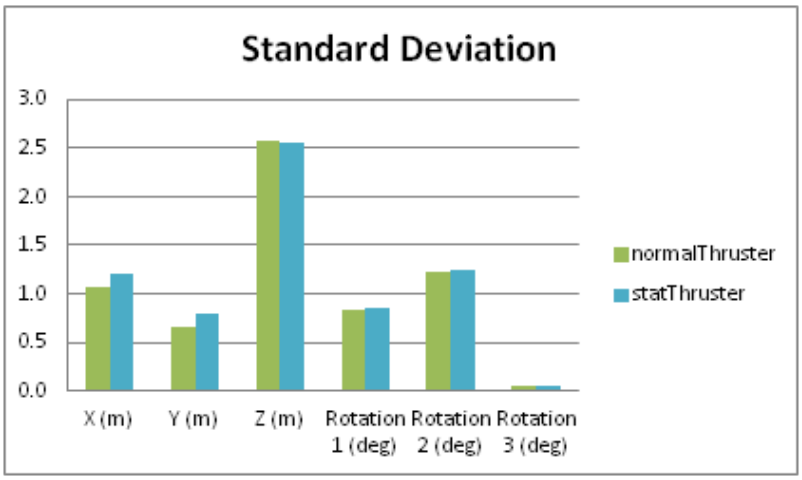

Figure 7.14: Standard deviation of motions for normalThruster and statThruster

magnitude of the standard deviations of the motions did not decrease, but were acutally slightly increased. The constant contribution to the PID controller cannot be recommended on the basis of these results.

7.3.4 Harmonically oscillating thruster forces

The dynamic positioning system governed by a PID controller did not induce any roll or pitch motions of significance and an attempt was made to induce increased roll motions with harmonically oscillating thruster forces. The thruster force from the PID controller acting in the global y-direction was replaced with a harmonic load oscillating with the mean up-crossing period of the roll motion from the simulation normalThruster. This simulation, harmonicThruster is described in Chapter 5.3.

The amplitude of the thruster forces in the simulation harmonicThruster was 3000 kN, which was chosen in an attempt to obtain the same standard deviation of the thruster forces in the global y-direction in the simulation normalThruster. The results show that the standard deviation of the global applied y-force was 15% smaller for harmonicThruster than for normalThruster, which can be seen in Figure 7.15. The reason why the harmonicThruster has a mean value is because it is given as the Applied

Load in the local y-direction and therefore has a small contribution from the thruster forces applied in the global x-direction.

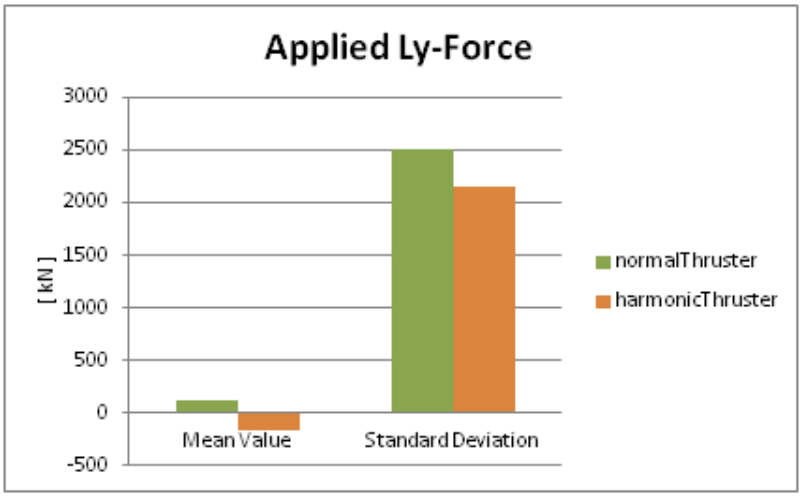

Figure 7.15: Mean value and standard deviation of applied load in the global y-direction for harmonicTruster and normalThruster.

The phase of the thruster forces in the global y- direction for the harmonicThruster simulation was chosen such that it should excite the roll motion. This can be seen in the extraction from the time-domain simulation in Figure 7.16. It should be noted that the coordinate system of the rotation and the applied force are rotated almost 180°relative to each other, as seen in Figure 3.1.

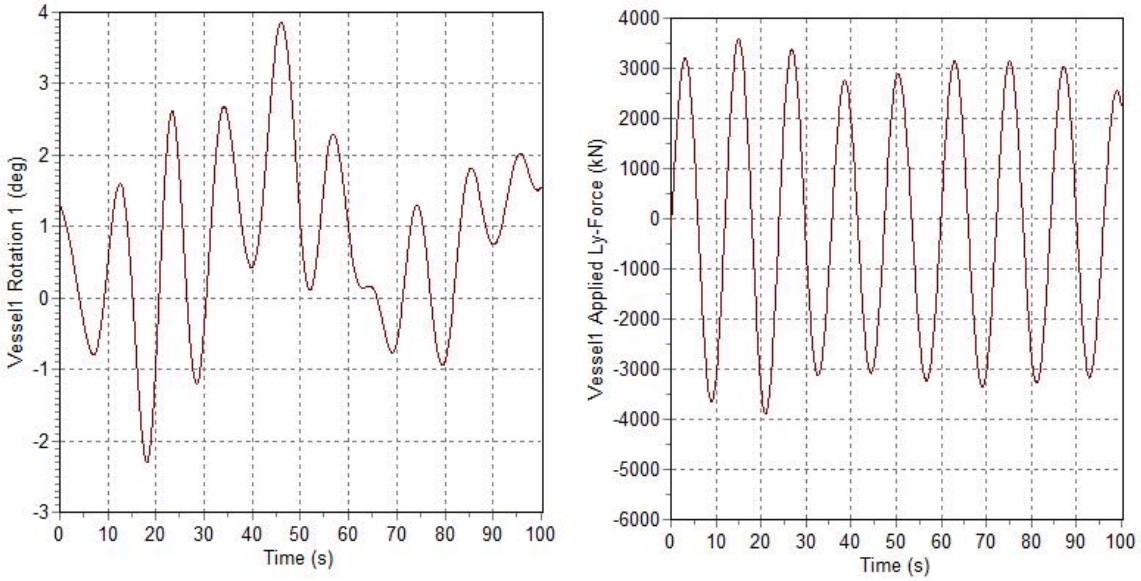

Figure 7.16: Extraction from the time-domain simulation harmonicThruster, rotation around global x-axis to the left and applied load in local y- direction to right.

The mean value and standard deviation from the simulation harmonicThruster is given in Figure 7.17 and Figure 7.18. The harmonic load increased the mean value of the offset in the global y-direction and decreased the mean roll angle. The standard deviation for the rotation around the global x- axis was increased by 6%, while the standard deviation of the applied force was decreased 15%. While the harmonic load did increase the standard deviation of the roll motion compared to the PID controller, the standard

deviation was still significantly smaller than what was registered on January 25th 2012 as will be seen in Chapter 7.4.

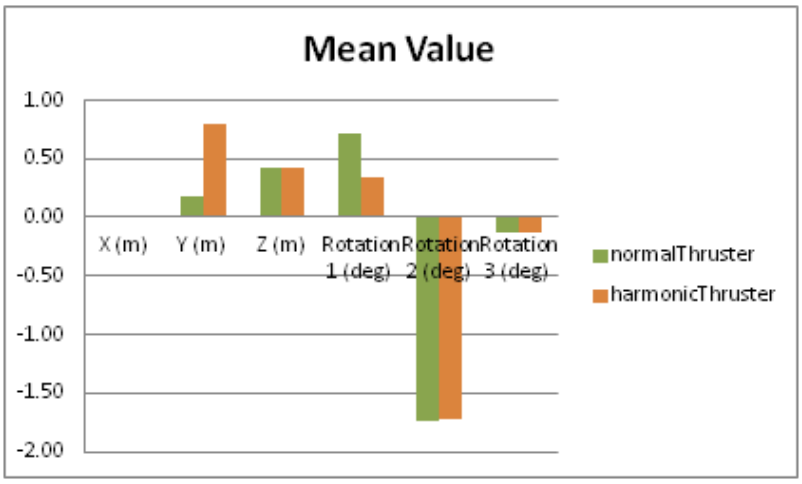

Figure 7.17: Mean value of motions for normalThruster and harmonicThruster

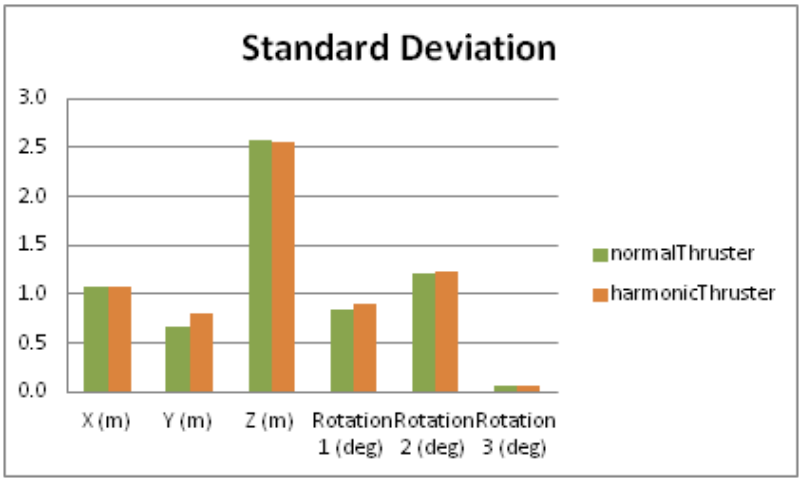

Figure 7.18: Standard deviation of motions for normalThruster and harmonicThruster

7.4 Comparison of time-domain simulations in OrcaFlex and registered time-history

The standard deviation for the motions from the simulations in OrcaFlex and the registered motions between 18:00 and 18:55 on January 25th 2012 are compared in Figure 7.19.

Figure 7.19 shows that the standard deviations for surge, sway and pitch with thruster forces is of the same magnitude as for the registered motions. The standard deviation in roll is, as for the calculations of Global Maritime, approximately half of those of the registered motions. The standard deviation in heave is approximately twice as large as the one for the registered motions.

A 20 minute time-history of the registered roll motion of COSL Pioneer on January 25th 2012 can be found in Figure 7.21 and the roll motion from the simulation normalThruster can be found in Figure 7.20. It would not be relevant to compare the

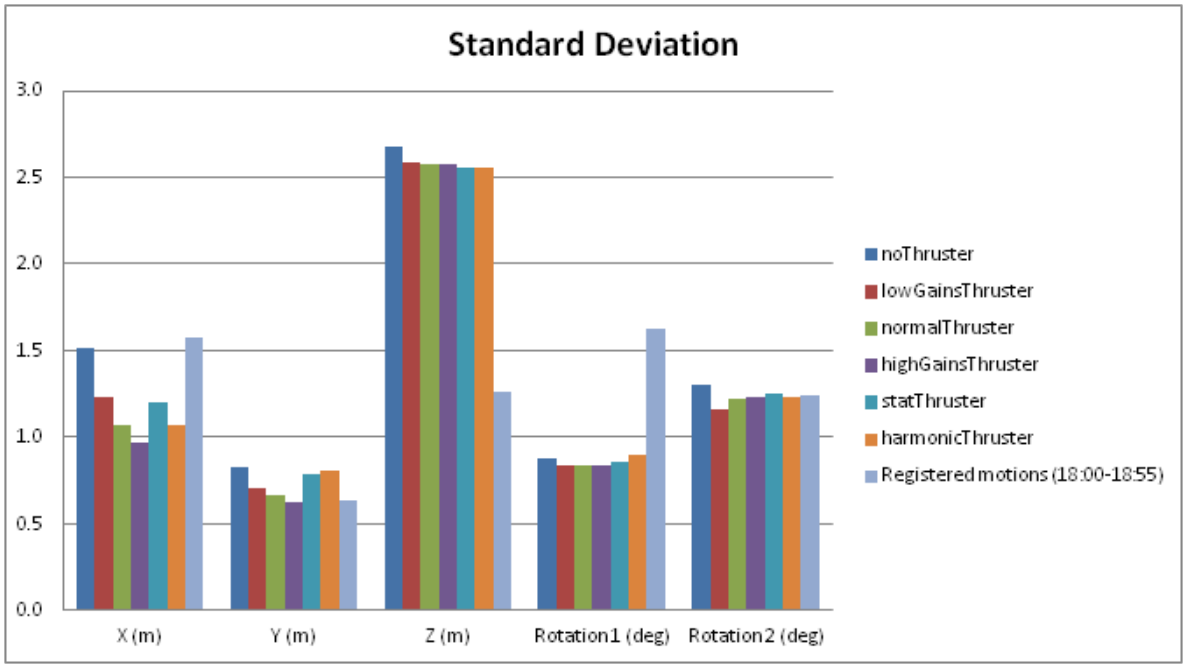

Figure 7.19: Standard deviation of motions for all simulations and for registered motions from January 25th 2012.

motions directly as the actual wave realizations are different, but it can be seen that the roll motions from January 25th 2012 have a slowly-varying component that the OrcaFlex-simulation is missing.

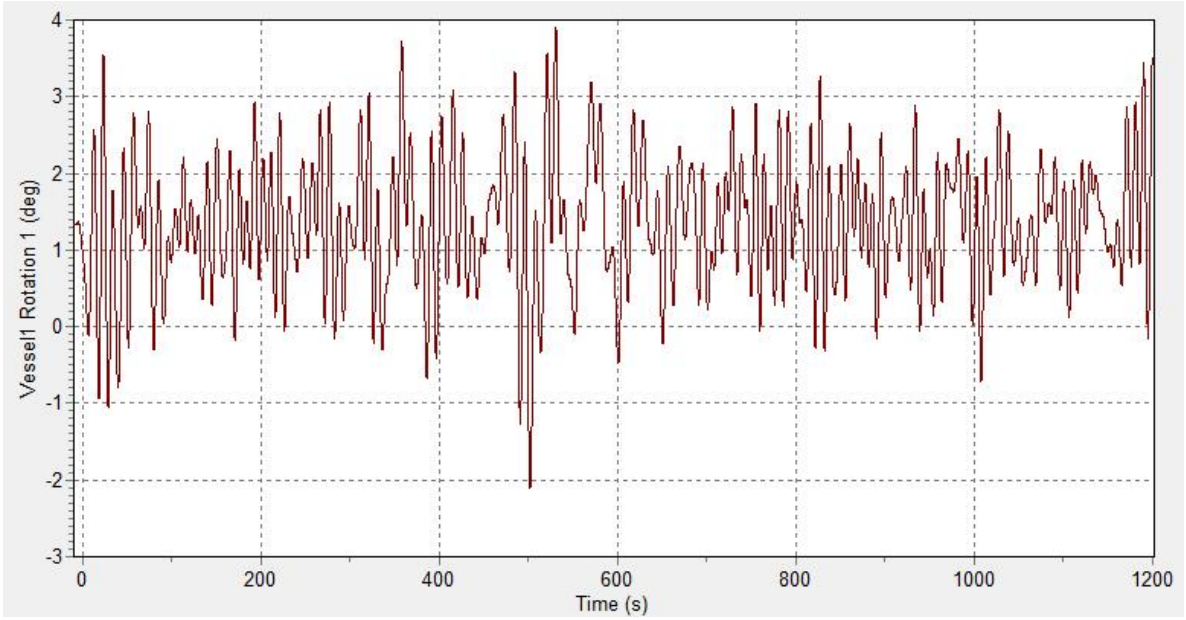

Figure 7.20: Time-domain roll motion for normalThruster

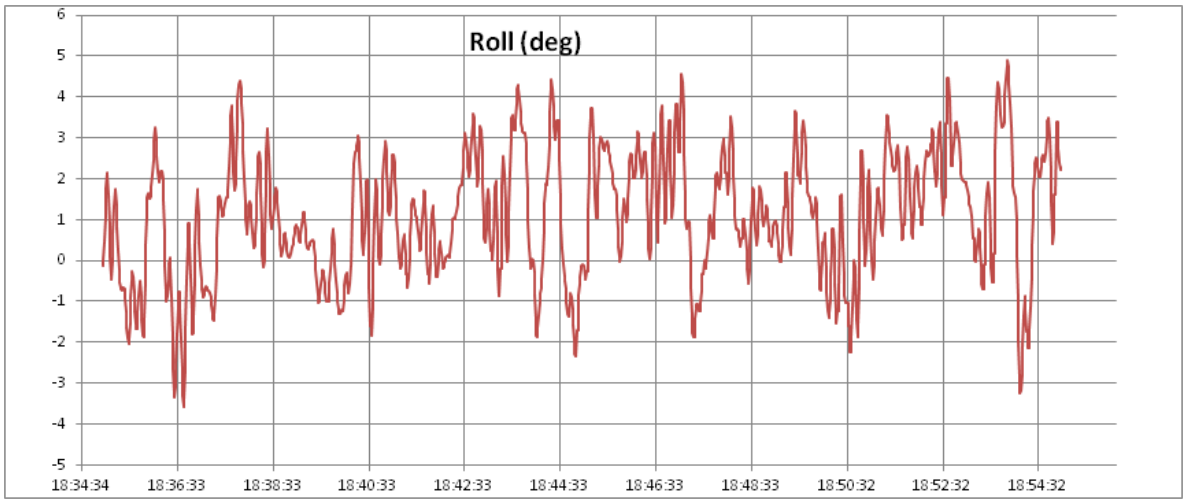

Figure 7.21: Registered roll motion of COSL Pioneer on January 25th 2012 between 18:35 and 18:55.

8 | Discussion and conclusions

8.1 Discussion of the results

None of the time-domain simulations were in agreement with the standard deviations of the registered motions. Many simplifications were made in order to assemble the computational model and several of these simplifications were quite extensive. This chapter will present and discuss sources of error and their implications.

8.1.1 Modelling of the thrusters

The main discrepancy in the physical modelling was the calculation and application of the thruster forces. The magnitude, direction and point of application are not consistent with reality. The forces from six thrusters located in six different places on the rig, which in reality may act in six different directions were simplified by two forces and a moment located at a fixed point in the global coordinate system. Since the applied thruster forces were acting in the global horizontal plane, they were not acting in the local horizontal plane of the rig and exerted therefore forces acting in the local z-direction of the vessel as well. Because the origin of the vessel coordinate system does not coincide with the origin of the global coordinate system, the yaw moment from the thrusters were not applied at the center of the vessel.

The program that calculated the thruster forces did not account for the limitations of the thrusters. The maximum available force from all six thrusters combined is 3450 kN, but all the simulations had maximum values of the resulting force of between 11 000 kN and 20 000 kN. Also, the moment from the thrusters was not calculated from the thruster forces, but was acting separately from the forces. None of the physical properties, such as cavitation issues or the Coanda effect, of the thrusters were included.

Given that the problems mentioned above were accounted for, the thruster forces would still not be consistent with reality, unless the calculation of the thruster forces were based on information about the actual dynamic positioning system. As mentioned in the introduction, real dynamic-positioning systems are very complex and are therefore not easily replicated. The implemented PID controller was very simple, not based on facts about the real DP system and attempted to counteract the wave-frequency motion as well as the low-frequency motion. The latter simplification decreased the period of oscillation of the thruster forces, which meant that it would become more difficult to induce resonance motion in roll because of the large natural period roll for COSL Pioneer.

The consequences of the approximations made when modelling the thrusters have probably been crucial, it is however not clear in what way this has affected the results. The only thing that is certain is that the magnitudes of the thruster forces are too large. This indicates that the results from the simulations noThruster and lowGainsThruster are probably more realistic than the others.

8.1.2 Modelling of the rig

The riser was not included in the calculations at all. The riser is not assumed to transfer any moment of significance due to its flex-joint connection, but if more accurate calculations are required, it should be included. The center of gravity was set based on a process of iterations in order to obtain the correct transverse metacentric height and should be fairly accurate, but is most likely not exact.

The quadratic transfer functions are jagged, which indicate that they may have a low degree of accuracy. This may have occurred because the panel model had too large or poorly distributed panels. Newman's approximation was applied for the calculation of the second-order wave drift forces and since there are several incoming directions, this is not necessarily a valid approximation for the required degree of accuracy.

Viscous damping has not been carefully evaluated. Five percent of the critical damping was added in heave for the calculation of the hydrodynamic data. The pontoons have relatively sharp edges that will cause eddy-making damping. Five percent of critical damping may be too little and the eddy-making damping is also dependent on the amplitude and frequency of the motion, which has not been taken into consideration. This could maybe explain the large standard deviation for the heave motion. Viscous damping in the other degrees of freedom was not included in the analysis and could lead to unrealistically large motions of the rig.

8.1.3 Modelling of the environment

The waves, wind and current were based on statistical values from January 25th 2012. The wind and current velocities were modelled as constant. The gusts of the wind will not be important for the low-frequency response, but slow variations in wind and current velocities could influence the results. No vertical variation of the wind was included, which presents another deviation from reality.

8.1.4 Dividing Period

As discussed in Chapter 4.3.5, the Dividing Period could have a significant impact on the results and its value was determined on the basis of a qualified guess. Also, if the low-frequency and wave-frequency responses oscillate with periods that are of similar magnitude, the Dividing Period would be impossible to set as it should be in between and far away from both.

8.1.5 Duration of the simulation

The duration of the simulations is 20 minutes, which is approximately 20 times the length of the natural period in roll and may be possibly too short to obtain valid statistical parameters. A sensitivity study should be performed to validate the length of the simulations.

8.2 Conclusions

The main goal of this thesis was to run time-domain analysis in order regenerate the motions of the drilling COSL Pioneer on January 25th 2012 and identify the cause of the excessive roll-motions that were registered. Time-domain analyses were performed but the statistical properties of the roll motions were not reproduced.

The thruster forces were calculated in a program written by the author and implemented in OrcaFlex as two forces and a moment acting in the earth-fixed horizontal plane. The thruster forces were calculated using an algorithm for a Proportional Integral Derivative controller. No clear conclusion could be drawn from these results regarding thruster-induced motions.

The deviations between the registered motions and the simulations are assumed to be predominantly caused by the simplifications regarding the thruster. The most severe simplifications of the thruster forces were the point of application, the direction of the forces and that the forces attempted to counteract all the horizontal motion of the rig and not only the low-frequency motion, as it should have. The increased frequency of oscillation of the thruster forces diminished the chances that resonance of the roll motion could not be excited by the thruster forces.

A harmonically oscillating force was applied in order to demonstrate the effect of thruster-induced roll motion. The harmonically oscillating force had a 15% smaller standard deviation than the PID controlled thruster forces, but still yielded an increase of the standard deviation in roll of 6%. This proved that the thrusters can increase the roll motion as long as the forces oscillate with the same period of oscillation and are in phase with the roll motion.

The second-order drift forces were suspected to be an alternative cause for the excessive roll motions, but the up-crossing period of the second-order drift forces was approximately 17 seconds (compared to the natural period in roll of approximately 53 seconds) and can from these results not be regarded as likely to be the cause. However, it is suspected that the quadratic transfer functions were inaccurate and it is possible that the drift-forces were modelled inaccurately and the second-order drift forces should therefore not be eliminated as a possible cause for the excessive roll motions.

The standard deviation in heave from the time-domain simulation was almost twice as large as that of the registered motions from January 25th 2012. The cause for this was not identified should therefore be further studied.

As the cause of the excessive motions was not identified and no excessive motions were reproduced, no recommendations for improvement can be given.

8.3 Suggestions for further work

Suggestions for further work on the modelling of the thruster forces is listed below in order of increasing degree of required amount of work.

1. Apply the thruster forces in the global coordinate system at the mean horizontal position of the vessel.
2. Apply the thruster forces in the coordinate system of the vessel
3. Perform more simulations and other variations of the controller gains and vary the proportional, derivative and integral gains separately.
4. Allow for coupled degrees of freedom in the PID controller and further refine the model to include restriction according to available power.
5. Apply a Kalman filter or experiment with increasing the Dividing Period such that the thruster forces can be calculated based on the low-frequency motion only. The Kalman filter is not implemented in OrcaFlex, so the filtration of the motions will then have to be performed by an External Function that needs to be written.
6. Expand the model of the thruster forces to include the thruster allocation and apply the correct thruster forces for all six thrusters at their actual location.
7. If the necessary information is available, refine the controller in accordance with the actual dynamic positioning system of COSL Pioneer

Other suggestions connected with other parts of the analysis:

1. Identify the cause of the excessive heave motions in the time-domain simulations.
2. Perform a sensitivity analysis to study the influence of the discretization of the panel model and adjust the panel model if necessary.
3. Calculate the quadratic transfer functions with shorter intervals between the periods.
4. Calculate full quadratic transfer functions and perform time-domain simulations without the use of Newman's approximation.
5. Perform a model test or use numerical methods to include the effects of viscous damping more accurately.
6. Include vertical variation of the wind and time- variation of the wind and current velocity.
7. Perform a sensitivity study in order to validate the length of the simulations.
8. Study the numerical methods of the applied software to see if the numerical methods have any influence on the results
9. There are many results from OrcaFlex that were not evaluated during the work of this thesis, such as other load components and study of the time-history for the other parameters. These results could provide useful data for further analyses and should be studied more closely. They should also be compared to real time-histories for COSL Pioneer if they are available.

10. If the calculations are in agreement with the registered motions and the motions were indeed thruster-induced, attempt to vary the settings of the dynamic positioning system such that the excessive motions can be reduced.

Bibliography

[1] A.J. Sørensen. Marine control systems. Lecture Notes.

[2] A.J. Sørensen and J.P. Strand. Positioning of small-waterplane-area marine constructions with roll and pitch damping. *Control Engineering Practice 8*, 2000.

[3] E. Huse and R. Børresen. Heave, pitch and roll damping of platforms and ships due to positioning thrusters. In *Offshore Tecnology Conference*, 1983.

[4] N.A. Jenssen. Mitigating excessive pitch and roll motions on semi-sibmersibles. In *Dynamic Positioning Conference 2010*, volume Konsberg Maritime AS, 2010.

[5] DNV. *Wadam User Manual*.

[6] WAMIT Inc. *Wamit User Manual*, 2011.

[7] J.N.Newman. *Marine Hydrodynamics*. The MiT Press, 1977.

[8] Frank M. White. *Fluid Mechanics*. McGraw-Hill, 2008.

[9] DnV. Correspondence with dnv software support, 2013.

[10] Odd M. Faltinsen. *Sea Loads on Ships and Offshore Structures*. Cambridge University Press, 1990.

[11] M.-H. Kim C.-H. Lee, J.N. Newman and D.K.P. Yue. The computation of second-order wave loads. In *1991 OMAE*, volume I A.

[12] T.F. Ogilvie. Second-order hydrodynamic effects on ocean platforms. In *International Workshop on Ship and Offshore Platforms*, 1983.

[13] Orcina. *OrcaFlex User Manual*, version 9.6a edition.

[14] Orcina. Correspondence with orcina software support, 2013.

[15] J. Chung and G.M. Hulbert. A time integration algorithm for structural dynamics with improved numerical disspiation: The generalized-α method. *Journal of Applied Mechanics*, 1993.

[16] ITTC. Testing and extrapolation methods, general density and viscosity of water, 1978.

[17] R.M. Isherwood. Technical note: A revised parametrisation of the jonswap spectrum. In *Applied Ocean Research*, volume 9, pages 47–50, 1987.

[18] R.E. Randall J.Zhang and C.A. Spell. On wave kinematics approximate methods. In *Offshore Technology Conference*, 1991.

[19] C.T. Stansberg and O.T. Gudmestad. Non-linear random wave kinematic models verified against measurements in steep waves. In *Proceedings of OMAE1996*, volume 1A, 1996.

[20] Ove T. Gudmestad C.T Stansberg and S.K. Haver. Kinematics under extreme waves. In *Proceedeings of OMAE2006*, 2006.

[21] R. E. Randall J. K. Longridge and J. Zhang. Comparison of experimental irregular water wave elevation and kinematic data with new hybrid wave model predictions. In *Ocean Engineering*, volume 3, pages 277–307, 1996.

[22] W.J. Brendling R.G. Standing and D. Wilson. Recent developments in the analysis of wave drift forces, low-frequency damping and response. In *OTC 5456*, 1987.

[23] Marilena Greco. Tmr 4215: Sea loads. Lecture Notes.

[24] P.J. Clark Š. Malenica and B. Molin. Wave and current forces on a vertical cylinder free to surge and sway. *Applied Ocean Research*, 17, 1995.

[25] A.J. Sørensen. A survey of dynamic positioning control systems. *Annual Reviews in Control*, pages 123–136, 2011.

[26] A.J. Sørensen. Control system design for dynamic positioning, 0000.

[27] Orcina. Orcfxapi help, 2013.

[28] Python. Python programming language – official website.

[29] Thor I. Fossen. *Marine Craft Hydrodynamics and Motion Control*. Wiley, 2011.

[30] A.J. Sørensen. Lecture notes - tmr4240 marine control systemsr. NTNU.

[31] J.-H. Kim Y.-S. Kim S.W. Hong S.A. Hong, B.-W. Nam and Y.-S. Kim. Second-order motion characteristics of a semi-submersible platform in waves. *International Journal of Ocean System Engineering*, 2011.

[32] AAD.J. Hermans. Low-frequency second-order wave-drift forces and damping. *Journal of Engineering Mathematics*, 1999.

[33] T.E. Schellin and A. Kirsch. Low-frequency damping of a moored semisubmersible obtained from simulated extinction tests and mean wave drift forces. *Applied Ocean Research*, 11(4), 1989.

[34] A. Voogt and J. Soles. Stability of drilling semi submersibles. In *10th International Symposium on Practical Design of Ships and Other Floating Structures*, 2007.

A | Mathematical details on how to find the velocity potentials

This appendix contains a rendering of the methods outlined in the Wadam User Manual[5], the Wamit User Manual[6] and Marine Hydrodynamics by Newman[7].

A.1 Application of Green's Theorem to find velocity potentials

This section explains the derivation of Equation A.8 which is applied in Wadam as explained in section A.2.

Let the two potentials ϕ and φ describe the fluid domain bounded by S with the volume V and let them satisfy the Laplace equation (Equation2.3). The application of the divergence theorem give Green's second identity.

$$\iint_S [\phi \frac{\partial \varphi}{\partial n} - \varphi \frac{\partial \phi}{\partial n}] dS = \iiint_V \nabla(\phi \nabla \varphi - \varphi \nabla \phi) dV \tag{A.1}$$

n is a unit normal vector pointing out of the fluid. Further calculations and the application of the Laplace equation gives

$$\begin{aligned} \iint_S [\phi \frac{\partial \varphi}{\partial n} - \varphi \frac{\partial \phi}{\partial n}] dS &= \iiint_V \nabla(\phi \nabla \varphi - \varphi \nabla \phi) dV \\ &= \iiint_V (\phi \nabla^2 \varphi + \nabla \phi \nabla \varphi - \varphi \nabla^2 \phi - \nabla \varphi \nabla \phi) dV \\ &= 0 \end{aligned} \tag{A.2}$$

The velocity potential at point (x,y,z) due to potential source of unit strength at point (ξ, η, ζ) is given as

$$\varphi = \frac{1}{4\pi r} = \frac{1}{4\pi \sqrt{(x-\xi)^2 + (y-\eta)^2 + (z-\zeta)^2}} \tag{A.3}$$

where (ξ, η, ζ) are given in the coordinates (x,y,z).

The next step is to insert φ from Equation A.3 in to Equation A.2, but the expression for φ does not satisfy the Laplace equation at the exact location of the source since denominator is zero there. To avoid this problem the surface S is replaced by the two surfaces S and S_ε, where S is the previous boundary and S_ε is a infinitesimal sphere surrounding the source. The surface of integration is no longer continuous, and strictly speaking Equation A.2 should no longer be valid. This is solved by introducing a small tube with infinitesimal radius connecting the surfaces S and S_ε. The contribution to the integral from the area of the tube goes to zero as its radius goes to zero and can therefore be omitted. The integration can then be performed over the surface S and the surface of the sphere with infinitesimal radius ε surrounding the point source as follows.

$$\frac{1}{4\pi} \iint_{S+S_\varepsilon} [\phi \frac{\partial}{\partial n}(\frac{1}{r}) - \frac{1}{r} \frac{\partial \phi}{\partial n}] dS = 0 \tag{A.4}$$

The equation may be rewritten as

$$\frac{1}{4\pi}\iint_S \left[\phi\frac{\partial}{\partial n}\left(\frac{1}{r}\right) - \frac{1}{r}\frac{\partial\phi}{\partial n}\right]dS = -\frac{1}{4\pi}\iint_{S_\varepsilon} \left[\phi\frac{\partial}{\partial n}\left(\frac{1}{r}\right) - \frac{1}{r}\frac{\partial\phi}{\partial n}\right]dS \tag{A.5}$$

The integration may be performed over either set of coordinates as the value of ϕ in Equation A.3 is unchanged if the source point and field point are switched. Equation A.6 performes the integration over ξ, η, ζ using that ϕ is assumed to be constant for very small ε. As ε becomes very small, the normal vector $\mathbf{n}$ is approximated by -$\mathbf{r}$. This gives

$$\begin{aligned}
-\frac{1}{4\pi}\iint_{S_\varepsilon} \left[\phi\frac{\partial}{\partial n}\left(\frac{1}{r}\right) - \frac{1}{r}\frac{\partial\phi}{\partial n}\right]d\xi &= -\frac{1}{4\pi}\iint_{S_\varepsilon} \phi\frac{\partial}{\partial n}\left(\frac{1}{r}\right)d\xi + \frac{1}{4\pi}\iint_{S_\varepsilon} \frac{1}{r}\frac{\partial\phi}{\partial n}d\xi \\
&= -\frac{1}{4\pi}\iint_{S_\varepsilon} \phi\frac{1}{r^2}d\xi + \frac{1}{4\pi}\iint_{S_\varepsilon} \frac{1}{r}\frac{\partial\phi}{\partial n}d\xi \\
&\approx -\frac{1}{4\pi}\phi(x,y,z)\frac{1}{\varepsilon^2}\underbrace{4\pi\varepsilon^2}_{\text{area of sphere}} + \underbrace{\frac{1}{4\pi}\iint_{S_\varepsilon} \frac{1}{r}\frac{\partial\phi}{\partial n}d\xi}_{\text{Goes to zero as } \varepsilon \text{ goes to zero}} \\
&\approx -\phi(x,y,z)
\end{aligned} \tag{A.6}$$

Inserting Equation A.6 into Equation A.5 gives the following equation for a source point inside the surface S.

$$\phi(x,y,z) = -\frac{1}{4\pi}\iint_S \left[\phi\frac{\partial}{\partial n}\left(\frac{1}{r}\right) - \frac{1}{r}\frac{\partial\phi}{\partial n}\right]d\xi \tag{A.7}$$

A source *on* the surface of S may be circumvented by half sphere with radius ε. A derivation analogue to the one of Equation A.7 gives

$$\phi(x,y,z) = -\frac{1}{2\pi}\iint_S \left[\phi\frac{\partial}{\partial n}\left(\frac{1}{r}\right) - \frac{1}{r}\frac{\partial\phi}{\partial n}\right]d\xi \tag{A.8}$$

For source place outside of S the integral is zero, in accordance with Equation A.2.

$$-\frac{1}{4\pi}\iint_S \left[\phi\frac{\partial}{\partial n}\left(\frac{1}{r}\right) - \frac{1}{r}\frac{\partial\phi}{\partial n}\right]d\xi = 0 \tag{A.9}$$

As $\frac{\partial\phi}{\partial n}$ is generally known for a moving body Equation A.8 can be used to find the unknown potential. According to Newman[7] there are computational advantages if the source potential is modified such that it satisfies the same boundary conditions as ϕ. The Green function, given in Equation A.10, may then substitute $\frac{1}{r}$ in the source potential given by Equation A.8.

$$G(\mathbf{x}, \boldsymbol{\xi}) = \frac{1}{r} + H(\mathbf{x}, \boldsymbol{\xi}) \tag{A.10}$$

The function H may be any function that satisfies the Laplace equation and can therefore be chosen such that G satisfies that boundary conditions of the fluid domain. If it also satisfies $\frac{\partial G}{\partial n} = 0$, the unknown term in Equation A.8 disappears. Inserting Equation A.10 into Equation A.8 gives

$$2\pi\phi(\mathbf{x}) + \iint_S \left[\phi(\boldsymbol{\xi})\frac{\partial G(\mathbf{x}, \boldsymbol{\xi})}{\partial n} - G(\mathbf{x}, \boldsymbol{\xi})\frac{\partial\phi(\boldsymbol{\xi})}{\partial n}\right]d\boldsymbol{\xi} = 0 \tag{A.11}$$

A.2 Application of Green's Theorem in Wadam

The application of Green's theorem in Wadam is described in the Wamit User Manual[6], Chapter 15 and given in this section.

A.2.1 Green's function

The Green function for finite water applied in Wadam is given by Equation A.12 and satisfies both the free surface and radiation conditions.

$$G(\mathbf{x},\boldsymbol{\xi}) = \frac{1}{r} + \frac{1}{r'} + 2\int_0^\infty dk \frac{(k+K)\cosh\big(k(z+H)\big)\cosh\big(k(\zeta+H)\big)}{k\sinh(kH) - K\cosh(kH)} e^{-kH} J_0(kR) \tag{A.12}$$

The parameters in the Green's functions are given by

$$\begin{aligned} r^2 &= (x-\xi)^2 + (y-\eta)^2 + (z-\zeta)^2 \\ r'^2 &= (x-\xi)^2 + (y-\eta)^2 + (z+\zeta+2H)^2 \\ K &= \frac{\omega^2}{g} \\ J_0(x) &= \text{Bessel function of zero order} \\ H &= \text{water depth} \end{aligned}$$

A.2.2 Fluid domain and velocity potentials

The fluid domain is bounded by the surface of the body, S_b, the free surface, S_{FS} and a far-field boundary, S_∞. The velocity potentials satisfying the Laplace equation in the domain are the radiation velocity potential, ϕ_R, the diffraction potential, ϕ_D and the potential of the incoming wave, ϕ_0.

Since the velocity potentials ϕ_0, ϕ_D and ϕ_R as well as the Green function, G, satisfy the free-surface boundary condition then the following simplification can be made.

$$\iint_{S_{FS}} \big[\phi\frac{\partial G}{\partial n} - G\frac{\partial \phi}{\partial n}\big] d\boldsymbol{\xi} = 0 \qquad \text{for } \phi = \phi_0, \phi_D \text{ or } \phi_R \tag{A.13}$$

Since the velocity potentials ϕ_D and ϕ_R become very similar to Green function, G, at the limits of the fluid domain then the following simplification can be made.

$$\iint_{S_\infty} \big[\phi\frac{\partial G}{\partial n} - G\frac{\partial \phi}{\partial n}\big] d\boldsymbol{\xi} = 0 \qquad \text{for } \phi = \phi_D \text{ or } \phi_R \tag{A.14}$$

This reduces Equation A.11 to Equation A.15 for the diffraction and radiation potentials.

$$2\pi\phi_(\mathbf{x}) + \iint_{S_b} \big[\phi(\boldsymbol{\xi})\frac{\partial G(\boldsymbol{\xi},\mathbf{x})}{\partial n_\xi} - \frac{\partial \phi}{\partial n} G(\boldsymbol{\xi},\mathbf{x})\big] d\boldsymbol{\xi} = 0 \qquad \text{for } \phi = \phi_D \text{ or } \phi_R \tag{A.15}$$

A.2.3 Radiation potential

Equation A.15 is valid for the radiation potential, ϕ_R, and thereby for all the individual components, φ_j (defined in Equation 2.7). This gives

$$2\pi\varphi_j(\mathbf{x}) + \iint_{S_b} \left[\varphi_j(\boldsymbol{\xi})\frac{\partial G(\boldsymbol{\xi},\mathbf{x})}{\partial n_\xi}d\boldsymbol{\xi} - \frac{\partial \phi_j}{\partial n}G(\boldsymbol{\xi},\mathbf{x})\right]d\boldsymbol{\xi} = 0 \tag{A.16}$$

Inserting Equation 2.8a into Equation A.16 yields Equation A.17, which is discretizised and implemented in Wadam. The discretisation is explained in Chapter A.2.5.

$$2\pi\varphi_j(\mathbf{x}) + \iint_{S_b} \left[\varphi_j(\boldsymbol{\xi})\frac{\partial G(\boldsymbol{\xi},\mathbf{x})}{\partial n_\xi}d\boldsymbol{\xi} - n_j G(\boldsymbol{\xi},\mathbf{x})\right]d\boldsymbol{\xi} = 0 \tag{A.17}$$

A.2.4 Excitation potential

Application of Equation A.11 with ϕ equal to the velocity potential of the incoming wave,ϕ_0, to the fictitious volume bounded by the free surface and the surface of the body gives

$$2\pi\phi_0(\mathbf{x}) + \iint_{S_b+S_{SF}} \left[\phi_0(\boldsymbol{\xi})\frac{\partial G(\boldsymbol{\xi},\mathbf{x})}{\partial n_\xi} - \frac{\partial \phi_0}{\partial n}G(\boldsymbol{\xi},\mathbf{x})\right]d\boldsymbol{\xi} = 0 \tag{A.18}$$

Insertion of Equation A.13 into Equation A.18 gives

$$2\pi\phi_0(\mathbf{x}) + \iint_{S_b+S} \left[\phi_0(\boldsymbol{\xi})\frac{\partial G(\boldsymbol{\xi},\mathbf{x})}{\partial n_\xi} - \frac{\partial \phi_0}{\partial n}G(\boldsymbol{\xi},\mathbf{x})\right]d\boldsymbol{\xi} = 0 \tag{A.19}$$

This is the integral for the fictitious volume inside the body and the normal vector is pointing out into the real fluid. By altering the normal vector to pointing into the fictitious fluid and out of the real fluid Equation A.19 may be rewritten as

$$2\pi\phi_0(\mathbf{x}) = \iint_{S_b} \left[\phi_0(\boldsymbol{\xi})\frac{\partial G(\boldsymbol{\xi},\mathbf{x})}{\partial n_\xi} - \frac{\partial \phi_0}{\partial n}G(\boldsymbol{\xi},\mathbf{x})\right]d\boldsymbol{\xi} \tag{A.20}$$

Equation A.21 is obtained by replacing ϕ with diffraction potential φ_D in Equation A.15.

$$2\pi\phi_D(\mathbf{x}) + \iint_{S_b} \left[\phi_D(\boldsymbol{\xi})\frac{\partial G(\boldsymbol{\xi},\mathbf{x})}{\partial n_\xi} - \frac{\partial \phi_D}{\partial n}G(\boldsymbol{\xi},\mathbf{x})\right]d\boldsymbol{\xi} = 0 \tag{A.21}$$

Inserting for $\phi_D = \phi_{exc} - \phi_0$ gives

$$\begin{aligned} 2\pi\phi_{exc}(\mathbf{x}) + \iint_{S_b} \Big[\phi_{exc}(\boldsymbol{\xi})\frac{\partial G(\boldsymbol{\xi},\mathbf{x})}{\partial n_\xi} - \underbrace{\frac{\partial \phi_{exc}}{\partial n}}_{=0 \text{ on } S_B} G(\boldsymbol{\xi},\mathbf{x})\Big]d\boldsymbol{\xi} \\ = 2\pi\phi_0(\mathbf{x}) + \iint_{S_b} \left[\phi_0(\boldsymbol{\xi})\frac{\partial G(\boldsymbol{\xi},\mathbf{x})}{\partial n} - \frac{\partial \phi_0}{\partial n}G(\boldsymbol{\xi},\mathbf{x})\right]d\boldsymbol{\xi} \end{aligned} \tag{A.22}$$

Inserting Equation A.20 into Equation A.22 gives Equation A.23 which is discretisised and implemented in Wadam. The discretization is explained in Chapter A.2.5.

$$2\pi\phi_{exc}(\mathbf{x}) + \iint_{S_b} \phi_{exc}(\boldsymbol{\xi})\frac{\partial G(\boldsymbol{\xi},\mathbf{x})}{\partial n_\xi}d\boldsymbol{\xi} = 4\pi\phi_0(\mathbf{x}) \tag{A.23}$$

A.2.5 Discretization

Equation A.17 and Equation A.23 are then discretizised by each panel in the panel model. The radiation and excitation potentials are taken to be constant over each panel. The integral Equation A.23 and Equation A.17 may then be discretizised for a model with N panels as given below.

$$2\pi\varphi(\mathbf{x}_i) + \sum_{k=1}^{N} D_{ik}\varphi_k = \sum_{k=1}^{N} S_{ik}\left(\frac{\partial\varphi}{\partial n}\right)_k \tag{A.24}$$

$$2\pi\phi(\mathbf{x}_i) + \sum_{k=1}^{N} D_{ik}\phi_k = 2\pi\phi_0(\mathbf{x}_i) \tag{A.25}$$

The coefficients in Equation A.24 are given by

$$D_{ik} = \iint_{S_k} \frac{\partial G(\boldsymbol{\xi}, \mathbf{x_i})}{\partial n_\xi} d\boldsymbol{\xi}$$
$$S_{ik} = \iint_{S_k} G(\boldsymbol{\xi}, \mathbf{x_i}) d\boldsymbol{\xi}$$

The integrals are enforced at the points $\mathbf{x}_i$ taken at the center of the panels. The set of equations given by Equation A.24 and Equation A.25 are used to find the radiation and excitation potentials which are used to compute the damping and added mass coefficients as well as the the load transfer functions.

B | The Generalised-α method

The Generalised-α method was presented by Chung and Hulbert [15] and is presented here. The basic form of the method is given for a linear system as

$$\mathbf{M}\ddot{\mathbf{X}} + \mathbf{C}\dot{\mathbf{X}} + \mathbf{K}\mathbf{X} = \mathbf{F} \tag{B.1}$$

where $\mathbf{X}$ is the vector of displacements. The method is given by Equations B.2-B.6.

$$\mathbf{p}_{n+1} = \mathbf{p}_n + \Delta t\mathbf{v} + \Delta t^2\big((1/2 - \beta)\mathbf{a}_n + \beta\mathbf{a}_{n+1} \tag{B.2}$$

$$\mathbf{v}_{n+1} = \mathbf{v}_n + \Delta t\big((1-\gamma)\mathbf{a}_n + \gamma\mathbf{a}_{n+1} \tag{B.3}$$

$$\mathbf{M}\mathbf{a}_{n+1-\alpha_m} + \mathbf{C}\mathbf{v}_{n+1-\alpha_f} + \mathbf{K}\mathbf{p}_{n+1-\alpha_f} = \mathbf{F}(t_{n+1-\alpha_f}) \tag{B.4}$$

$$\mathbf{p}_{n+1-\alpha_f} = (1-\alpha_f)\mathbf{p}_{n+1} + \alpha_f\mathbf{p}_n \tag{B.5a}$$

$$\mathbf{v}_{n+1-\alpha_f} = (1-\alpha_f)\mathbf{v}_{n+1} + \alpha_f\mathbf{v}_n \tag{B.5b}$$

$$\mathbf{a}_{n+1-\alpha_m} = (1-\alpha_m)\mathbf{a}_{n+1} + \alpha_m\mathbf{a}_n \tag{B.5c}$$

$$t_{n+1-\alpha_f} = (1-\alpha_f)t_{n+1} + \alpha_f t_n \tag{B.5d}$$

α_f, α_m, β and γ are algorithmic parameters that need to be determined. p, v and a are the estimated displacements, velocities and accelerations, respectively. The initial conditions are given by

$$\mathbf{p}_0 = \mathbf{X}(0) \tag{B.6a}$$

$$\mathbf{v}_0 = \dot{\mathbf{X}}(0) \tag{B.6b}$$

$$\mathbf{a}_0 = \mathbf{M}^{-1}(\mathbf{F}(0) - \mathbf{C}\mathbf{v}(0) - \mathbf{K}\mathbf{d}(0) \tag{B.6c}$$

C | Separate python script: PIDthruster.py

```
import sys
import math
import OrcFxAPI

class thrust(object):

  # Setting initial values. 'Initialise' is only run once.
  def Initialise(self, info):

      # Reading parameters from OrcaDlex data form:
      paramsDict = {}
      for key, value in info.ObjectParameters.items():
          paramsDict[key] = float(value)
      self.params = OrcFxAPI.objectFromDict(paramsDict)

      # Collecting the time-step from the OrcaFlex model
      self.timeStep = info.Model.general.ImplicitConstantTimeStep

      # There is one instance of this external function
      # per data item that uses it. As long as the applied
      # load calculations are uncoupled, each instance
      # will keep track of the required data in the
      # attributes of each instance.
      self.int = 0.0
      self.intLastIteration = 0.0
      if info.DataName.startswith('GlobalAppliedForceX'):
          self.prevpos = self.params.target1
          self.prevposLastIteration = self.params.target1
          self.target = self.params.target1
          self.kp = self.params.kp1
          self.ki = self.params.ki1
          self.kd = self.params.kd1
          self.kd = self.params.kd1
          self.stat = self.params.stat1
      if info.DataName.startswith('GlobalAppliedForceY'):
          self.prevpos = self.params.target2
          self.target = self.params.target2
          self.kp = self.params.kp2
          self.ki = self.params.ki2
          self.kd = self.params.kd2
          self.prevposLastIteration = self.params.target2
          self.stat = self.params.stat2
      if info.DataName.startswith('GlobalAppliedMomentZ'):
          self.prevpos = self.params.target6
          self.prevposLastIteration = self.params.target6
          self.target = self.params.target6
          self.kp = self.params.kp6
          self.ki = self.params.ki6
          self.kd = self.params.kd6
          self.stat = self.params.stat6
```

```
# 'Calculate' is run for each iteration of each time step
# and calculates the forces based on the current position
def Calculate(self, info):
    if info.DataName.startswith('GlobalAppliedForceX'):
        actual = info.InstantaneousCalculationData.Position[0]
    elif info.DataName.startswith('GlobalAppliedForceY'):
        actual = info.InstantaneousCalculationData.Position[1]
    elif info.DataName.startswith('GlobalAppliedMomentZ'):
        Xaxis = info.InstantaneousCalculationData.Orientation[0]
        actual = math.degrees(math.atan2(Xaxis[1], Xaxis[0]))
    else:
        raise Exception('Cannot find name of value to be determined')

    # If it's a new time step then 'prevpos' and 'int ' are
    # updated to be the values from the previous iteration of
    # the implicit solver, if it's the first time step then
    # they will take the initial values that were set in
    # Initialise:
    if info.NewTimeStep:
        self.prevpos = self.prevposLastIteration
        self.int = self.intLastIteration

    # Calculating the error and the forces corresponding to
    # the three terms in the PID controller:
    error = actual-self.target
    Fp = -self.kp*error
    Fi = self.int - self.ki*error*self.timeStep
    Fd = -self.kd*(actual-self.prevpos)/self.timeStep

    # Storing data from this iteration ready to be used if
    # this is the last iteration for the current time step:
    self.prevposLastIteration = actual
    self.intLastIteration = Fi

    # The force from the thrusters is sent back to OrcaFlex
    # and the data item (Applied Load) that was asked for
    info.Value = Fp+Fi+Fd+self.stat
```

D | Separate python script: harmonicThruster.py

```
import sys
import math
import OrcFxAPI

class thrust(object):

  def Calculate(self, info):

    # Calculates value of the harmonic load:
    info.Value = -3000*math.sin((2*math.pi/12)*info.SimulationTime)
```

E | Wadam Input

ENVIRONMENT	
Gravity	9.80665 $^{m}/_{s^2}$
Water density	1025 $^{kg}/_{m^3}$
Water kinematic viscosity	1.609E-6 $^{m^2}/_{s}$
Water depth	109 m
Frequency Set	(2.5s - 9s): Interval of 0.25s (9s - 11s): Interval of 0.5s (11s - 17s): Interval of 1s (17s - 21s): Interval of 0.5s (21s - 30s): Interval of 1s
Direction Set	0°-180°, interval of 15°
HYDRO STRUCTURE	
Panel Model	T11.FEM
Translation of model	-15.75 m
Symmetry planes of panel model	None
Number of panels	6628
MASS MODEL	
Coordinate system	COG Centered Coordinate system
Buoyancy	Calculated from panel model
Total mass	34 330 000 kg
Center of gravity	-0.0454 m, 0 m, 4.87 m
Radii of gyration	rx = 39.5 m, ry = 38.9 m, rz = 44.8 m

Table E.1: Wadam input, Physical data

EXECUTION DIRECTIVES	
Tolerance waterline	5%
Tolerance center of gravity	5%
Characteristic length	104.5 m
Drift Forces	Pressure integration (6DOF)
Roll damping	None
Equation solver	Direct matrix solver, maximum iteration size: 15 000
Print	Normal print
Result files	- SIF formatted - Calculate eigenvalues - Use global origin as reference point
Logarithm Singularity	Analytical
Numerical integration	One node gauss
Panel dimension	Maximum diagonal
Other	- Save temp. Wamit files - Calculate mass matrices in HydroD

Table E.2: Wadam input, Execution Directives

F | OrcaFlex Input

F.1 General data

STATICS	
Statics method	Whole System Statics
Buoy degrees of freedom included in Static Analysis	None
Starting Velocity	None
Statics convergence parameters:	
- Max iterations	5000
- Tolerance	1E-6 (Default value)
- Min Damping	1 (Default value)
- Max Damping	10 (Default value)
DYNAMICS	
Duration Build-up	10 s
Duration Stage 1	1200 s
Logging:	
- Precision	Single
- Target Sample Interval	0.1 s
INTEGRATION AND TIME STEPS	
Integration method	Implicit
Time step	0.1 s
Maximum number of iterations	100
Tolerance	25E-6
RESULTS	
Spectral Density Fundamental Frequency	0.01 Hz
DRAWING	
North Direction defined	0 deg

Table F.1: OrcaFlex input, General Data

F.2 Environment

SEA	
Surface Z	0 m
Kinematic viscosity	1.609E-6 m^2/s
Temperature	4 °C
Reynolds Number Calculation	Not applied
SEA DENSITY	
Density Variation	None
Water density	1.025 ton/m^3
SEABED	
Type	Flat
Seabed Origin	(0m,0m,-109m)
Direction	Not applied
Slope	0
Seabed Model	Linear
Normal Stiffness	100 $kN/m/m^2$
Shear Stiffness	0 $kN/m/m^2$
Damping	0

Table F.2: OrcaFlex input, Sea and Seabed

WAVES	
Simulation Time Origin	0 s
Kinematic Stretching model	Extrapolation stretching
User Specified Seeds	12345
Spectrum Discretisation Method	9.5d
Direction	-28 deg
Significant Waveheight, H_S	8.8 m
Zero Crossing Period	9.2 s
Wave Origin	(0m,0m)
Wave Time Origin	0 s
Wave Type	JONSWAP
γ	2.7
Peak Frequency, f_m	0.0831 Hz
Peak Period, T_p	12.0337 s
Wave Directions	
- Spreading Exponent	10
- Number of Directions	9
Number of Wave Components per Direction	100 (Default)
Relative Frequency Range	
- r_{min}	0.5 (Default)
- r_{max}	10 (Default)
Maximum Component Frequency Range	Not limited

Table F.3: OrcaFlex input, Waves

CURRENT	
Ramp During Build-Up	No
Horizontal Current Variation	No
Vertical Current Variation	
- Method	Power Law
- Speed Surface	0.5 m/s
- Speed Seabed	0 m/s
- Exponent	30
- Direction	0 deg
WIND	
Include Wind Loads on	Vessels and Lines
Vertical Wind Variation	None
Air Density	0.0013 ton/m^3
Air Kinematic Viscosity	15E-6 m^2/s
Wind Type	Constant
Wind Speed	25.8 m/s
Wind Direction	26 deg

Table F.4: OrcaFlex input, Wind and Current

F.3 Vessel

VESSEL	
Length	104.5 m
Initial Position	x=0m, y=0m, z=0m, heel=0°, trim=0°, heading=0°
Calculation	
- Included in Static Ananlysis	6 DOF
- Primary Motion	Calculated (6 DOF)
- Superimposed Motion	None
- Included Effects	Applied Loads, Wave Load(1st order), Wave Drift Load(2nd order), Wave Drift Damping, Added Mass and Damping, Manoeuvring Load, Current Load and Wind Load
- Primary Motion is Treated as	Both low- and wave- frequency
- Dividing Period	25s
Applied Loads	
- Point of Application	(0m,0m,-16.1m)
- Local Applied Load X	PIDThruster
- Local Applied Load Y	PIDThruster
- Local Applied Moment Z	PIDThruster
Multiple Statics	No
VESSEL TYPE	
Structure	
Vessel Typical Length	104.5 m
Mass	34 330 ton
(Radii of Gyration)	(r44=39.5m, r55=38.9m, r66=44.6m)
Moment of Inertia	I44=53 563 ton·m^2, I55=51 948 ton·m^2, I66=68 288 ton·m^2
Center of Gravity	x=-0.0454m, y=0m, z=4.87m

Table F.5: OrcaFlex input, Vessel data 1

VESSEL TYPE	
Conventions	
Displacment RAO rotation amplitude	Not applied
Waves are referred to by	Periods
RAO phases are	'Leads' in 'degrees' relative to wave 'crest'
Postive directions	Surge is 'forward', sway is 'port', heave is 'up', roll is starboard 'down', pitch is bow 'down', yaw is bow to 'port'
Symmetry	XZ-plane
Displacement RAOs	None
Load RAOs	
Imported from	Wamit output file calculated in Wadam (Stop Before Second Force)
Origin	0m,0m,0m
Phase Origin	0m,0m,0m
Wave Drift QTFs	
Specification Method	Newman's approximation
Imported File	Wamit output file calculated in Wadam
Origin	0m,0m,0m
Stiffness, Added Mass and Damping	
Reference origin	x=-0.045m, y=0m, z=4.87m
Equilibrium position	z=4.87m, Heel=0°, Trim=0°
Imported file, damping and added mass	Wamit output file calculated in Wadam (Stop Before Second Force)
Restoring coefficients	C33=8 319kN/m C34=-0.019kN/deg C35=-0.806kN/deg C44=908 374 kNm/deg C45=0.920kNm/deg C55=1 943 140kNm/deg
Other Damping	None
Current Load	
Areas and area moment	Surge:655m^2 Sway:1263m^2 Yaw:131984m^3
Load Coefficients	From FORCE wind tunnel tests
Current load origin	-26.5m, -26m, -8.75m
Wind Load	
Areas and area moment	Surge:1975m^2, Sway:2231m^2, Yaw:233140m^3
Load Coefficients	From FORCE wind tunnel tests
Wind load origin	-26.5m, -26m, 24m

Table F.6: OrcaFlex input, Vessel data 2

F.4 Anchor Lines

LINES: End X- and Y-Coordinates		
Line number	**End A (Global axes)**	**End B (Vessel axes)**
Line 1	(-1625m, 458m)	(29.7m, -33.9)
Line 2	(-902m, 1716m)	(22.8m, -33.9m)
Line 3	(576m, 1800m)	(-23.4m, -34m)
Line 4	(1446m, 776m)	(-30.1m, -34.1m)
Line 5	(1605m, -527m)	(-29.7m, 34m)
Line 6	(1019m, -1941m)	(-22.9m, 34m)
Line 7	(-667m, -2089m)	(23.3m, 34.1m)
Line 8	(-1711m, -913m)	(29.9m, 34.1m)

Table F.7: OrcaFlex input, Anchor Line End Coordinates

LINES	
Include Torsion	No
Top End	End B
P-y model	None
Connected to object	End A: Anchored, End B: Vessel1
End Orientation	Azimuth: Calculated by OrcaFlex Declination, Gamma = 0
Height above Seabed	0m
Release at start of stage	Not applicable
Connection stiffness	None
Included in Statics	Catenary
Full Statics	Yes
Include Seabed Friction	Yes
Expansion Factor	None
Clash Check	No
Bre-bent curvature	No
Contents	None (Density = 0)
Catenary convergence	(Default values)
- Max iterations	100
- Delta	-5E-9
- Tolerance	50E-9
- Min damping	1
- Shooting factor	1.5
- BackTrack factor	2
- Mag.of Std. Error	0.2
- Mag. of Std. Change	0.6
Full Statics Convergence	(Default values)
- Method	Line Search
- Max iterations	400 (except for Line 5:2000)
- Delta	Not applied
- Tolerance	1E-6
- Min damping	1
- Max damping	10
Drag & Wake Formulation	
- Drag formulation	Standard
- Reacts to wake	No
- Generates wake	No
VIV	Not applied
Results	Log results. Arc length axis: Horizontal

Table F.8: OrcaFlex input, Lines, Computational choices

LINE TYPES			
Name	**Chain NVR4-76**	**Chain NVR4-84**	**WIRE (6x49 WS+IWRC)**
Category	General	General	General
Wizard input diameter	0.076 m (D_{bar})	0.084 m (D_{bar})	0.090
Outer diameter	*0.137 m	*0.151 m	0.090 m
Inner diameter	0 m	0 m	0 m
CG Offset	Not applied	Not applied	Not applied
Bulk modulus	Infinity	Infinity	Infinity
Mass	0.1127 ton/m	0.134 ton/m	0.032 ton/m
Compression limited	Yes	Yes	No
Allowable tension	6 003 kN	7 210 kN	7250 kN
Minimum Bending radii	Not applied	Not applied	Not applied
Bending stiffness	0.1kN	0.1 kN	0.1 kN
Axial stiffness	508 158 kN	620 973 kN	667 983 kN
Poisson ratio	0.3	0.3	0.3
Torsional Stiffness	0	0	0
Drag coefficient X/Y-dir	2.6	2.6	1.8
Drag coefficient Z-dir	1.4	1.4	0
Lift coefficients	0	0	0
Drag/lift diameters	0.076 m	0.084 m	0.090 m
Added Mass coefficient X/Y-dir	1	1	1
Added Mass coefficient Z-dir	0.08	0.08	0.08
Inertia coefficients X/Y/Z	$1+C_a$	$1+C_a$	$1+C_a$
Contact Diameter	*0.255 m	*0.281 m	0.090 m
Line Clashing	None	None	None
Stress Diameters	*0.137 m	*0.151 m	0.090 m
Allowable Stress	Not applied	Not applied	Not applied
Tensile Stress Loading factor	1	1	1
Bending Stress Loading factor	1	1	1
Shear Stress Loading factor	1	1	1
Torsional Stress Loading factor	1	1	1
Seabed Friction Coefficients	0.6	0.6	0.6

Table F.9: OrcaFlex input, Line Types. Values marked with * are calculated by the OrcaFlex Line Wizard

LINE SECTIONS				
Line	**Segment**	**Segment type**	**Segment Length [m]**	**Target Segment length [m]**
Line1	Section 1	NVR4-84	240	10
Line1	Section 2	NVR4-84	10	2
Line1	Section 3	NVR4-76	10	2
Line1	Section 4	NVR4-76	889	10
Line1	Section 5	NVR4-76	40	2
Line1	Section 6	NVR4-76	64	10
Line1	Section 7	NVR4-76	10	2
Line1	Section 8	WIRE (6x49 WS+IWRC)	10	2
Line1	Section 9	WIRE (6x49 WS+IWRC)	388	10
Line2	Section 1	NVR4-84	1263	10
Line2	Section 2	NVR4-84	40	2
Line2	Section 3	NVR4-84	200	10
Line2	Section 4	NVR4-84	10	2
Line2	Section 5	WIRE (6x49 WS+IWRC)	10	2
Line2	Section 6	WIRE (6x49 WS+IWRC)	388	10
Line3	Section 1	NVR4-84	1331	10
Line3	Section 2	NVR4-84	40	2
Line3	Section 3	NVR4-84	132	10
Line3	Section 4	NVR4-84	10	2
Line3	Section 5	WIRE (6x49 WS+IWRC)	10	2
Line3	Section 6	WIRE (6x49 WS+IWRC)	340	10
Line4	Section 1	NVR4-84	240	10
Line4	Section 2	NVR4-84	10	2
Line4	Section 3	NVR4-76	10	2
Line4	Section 4	NVR4-76	646	10
Line4	Section 4	NVR4-76	646	10
Line4	Section 5	NVR4-76	40	2
Line4	Section 6	NVR4-76	307	10
Line4	Section 7	NVR4-76	10	2
Line4	Section 8	WIRE (6x49 WS+IWRC)	10	2
Line4	Section 9	WIRE (6x49 WS+IWRC)	340	10

Table F.10: OrcaFlex input, Sections and segments, Lines 1-4

LINE SECTIONS				
Line	**Segment**	**Segment type**	**Segment Length [m]**	**Target Segment length [m]**
Line5	Section 1	NVR4-84	240	10
Line5	Section 2	NVR4-84	10	2
Line5	Section 3	NVR4-76	10	2
Line5	Section 4	NVR4-76	817	10
Line5	Section 5	NVR4-76	40	2
Line5	Section 6	NVR4-76	136	10
Line5	Section 7	NVR4-76	10	2
Line5	Section 8	WIRE (6x49 WS+IWRC)	10	2
Line5	Section 9	WIRE (6x49 WS+IWRC)	388	10
Line6	Section 1	NVR4-76	830	10
Line6	Section 2	NVR4-76	40	2
Line6	Section 3	NVR4-76	133	10
Line6	Section 4	NVR4-76	10	2
Line6	Section 5	WIRE (6x49 WS+IWRC)	10	2
Line6	Section 6	WIRE (6x49 WS+IWRC)	1131	10
Line7	Section 1	NVR4-76	854	10
Line7	Section 2	NVR4-76	40	2
Line7	Section 3	NVR4-76	109	10
Line7	Section 4	NVR4-76	10	2
Line7	Section 5	WIRE (6x49 WS+IWRC)	10	2
Line7	Section 6	WIRE (6x49 WS+IWRC)	1131	10
Line8	Section 1	NVR4-84	490	10
Line8	Section 2	NVR4-84	10	2
Line8	Section 3	NVR4-76	10	2
Line8	Section 4	NVR4-76	809	10
Line8	Section 5	NVR4-76	40	2
Line8	Section 6	NVR4-76	144	10
Line8	Section 7	NVR4-76	10	2
Line8	Section 8	WIRE (6x49 WS+IWRC)	10	2
Line8	Section 9	WIRE (6x49 WS+IWRC)	388	10

Table F.11: OrcaFlex input, Sections and segments, Lines 5-8

F.5 Buoys

CLUMPS		
Name	**Buoy5**	**Buoy10**
Mass	0.1 ton	0.2 ton
Volume	4.97 m^2	9.94
Height	2.71 m	3.41 m
Align with	Line axes	Line axes
Drag area, X/Y-dir	3.67	5.83
Drag area, Z-dir	1.83 m	2.91 m
Drag coefficient	1.5	1.5
Added mass coefficient	1	1

Table F.12: OrcaFlex input, Subsurface Buoys